ENVIRONMENTALLY-BENIGN FLAME RETARDANT NANOCOATINGS FOR FOAM AND FABRIC

A Dissertation

by

AMANDA ASHLEY CAIN

Submitted to the Office of Graduate and Professional Studies of
Texas A&M University
in partial fulfillment of the requirements for the degree of

DOCTOR OF PHILOSOPHY

Chair of Committee,	Jaime C. Grunlan
Committee Members,	Jodie Lutkenhaus
	Abraham Clearfield
	Xinghang Zhang
Head of Department,	Ibrahim Karaman

December 2014

Major Subject: Materials Science and Engineering

Copyright 2014 Amanda Ashley Cain

ABSTRACT

Halogen-additives are cost effective flame retardants (FRs) that scavenge H• and OH• radicals in the gas phase, but are under significant scrutiny due to the toxic smoke they release and their potential to leach out into the environment and possibly bio accumulate. One fire retarding solution is using layer-by-layer (LbL) assembly, which is a simple, bottom-up processing technique, to create functional nanocoatings through sequential adsorption of materials with complementary functional groups for the purpose of inhibiting or suppressing the combustion cycle. Inspiration for first applying polymer/clay thin films (i.e., nanobrick walls) as flame retardant (FR) coatings to polyurethane foam via LbL came from the final stage of a proposed flame suppression mechanism in a melt-mixture of polymer and clay, which depicts a physical barrier created from the build-up of impermeable flakes and carbonized char.

Intumescing nanobrick wall assemblies comprised of nitrogen and phosphorus-containing polymers (mortar) and clay platelets (bricks) were deposited on flexible polyurethane foam using layer-by-layer assembly. Four trilayers of the poly(allylamine hydrochloride) (PAH)/poly(phosphate sodium salt) (PSP)/montmorillonite (MMT) nanobrick wall assembly (< 3 wt% coating addition) are necessary to cut the pkHRR of polyether-based polyurethane by 54.8%, relative to control, uncoated foam

The influence of clay aspect ratio and composition on fire behavior of coated polyurethane foam was studied as a function of polymer/clay (montmorillonite or vermiculite (VMT)) layers deposited and nanocoating weight addition. A single bilayer

(BL) of polyethylenimine (PEI) and formulated-vermiculite clay, which adds only 3.2 wt% to the foam, successfully prevented formation of a melt pool of burning polymer and reduced peak heat release rate and total smoke release by 54% and 31%, respectively. MMT-nanobrick walls require 4 BL to match the fire performance of single BL VMT-nanobrick walls.

Aqueous coacervation was investigated as a single step process to deposit flame retardant nanocoatings on textiles quickly. Cotton soaked in environmentally-benign PSP/PEI complex for 1 min resulted in a 16.7% residue after vertical flame testing and a 52.7% reduction in total heat release in comparison to uncoated cotton in micro combustion calorimetry. Nanocoatings produced from a 10 min immersion result in fabric capable of self-extinguishing during vertical flame testing.

DEDICATION

I dedicate this dissertation to my Dad, Mom, & Granny, and in loving memory of my Paw Paw, Howard Friday. You instilled within me the importance of hard work and higher education. Thank you for always encouraging me to work diligently and persist, stay rooted in knowledge of the Gospel's truths, stand firm on faith even in challenging situations, and pursue my passions with all my heart in a manner that glorifies the Lord.

ACKNOWLEDGEMENTS

More people deserve acknowledgement for their support of this work than I can mention. First, I would like to express my gratitude to my advisor, Dr. Jaime Grunlan. I appreciate his contributions of time and funding to make my Ph.D. experience productive and stimulating. Thank you for encouraging my research and for allowing me to grow as a research scientist. I would also like to thank my committee members, Jodie Lutkenhaus, Abraham Clearfield, Zhang Xinghang, and Andreas Holzenburg for taking time out of their busy schedules for serving on my Ph.D. committee and for their insight. I appreciate the assistance of Oren Regev (of Ben-Gurion University of the Negev) and E. Ann Ellis (of the Microscopy and Imaging Center at Texas A&M University) for their investment in me and my research.

The group members of the Polymer NanoComposites Lab have contributed immensely to my personal and professional time at Texas A&M. I owe a great debt of gratitude to my outstanding undergraduate assistants, Morgan Plummer, Shannon Murray, Arturo Mateos, and Craig Nolan, who put in countless hours and gave valuable feedback on this research. I also acknowledge the tremendous amount of help I received from former and current graduate students of the Polymer Nanocomposites Lab, Dr. Yong Tae Park, Dr. Yu-Chin Li, Dr. You-Hao Yang, Dr. Galina Laufer, Dr. Gregory Moriarty, Bart Stevens, Ping Tzeng, Kevin Holder, Fangming Xiang, Tyler Guin, Blake Teipel, Dr. Marcus Leistner, and Taylor Smith. A special thanks to Dr. Morgan Priolo. Thank you for your advice and for all your time, sound-boarding ideas – you are a great

mentor and friend. The success of my research was also facilitated on a daily basis by the excellent staff of both the Department of Mechanical Engineering and the Department of Materials Science & Engineering, with outstanding advisement from Coordinator, Jan Gerston. Special thanks to Aishwarya Sooresh, Shamik Basu, Xiayan Huang, Youxing Chen, and Alper Evirgen - I am so happy that my friendship with you all has extended well beyond our MSEN 601 study sessions.

I am deeply thankful to my church family – especially the Forbes and our life group - for their friendship, encouragement, support, and prayers. I wish to express my sincere thanks to my best friend, David Hagen, and his wonderful family for supporting me. Your leadership in the research group and support during my time at Texas A&M is invaluable. I am so deeply blessed by your encouragement, support, and unwavering faith in the Lord. I especially am grateful for my Mom, Dad, and Granny. You taught me about hard work, persistence and self-respect, and instilled within me qualities and values that have me standing on a solid foundation, where I know the Lord, and have full assurance in His provision. You have always expressed how proud you are of me and how deep your love is for me. Words cannot express how grateful I am for the sacrifices you have made and the prayers you have raised on my behalf.

Finally, and most importantly, I thank God, for his steadfast love and provision through all the difficulties. I have experienced Your guidance day by day. I will keep on trusting You for my future. Thank you, Lord. “For I am not ashamed of the gospel, because it is the power of God that brings salvation to everyone who believes” Romans 1:16.

NOMENCLATURE

AFM	Atomic force microscopy
ASTM	American Society for Testing and Materials
BL	Bilayer
CNT	Carbon nanotube
CH	Chitosan
DWNT	Double-walled carbon nanotube
EDX	Energy-dispersive X-ray spectroscopy
Eff Hc	Effective heat of combustion
EPTMAC	N-(2,3 epoxypropyl)trimethylammonium chloride
FR	Flame retardant
HRR	Heat release rate
LbL	Layer-by-layer
LCST	Lowest critical solution temperature
MCC	Microscale combustion calorimeter
MMT	Montmorillonite
MWNT	Multi-walled carbon nanotubes
NFC	Nanofibrillated cellulose
OTR	Oxygen transmission rate
PA	Phytic acid
PAA	Poly(acrylic acid)

PAAm	Poly(allylamine)
PAH	Poly(allylamine hydrochloride)
PDDA	Poly(diallyldimethyl ammonium chloride)
PEI	Branched polyethylenimine
PET	Poly(ethylene terephthalate)
pkHRR	Peak heat release rate
PLA	Poly(lactic acid)
PNC	Polymer nanocomposites
PNIPAAM	Poly(N-isopropylacrylamide)
POSS	Polyhedral Oligomeric Silsesquioxane
PSP	Poly(phosphate sodium salt)
PU	Polyurethane
QCM	Quartz crystal microbalance
QL	Quadlayer
SEM	Scanning electron microscopy
SWNT	Single-walled carbon nanotubes
TEM	Transmission electron microscopy
TGA	Thermogravimetric analysis
THR	Total heat release
TL	Trilayer
VMT	Vermiculite

TABLE OF CONTENTS

Page

LIST OF FIGURES

FIGURE Page

FIGURE Page

FIGURE Page

FIGURE Page

LIST OF TABLES

CHAPTER I

INTRODUCTION*

1.1 Background

Fire represents an exothermic chemical reaction that consumes all carbon-based materials and grows when supplied with a sufficient amount of heat and oxygen.[1] The overwhelming presence of flammable polymeric materials in household, automotive, and insulation applications has necessitated the need for effective flame retarding treatments that are sustainable and cost-effective.[2] Flexible polyurethane (PU) foams are porous, open-celled thermoplastic materials that tend to smolder, flow, and pyrolyze under fire conditions due to their insulating behavior, low thermal inertia, and open structure.[3] The addition of flame retarding additives is a common technique used to reduce the fire risk of these materials, but has been criticized on both environmental and functional grounds. Halogen-additives are cost effective flame retardants (FRs) that scavenge H• and OH• radicals in the gas phase,[4] but are under significant scrutiny due to the toxic smoke they release and their potential to leach out into the environment and possibly bio accumulate.[5-7]

---

*Parts of this chapter are reprinted with permission from Mateos, A. J.; Cain, A. A.; Grunlan, J. C., Large-Scale Continuous Immersion System for Layer-by-Layer Deposition of Flame Retardant and Conductive Nanocoatings on Fabric. *Industrial & Engineering Chemistry Research* **2014,** *53*, 6409-6416. © 2013 American Chemical Society, and from Cain, A. A.; Nolen, C. R.; Li, Y.-C.; Davis, R.; Grunlan, J. C., Phosphorous-filled Nanobrick Wall Multilayer Thin Film Eliminates Polyurethane Melt Dripping and Reduces Heat Release Associated with Fire. *Polymer Degradation and Stability* **2013,** *98*, 2645-2652. © 2013 Elsevier.

Toxicity and environmental impact concerns are driving the search for halogen-free flame retardants such as mineral fillers,[8-12] silicon-containing compounds,[13-15] carbon nanotubes,[15-18] and inorganic platelets.[19-21] Polymer nanocomposites prepared with montmorillonite clay have gained significant attention due to several successful demonstrations of reductions in peak heat release rates (pkHRR) and elimination of thermoplastic melt-dripping.[22-27] A proposed mechanism suggests that upon exposure to fire, mobile pyrolysis bubbles bring nanofiller to the surface to form a barrier that limits exchange of volatiles.[28] This char structure, that acts as armor, is a condensed phase flame retardant that slows the rate at which mass transfers through physical action.[29]

Flame retardant multilayer thin films can be fabricated via layer-by-layer (LbL) assembly on the surface of the substrate, precisely where the protective barrier is needed.[30] LbL assembly is a simple, bottom-up processing technique used to create functional nanocoatings through sequential adsorption of materials with complementary functional groups.[31] A schematic representation of the LbL deposition process is depicted in Figure 1.1, where steps 1 – 4 are repeated until the desired number of layers are deposited. A single bilayer (BL) refers to a pair of complementary layers (typically positively and negatively charged) deposited using the LbL technique, but the concept also extends to trilayers (TL) and quadlayers (QL).[32-35] Thin film growth can be characterized by a variety of interactions (hydrogen bonding,[36-38] hydrophobic interactions,[39] etc.), but is typically driven by charge overcompensation on the surface of the last layer deposited.[40-43] In addition to flame retardant coatings, these multilayer constructions have been engineered to demonstrate a breadth of properties including

antireflection,[44-45] electrical conductivity,[46-48] hydrophobicity,[49-51] and gas barrier.[35, 52-53] Diverse building blocks, such as titanium nanoparticles,[54-55] clay nanoplatelets,[56-58] carbon nanotubes,[59-60] proteins,[61-62] and quantum dots,[63-64] have been incorporated into these thin film assemblies in effort to tailor the strength, barrier behavior, optical, and electrical properties.

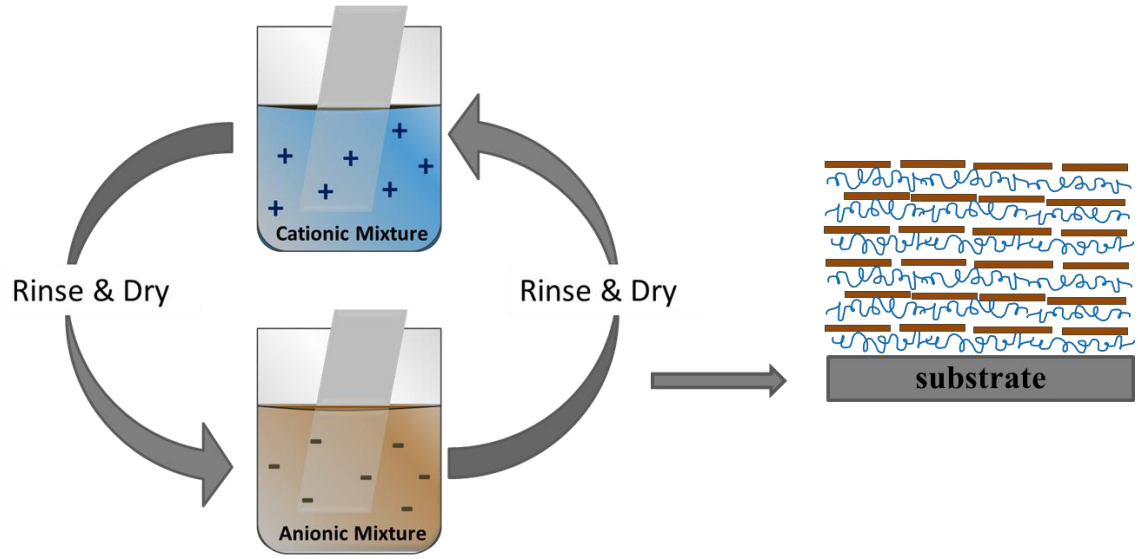

Figure 1.1. Layer-by-layer deposition process used to prepare functional thin films from aqueous mixtures. Steps 1 – 4 are repeated until the desired number of layers are deposited on a substrate.

1.2 Objective and Dissertation Outline

Cotton fabric and polyurethane foam were chosen to be used as model substrates throughout this dissertation because of their common use (in home furnishing, automobiles, and apparel) and highly flammable nature. Flame retardant thin films comprised of polyelectrolytes, clay platelets, and carbon nanotubes, were fabricated

using layer-by-layer assembly and deposited on these complex, three dimensional substrates to interfere with the combustion cycle and impart anti-flammability. The objective of this research was to develop flame retardant nanocoatings and examine their effectiveness in creating a protective barrier that shields the substrate from heat (and direct contact with the flame), and reduces smoke release. The ultimate goal of this body of work was to create nanocoatings for both open-celled polyurethane foam and cotton fabric that are capable of extinguishing flames when each substrate was exposed to fire.

Chapter II provides a brief overview of flame retardants. First, the combustion process of polymers and general flame retardant mechanisms are reviewed, followed by flame retardant strategies. The second part of this chapter reviews LbL assembly, with special emphasis on how this technique has been used to create unique flame retardant thin films.

Chapter III examines the combination of two flame-retarding mechanisms that are paired into a single nanocoating system using layer-by-layer assembly. This unique trilayer thin film is composed of sodium montmorillonite (MMT), poly(allylamine hydrochloride) (PAH), and poly(phosphate sodium salt) (PSP). Growth and composition were characterized using ellipsometry and quartz crystal microbalance (QCM). Thin films were deposited onto flexible polyurethane (PU) foam, and the flammability of control and coated samples was evaluated with small scale torch burn testing and cone calorimetry (ASTM E-1354-07).

Chapter IV investigates the effect of nanoplatelet aspect ratio and elemental composition on multilayer growth and structural composition with scanning electron

microscopy (SEM), transmission electron microscopy (TEM), ellipsometry, and QCM. Polymer/clay nanobrick wall thin films are comprised of polymeric mortar and MMT or vermiculite (VMT) clay bricks. Fire behavior of coated flexible polyurethane foam was compared as a function of the number of layers deposited and as a function of weight addition to the foam. Flammability was assessed using cone calorimetry (ASTM E-1354-07) and thermogravimetric analysis.

Chapter V describes a novel aqueous polyelectrolyte coacervate that was investigated as a means to quickly deposit flame retardant nanocoatings on textiles in a single step. Fabric was soaked in an aqueous complex of PSP and branched polyethylenimine (PEI). The weak polyelectrolytes are drawn toward one another through ionic interaction, and coalesce into a network around individual cotton fibers. Flammability of fabric coated with different "OnePot" weight additions were evaluated using a vertical flame test and a micro combustion calorimeter (MCC).

Chapter VI provides some conclusions and direction for future research. This dissertation investigates flame retardant nanocoatings that provide fire protection through condensed phase mechanisms. One exciting approach to reducing flammability of polyester-based fabrics would be to create an intumescing flame retardant coating using amine-functionalized cellulose nanofibers and PSP. Creating a thermally insulating barrier for polyurethane foam using pyrene-modified polymers and carbon nanotubes is one study that remains to be completed. These coatings also show promise for flame retardant and antistatic applications. The OnePot concept (chapter V) and Few Clay Layers approach (chapter IV) are two examples of effective flame retardant

systems that minimize processing steps and time necessary to deposit the nanocoating. Improving coating durability to withstand multiple wash cycles is another key topic of future work that is vital to commercialization.

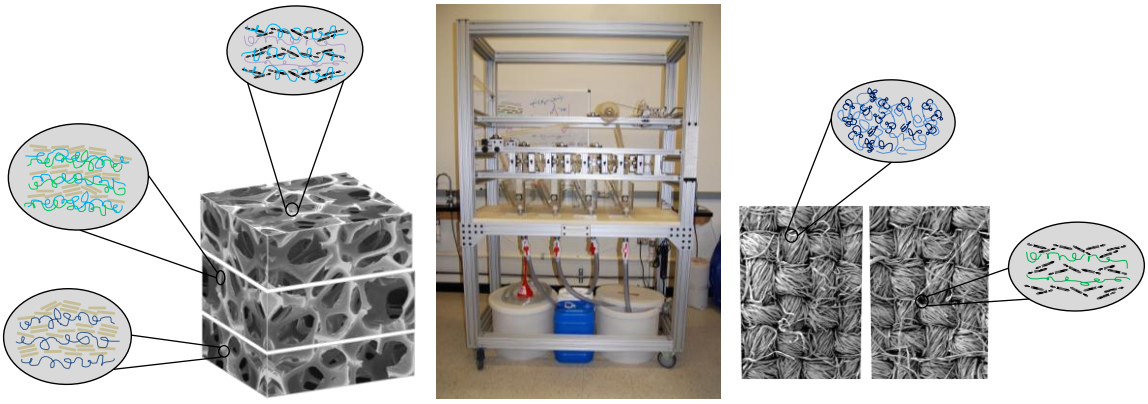

Figure 1.2. Schematic overview of coatings with flame retardant (left to right: VMT-based nanobrick wall, intumescent mortar and MMT-based nanobrick wall, MWNT-based, and intumescent systems) and antistatic (polydiallyldimethylammonium chloride/MWNT-based systems) properties.

CHAPTER II

LITERATURE REVIEW*

2.1 Polymer Combustion and Flame Retardant Fundamentals

Polymers are natural and synthetic compounds of high molecular weight composed of smaller repeat units (mers) that are covalently bonded together.[65] In a fire, physical and chemical changes degrade and break down polymeric materials into fragments and combustible species, which liberates stored energy and fuels the combustion process.[66] Polymer degradation typically occurs through four mechanisms: (1) end-chain and (2) random chain scission (where monomer units are cleaved from chain ends or at random polymer backbone locations), (3) chain stripping (individual atoms or pendant groups are cleaved from the polymer chain), and (4) crosslinking (formation of bonds between polymer chains).[67] Bonds with the lowest dissociation energies will be degraded first. Polymer chemical structure influences these kinetic processes and the resulting degradation products. For example, the presence of oxygen or double bonds in polymer backbones weakens thermal stability, whereas aromatic rings in polymer backbones and the presence of crosslinking tend to strengthen the

---

*Parts of this chapter are reprinted with permission from Cain, A. A.; Nolen, C. R.; Li, Y.-C.; Davis, R.; Grunlan, J. C., Phosphorous-filled Nanobrick Wall Multilayer Thin Film Eliminates Polyurethane Melt Dripping and Reduces Heat Release Associated with Fire. *Polymer Degradation and Stability* **2013,** *98*, 2645-2652. © 2013 Elsevier, and from Cain, A. A.; Murray, S.; Holder, K. M.; Nolen, C. R.; Grunlan, J. C., Intumescent Nanocoating Extinguishes Flame on Fabric Using Aqueous Polyelectrolyte Complex Deposited in Single Step. *Macromolecular Materials and Engineering* **2014**,in press. © 2014WILEY-VCH.

thermal stability of a given polymer.[68] High temperature-resistant polymers typically exhibit decomposition temperatures > 400°C.[69]

In addition to classifying materials by their chemical structure, synthetic polymers are often grouped into the following three basic categories: thermoplastic, thermoset, and elastomer.[70] Elastomeric polymers are rubbery networks (with low glass transition temperatures and low crosslink densities) that are capable of undergoing large elastic deformations. Thermoplastics are moldable polymeric materials that soften and melt before decomposing. Thermosetting materials do not melt (crosslinks prevent movement of molecular chains) and undergo irreversible chemical changes when decomposing, evolving volatiles and yielding char. Thermogravimetric analysis (TGA), which measures changes in mass as a function of temperature (or time), has been paired with evolved gas analysis (such as FTIR and mass spectroscopy) to evaluate various polymeric decomposition pathways.[71-72] Micro combustion calorimetry (MCC) and cone calorimetry tests assess heat release and flammability through oxygen-consumption calorimetry by exposing samples to heating rates that mimic fire type conditions.[73] Equations 1 – 7 show the Bolland and Gee reaction scheme for initiation (1), propagation (2 and 3), termination (4, 5, and 6), and chain branching mechanisms (7) that occurs to polyolefin polymers during thermal and photooxidation, where RO• represents oxygen- and carbon-centered radicals and R• represents polymer alkyl radicals:[74]

$$RH + Heat \rightarrow R\bullet + \bullet H \quad (1)$$

$$R\bullet + O_2 \rightarrow RO_2\bullet \quad (2)$$

$RO_2\bullet + RH \rightarrow ROOH + R\bullet$ (3)

$R\bullet + R\bullet \rightarrow R - R$ (4)

$RO_2\bullet + R\bullet \rightarrow ROOR$ (5)

$RO_2\bullet + RO_2\bullet \rightarrow$ Products (6)

$ROOH \rightarrow RO\bullet + \bullet OH$ (7)

Heat generated from flaming combustion breaks down polymer chain structures, releasing fuel into the gas phase that generates smoke.[75] Degradation products that escape from the polymer surface and mix with an oxidative atmosphere will ignite if the temperature is sufficient. Degradation continues as heat is conducted and radiated back to the surface. Highly reactive H• and OH• radicals found at the flame front are critical driving forces for flame spread.[74] When temperature rises sufficiently, condensed phase degradation occurs at the interface between the flame and the polymeric surface.[76] Flame spread is also associated with heat of combustion. Figure 2.1 is a schematic representation of a combustion cycle that can be established if heat requirements are met in the vapor and/or condensed phases.[77]

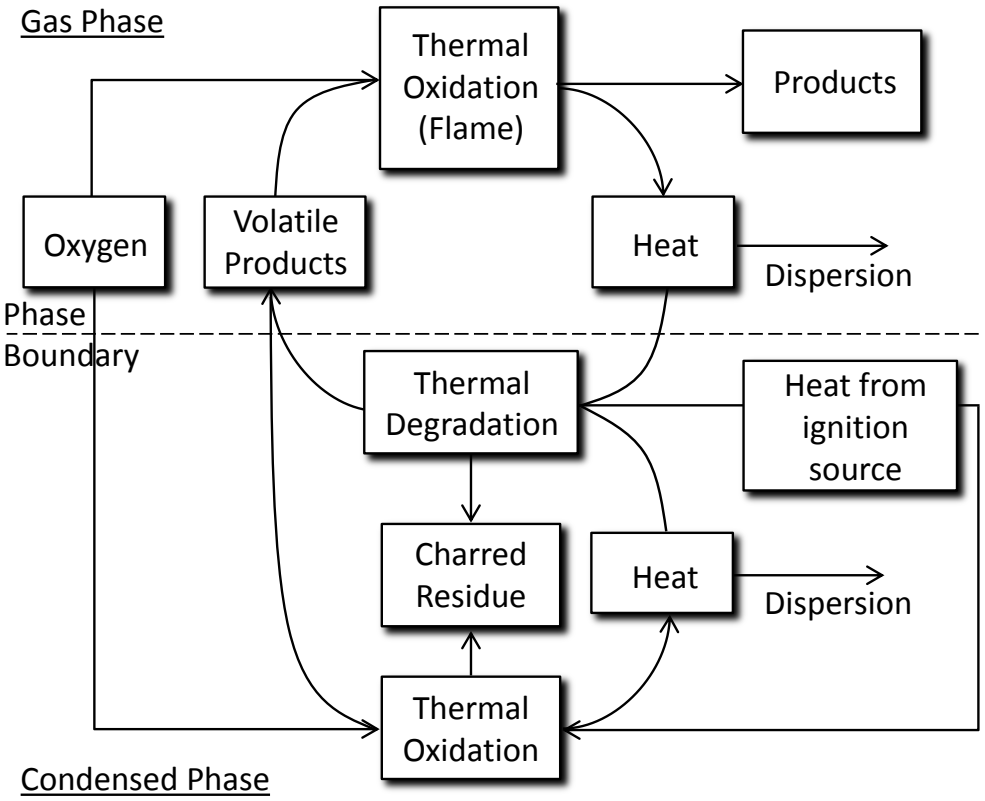

Figure 2.1. Self-sustained polymer combustion cycle. Adapted with permission.[78]

Rigid polyurethane, which is widely used in the building industry due to its heat insulating properties, and flexible polyurethane, commonly used in upholstered furniture, are highly flammable materials susceptible to fast flame-spread and high heat release. Urethane linkages have been observed to dissociate at temperatures as low as 200℃.[79] Polyether and polyester units thermally degrade and regenerate isocyanate and diol precursor groups, respectively, indicated schematically in Figure 2.2.[80] Aside from applying fabric coverings for fire protection, which can rip and expose underlying unprotected material, lower flammability polymers could be worked into formulations or

could be substituted in the market for typical commodity polymers like PU and cotton. Despite their promise, economics (cost and processing) tends to limit the use of high stability polymers.[81] Another fire retarding solution consists of elements/substances that are applied to (or added to) the polymeric materials for the purpose of inhibiting or suppressing the combustion cycle by interfering with ignition, slowing burning, modifying decomposition and pyrolysis, or reducing evolved heat and/or flame spread.[82] These flame retardants (FRs) can be classified into the following three mechanism categories: (1) gas phase, (2) endothermic, or (3) char forming.[81, 83] Whereas gas phase FRs interfere with the chain branching mechanism by scavenging free radicals,[84] char forming systems mainly inhibit the combustion cycle in the condensed phase by creating a thermal barrier that slows release of gases and reduces mass transfer.[85] Endothermic flame retardants interfere with combustion heat requirements in both gas and condensed phases by endothermically decomposing, yielding non-flammable gas that isolates the flame from its oxygen supply, and forming residue in the condensed phase.[86]

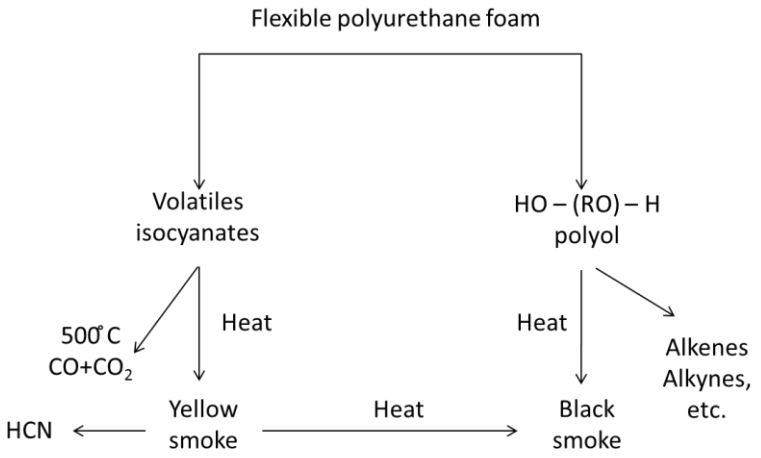

Figure 2.2. Schematic illustration thermal degradation of flexible polyurethane foam. Adapted with permission.[79]

2.2 Flame Retardant Technology

A myriad of flame retardants have been employed to suppress or inhibit the combustion process. Traditional flame retardants described in this overview include halogenated FR, phosphorous-containing FR, mineral fillers, and polymer nanocomposites.

2.2.1 Halogen-based Flame Retardant

As a polymer is undergoing thermal oxidative degradation, the consumption of atmospheric oxygen, the generation of highly reactive H• and OH• radicals (8), and the oxidation of CO to CO_2 propagate chain branching reactions (9).

$$H\bullet + O_2 \rightarrow OH\bullet + O \quad (8)$$

$$HO\bullet + CO \rightarrow CO_2 + H \quad (9)$$

Halogenated compounds incorporate elements from the Group VII (in the periodic table) and have the ability to function as flame retardants in both the gas and condensed phases. Whereas the low bond strength for iodine compounds is not sufficient to endure typical environmental exposure, the high bond strength of fluorine compounds results in their unreactive character.[87] Organobromine and organochloride compounds are most commonly used to increase thermal stability of polymers because the bond energies for these carbon-halogen bonds is within a temperature range in which the halogen can be released to combat the combustion free radical reaction.[81] Upon the addition of heat, halogen (or halide) atoms are released and react with hydrogen atoms of the fuel to produce hydrogen halides (HX). By competing with and diluting the availability of H• (and OH•) radicals necessary for chain branching during thermal oxidation, these flame retardants act as flame inhibitors (10).[88]

$$H\bullet + HX \rightarrow H_2 + X\bullet \qquad (10)$$

The halogen radical can further interact with combustible gases to regenerate the hydrogen halide (HX) flame inhibitor.[89] Elements such as zinc borate[90] and antimony oxide[91-92] have been paired with halogen compounds to increase flame retarding efficiency.[81] Despite their ability to reduce polymers' fire threat, the mechanism by which they inhibit radical propagation increases smoke and produces partially combusted polymer (CO), which increases toxic gas release.[93-94] Several efforts have been made to develop and enhance performance of non-halogenated materials due to environmental persistence of halogen-containing FR.[95]

2.2.2 Phosphorous-based Flame Retardants

Depending on their chemical structure and their interaction with polymer and/or added synergists, phosphorous-compounds can interfere in the combustion cycle in both vapor and condensed phases by either volatilizing into the gas phase (HPO_2•, PO•, PO_2•, and HPO•)[96] (and scavenging H• and OH• radicals) or decomposing in the condensed phase (catalyzing char accumulation on the polymer surface).[4, 97] Unlike halogenated flame retardants, phosphorous tends to be effective at high heat flux conditions, especially when paired with polymers that have high oxygen content.[81] For instance, cellulose exothermically decomposes into smaller carbohydrate units like laevoglucosan and flammable volatiles when exposed to temperatures in the 280-320°C range (Figure 2.3).[98] Phosphorus-containing flame retardants can act in the condensed phase, breaking down into an acidic form (i.e., polyphosphoric acid), which phosphorylates hydroxyl groups on the polymeric surface, catalyzing char formation. This conversion of combustible materials into more thermally stable phosphorocarbonaceous residue not only means less of the original material is consumed by the combustion process, it also functions as a heat shield to the underlying portion of the substrate.[99] This category of flame retardants generally tends to reduce the highly exothermic oxidation of CO to CO_2 (at the cost of increased smoke and soot production and CO vapor generation).[100]

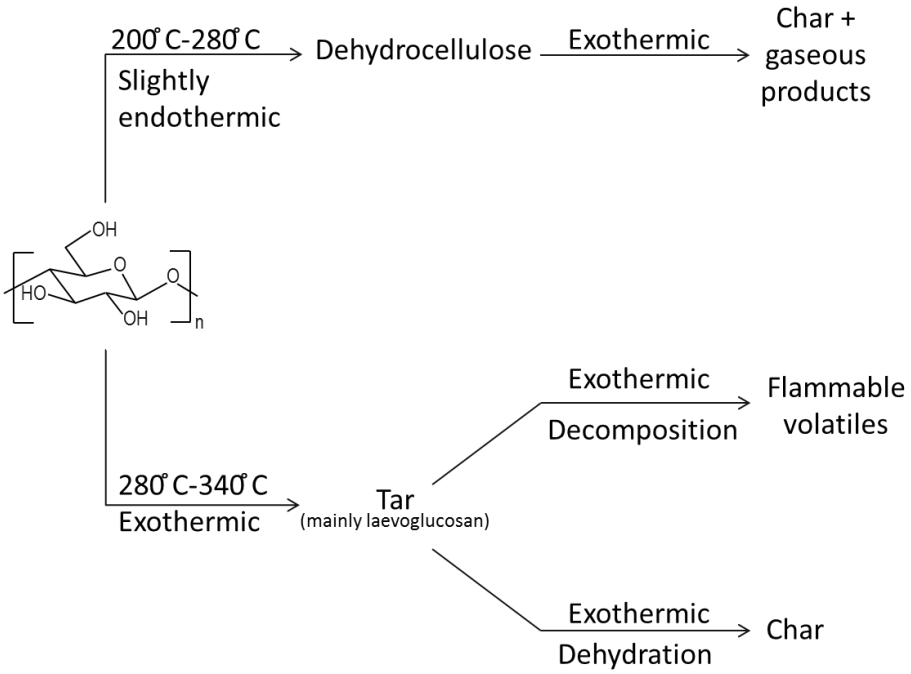

Figure 2.3. Basic scheme illustrating the decomposition of cellulose. Adapted with permission.[98]

Intumescence is a condensed phase flame retardant mechanism that involves the formation of a thermally insulating barrier layer along the polymer surface as the result of a foaming chemical reaction that reduces heat flow to a material.[101] Many approaches involve pairing a phosphorous-based acid with a char forming polymer and a blowing agent,[102] but several ingredients have been investigated.[103-105] Traditionally, when heated beyond a critical temperature, the acidic species (e.g., ammonium polyphosphate) catalyzes char formation through esterification and dehydration of the carbon-rich source (e.g., pentaerythritol). As the blowing agent (e.g., melamine) decomposes, evolved gases form bubbles that expand phosphorocarbonaceous material into a swollen multicellular char.[106] The described mechanism is depicted in Figure 2.4.[81] Thick intumescent

coatings are commonly used to impart fire resistance to structural steel, which allows the metal to better maintain its load-bearing strength as temperature increases during a fire.[101, 107-108]

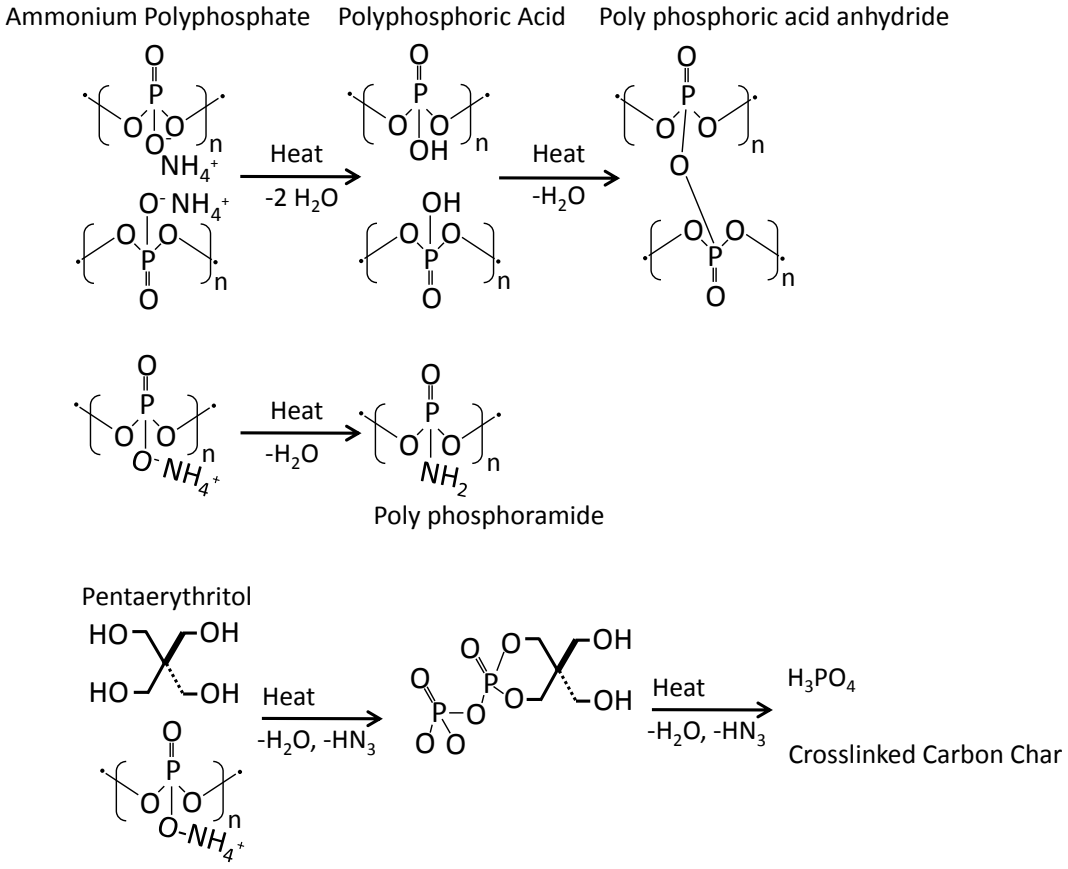

Figure 2.4. Intumescent flame retardant chemical reactions. Adapted with permission.[81]

2.2.3 Mineral Filler Flame Retardants

Inorganic and inert filler is added to polymer matrices not only as a substitute for combustible material, but also to improve their behavior at high temperatures. Metal

hydroxides (aluminum tri-oxide (ATH) and magnesium di-hydroxide (MDH)), hydroxyl carbonates (magnesium and calcium), and zinc borates are common examples of this class of FRs that work through an endothermic cooling mechanism.[81] As depicted in reactions 11 and 12, when the applied heat reaches a critical temperature, mineral fillers decompose, absorbing energy (which cools the condensed phase) and producing non-flammable gases (i.e., water, carbon dioxide, hydrogen chloride, sulfur dioxide) which dilute combustible volatiles.[4] Although mineral fillers are typically nontoxic, high loading levels (20-60 wt%) are necessary for this material to be an effective flame retardant.[109] The window of performance can be tuned to fit the specific polymer matrix in regards to its processing temperature range and onset degradation temperature. For instance, ATH's endothermic decomposition temperature falls between 180-200℃, while the endothermic degradation of MDH occurs between 300-330℃.[85] Once all of

$$2Al(OH)_3 + Heat \rightarrow Al_2O_3 + 3H_2O \text{ (1050 kJ/kg)} \quad (11)$$

$$Mg(OH)_2 + Heat \rightarrow MgO + H_2O \text{ (1300 kJ/kg)} \quad (12)$$

the nonflammable gases have been released, the filler becomes part of the solid phase. In some cases, char formation is promoted. In particular, when boron compounds such as $2ZnO{\cdot}3B_2O_3{\cdot}3.5H_20$ are used in conjunction with oxygen-containing polymers, the inorganic material endothermically decomposes into boric acid and boron oxide. The former aids in dehydrating the polymer, while the latter produces a glassy, insulating layer.[4] Mineral and inert fillers have also been incorporated as smoke suppressants.[110-111]

2.2.4 Polymer Nanocomposites

Polymer nanocomposites are polymers that have fillers with at least one dimension on the order of nanometers dispersed within the matrix.[112] In general, nanofillers are classified by their geometry: as zero-dimensional nanoparticles with diameters less than 100 nm (colloidal silica, carbon black, POSS), one-dimensional fibrous materials (carbon fiber, carbon nanotubes), or two-dimensional layered nanostructures with high aspect ratios, typically ranging from 30-1000 (MMT, VMT, graphene oxide).[113] Figure 2.5 illustrates nanoparticles and their corresponding aspect ratios.

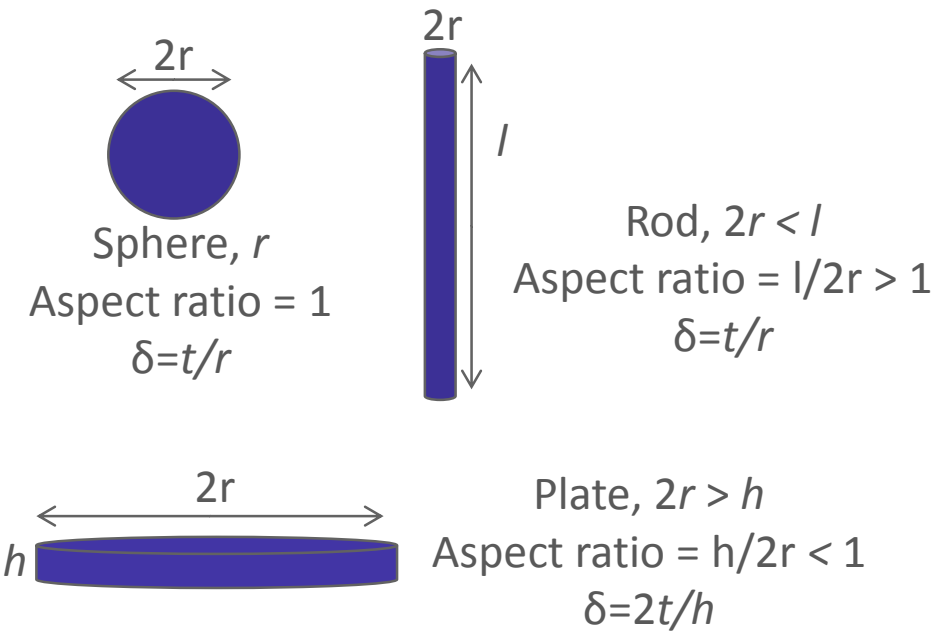

Figure 2.5. Schematic of 0D (sphere), 1D (rod), and 2D (platelet) nanoparticles and their corresponding aspect ratios. Adapted with permission.[23]

Although one strong driving force for investigating nanofiller incorporation has been reinforcement to the polymer matrix,[114-118] it is well known that the unique properties of nanoparticles can be combined to synergistically create interesting physical properties.[119-120] The exhibited properties are associated with the final structure and composition of the nanocomposite, which is influenced by the processing technique.[121] Large research efforts have been devoted to the development of incorporating nanofiller in polymer matrices (e.g., exfoliation-adsorption, in situ intercalative polymerization, melt interaction, template synthesis).[122-123] Transmission electron micrographs, and corresponding illustrations in Figure 2.6, demonstrate three morphologies observed when nanomaterials, such as nanoclays, are dispersed within the bulk phase.[124] Immiscible morphologies, where tactoids (stacks of silicate platelets) are incorporated in the matrix, produce micro (and macro) phase separation due to agglomeration.[125] In addition to blending and thorough mixing, chemical modification and surface functionalization are often required to achieve complete dispersion and good particle exfoliation.[126-127] Using these inclusion techniques often enhances particle-matrix interfacial adhesion, which tends to improve mechanical properties (e.g., impact strength, interlamellar shear strength, delamination resistance)[128-130] and thermal behavior.[131-132]

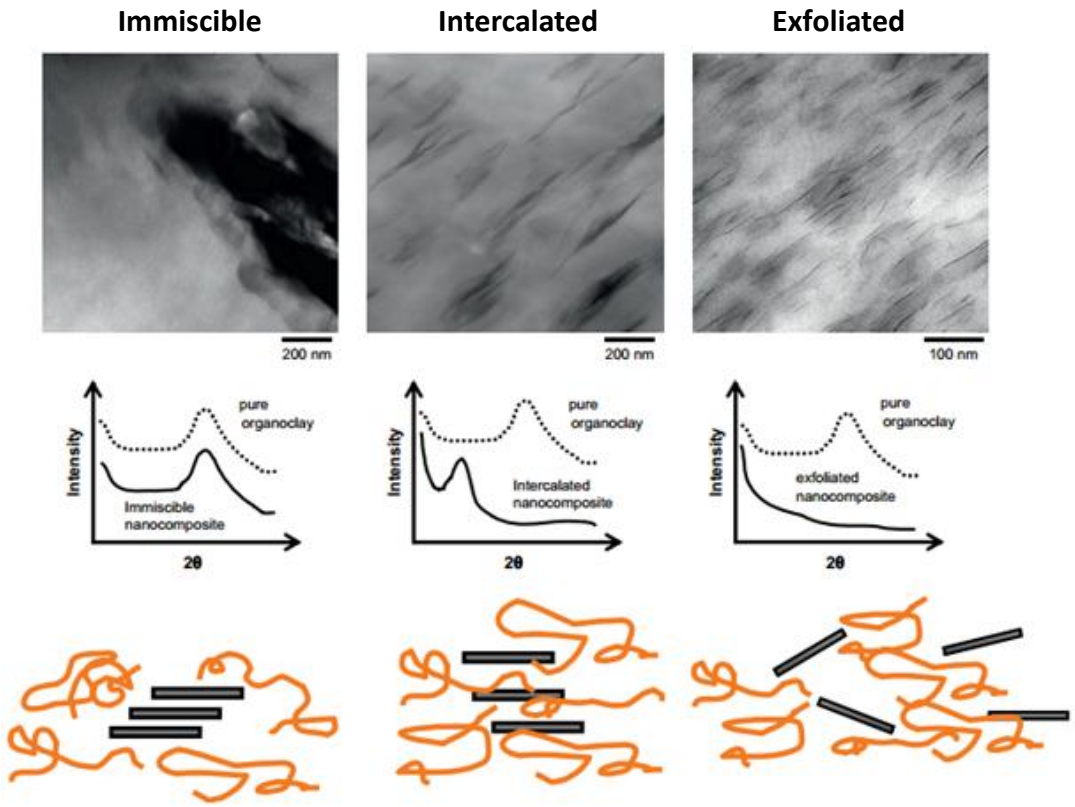

Figure 2.6. Varying of different states of dispersion of organoclays in polymers with corresponding WAXS and TEM results. Adapted with permission.[124]

The inclusion of nanofillers within a polymer matrix for the purpose of enhancing thermal stability and fire performance is an active area of research.[133-134] Polymer nanocomposites themselves are condensed phase flame retardants that form a physical barrier that insulates the interior of the specimen and slows mass transport of fuel into the gas phase.[135] Camino *et al.* created a schematic representation to depict the formation of the protective barrier formed when polymer nanocomposites decompose and described the process as a labyrinth barrier effect (Figure 2.7).[28] When an ethylene-co-vinyl acetate (EVA)-organoclay composite is exposed to an external heating source

and is ignited, the dispersed nanoclay is brought to and oriented along the surface of the specimen through ablative reassembly. The result is the formation of a protective char-silicate barrier.

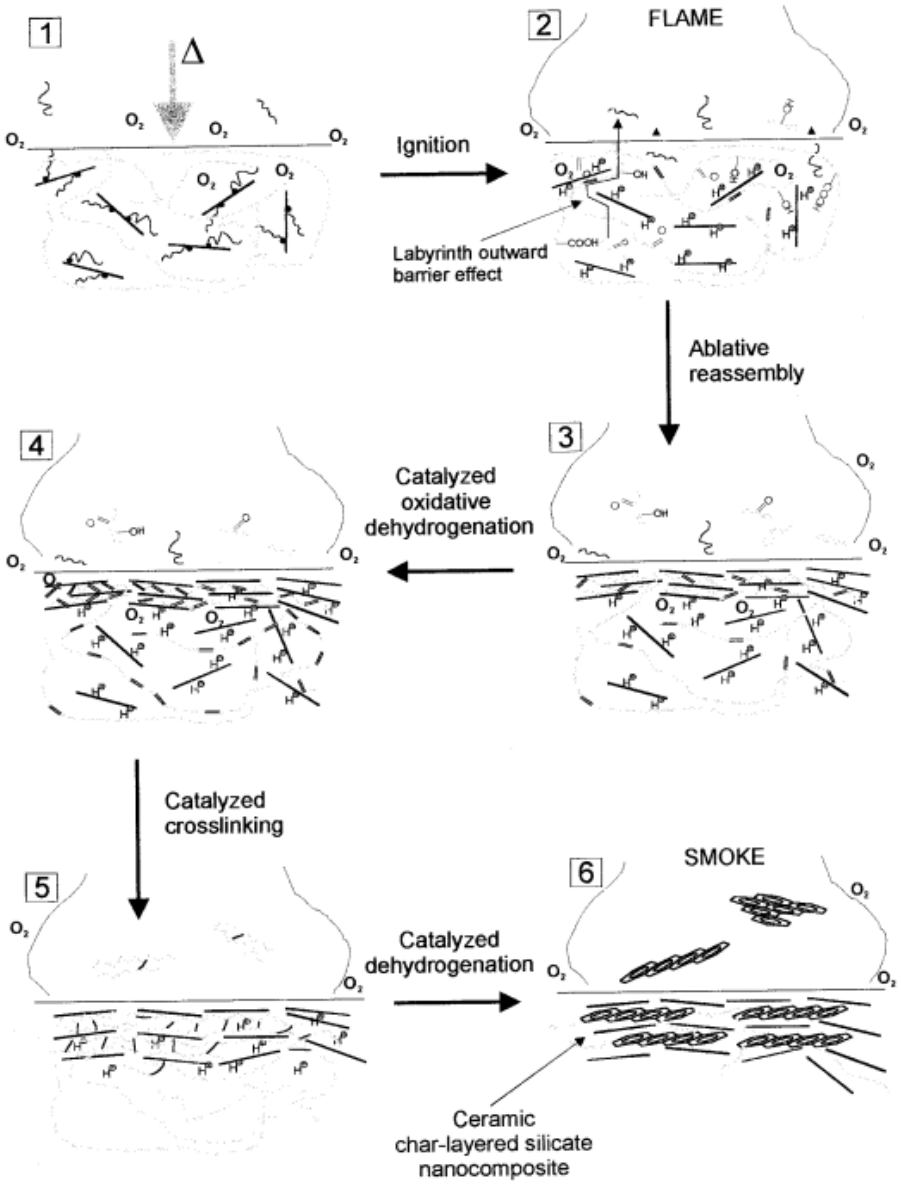

Figure 2.7. Schematic representation of combustion and ablative reassembly of a nanocomposite during burning. Reprinted with permission.[28]

Cone calorimetry is an excellent technique used to quantitatively assess fire performance (e.g., time to ignition, heat release rate (HRR), peak heat release rate (pkHRR), total mass loss, total heat release (THR)) through the use of oxygen consumption calorimetry.[73] Samples are exposed to a heat flux (10-100 kW/m^2) generated from an electric heater, and data is collected as a function of time. A decrease in the rate in which fuel is released corresponds to HRR. It is generally recognized that polymer nanocomposites significantly reduce pkHRR, but do not alter the sample's overall heat release. The filler-rich barrier produced when the specimen is exposed to a critical temperature is able to delay mass loss such that the heat release remains low throughout the combustion process (i.e., reduced pkHRR). Formation of the physical barrier and its associated flammability properties are largely influenced by the concentration and dispersion of nanofiller.[136-137] This concept is depicted in Figure 2.8,[137] where the scenario with lower nanotube content (a) forms discrete islands and the sample with higher nanotube content (b) generates a continuous protective layer. A discontinuous char layer, which could also be a result of poor nanofiller dispersion or agglomeration during combustion, yields inferior thermal protection. It has been suggested that the aspect ratio of the dispersed particles not only influences continuous network formation, but also could be a parameter used to tune the concentration necessary to form a networked char barrier.[136]

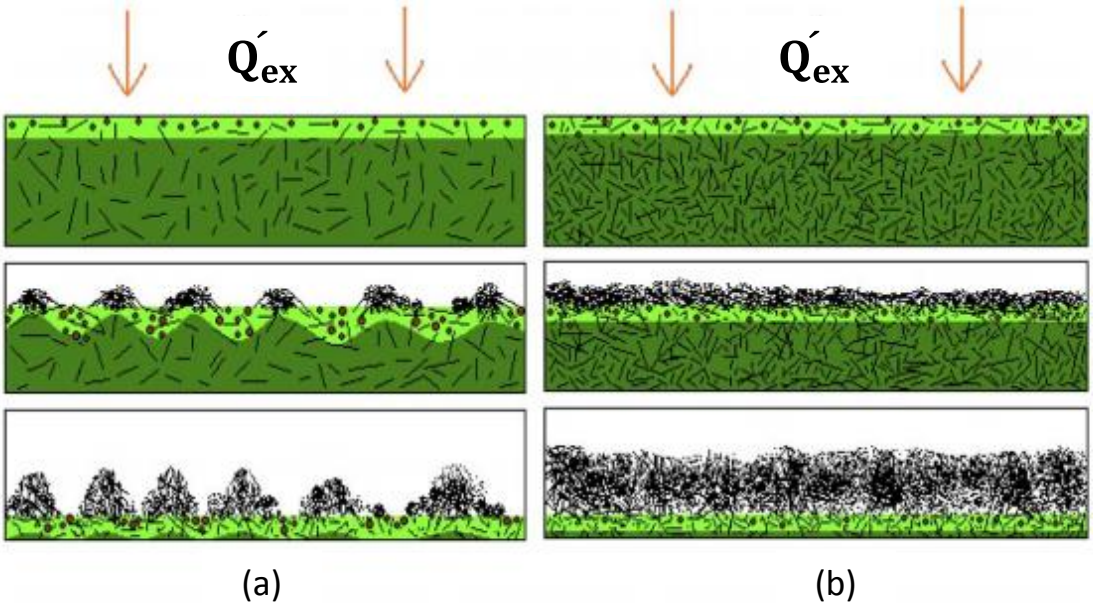

Figure 2.8. Schematic of the formation of islands (a) and of a network structured layer (b) in a carbon-nanotube-filled nanocomposite during burning. Light color represents a melt layer. Circles are bubbles. Adapted with permission.[137]

2.3 Layer-by-layer Assembly

As mentioned in Chapter 1, layer-by-layer assembly is an extremely popular thin film deposition technique used to create multilayered, multifunctional nanocoatings (typically < 1 μm thick). Although multilayer build-up of oppositely charged colloidal particles was first reported by Iler in 1966,[138] and layer-by-layer principles have been observed in the interim period, Decher, and collaborators established LbL as a versatile bottom-up processing technique in the 1990s.[139-142] Unlike the Langmuir-Blodgett assembly, which also has been widely employed to create ultrathin films,[143-145] layer-by-layer assembly is an ultra-low-cost technique capable of incorporating a myriad of building block components. Build-up of nanoscale films was first proposed as a dip-coating process where substrates are alternately exposed to oppositely charged solutions (see Figure 1.1). Figure 2.9 illustrates several methods of fabrication that have since been developed in an effort to enhance precision of deposited layers and decrease processing time (i.e., spraying[146-149] and spin-coating[150-151]). Individual layer thicknesses, which range from < 1 to 100 nm, can be tuned with the component-type,[43] the sequence of assembly,[152] or with altering conditions of the deposition mixture (such as ionic strength,[153-155] pH,[156-159] temperature,[160-162] counterion,[163-164] and deposition time[165]). Nano- and microscale control during fabrication of organic-inorganic multilayers creates a freedom of design to engineer customized nano-systems for a range of applications.

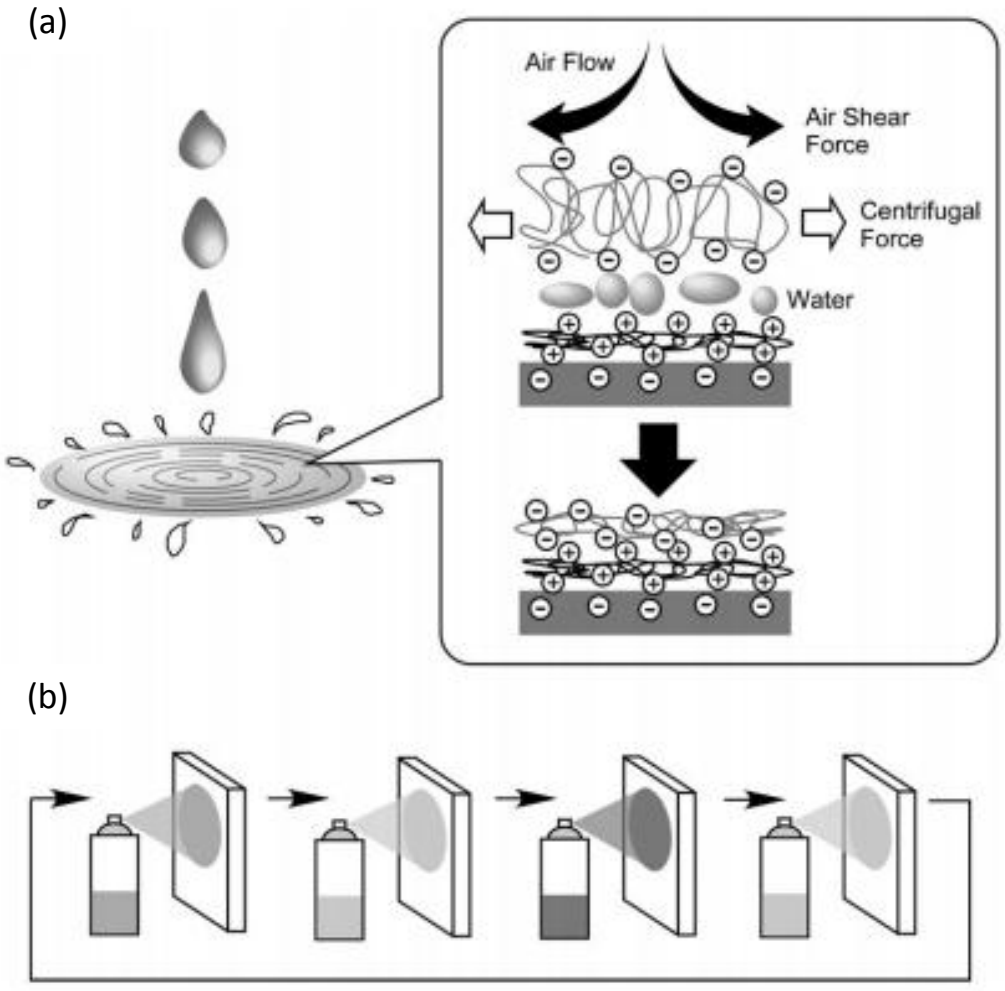

Figure 2.9. Illustrations of (a) spin-coating LbL assembly and (b)spraying LbL assembly. Reprinted with permission.[166]

Although layer-by-layer assembly has been used to created stratified multilayer architectures on flat two-dimensional substrates,[167-172] the LbL technique is highly suited to engineer nanocoatings to liquid-accessible surfaces (i.e., non-planar materials such as particles,[173-174] textiles,[51, 175-178] and open-celled foam[179]). Considerable efforts have been made to impart multifunctional properties to base substrates and to create core-shell

colloidal particles that could be used exclusively or as building blocks within a larger multilayer system.[180-181] As shown in Figure 2.10, once the nanoparticle template is removed, the well-organized multilayer shell becomes a capsule that can deliver a payload.[182] Crosslinked nanoporous polymer spheres of poly(acrylic acid) (PAA) and poly(allylamine hydrochloride) (PAH) were prepared on mesoporous silica particle templates, which were removed with dilute hydrofluoric acid.[183] Wang *et al.* used TEM and SEM to demonstrate the spherical shape is retained (the structure does not collapse when the nanoparticle is dissolved) and to characterize morphology and porosity of the core-shell particles (Figure 2.11). Similarly, multilayers can be deposited via layer-by-layer assembly onto templates (e.g., planar surfaces with cylindrical pores[184-185]) to fabricate nanotubes.[186] Self-standing tubular structures can be obtained once the template is selectively removed. Tube diameter and length are controlled by the membrane's pore dimension, while thickness and microstructure are variables controlled with experimental conditions and building constituents. Several investigations have focused on refining synthesized nanostructured materials for biomedical applications, such as drug delivery and gene therapy.[187-195] Biopolymers have been incorporated into multilayer assemblies in an effort to compatibilize implants and often simultaneously act as site specific drug delivery systems with tuned release profiles.[62, 196-199]

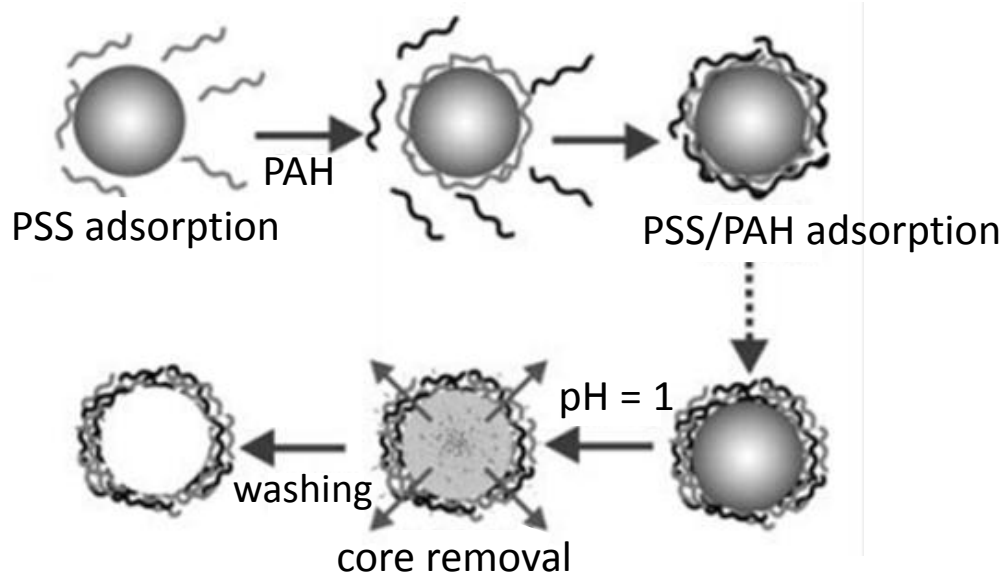

Figure 2.10. Schematic of polyelectrolyte multilayers deposited on capsules, and the subsequent hollow shell obtained after the removal of the nanoparticle template. Adapted with permission.[182]

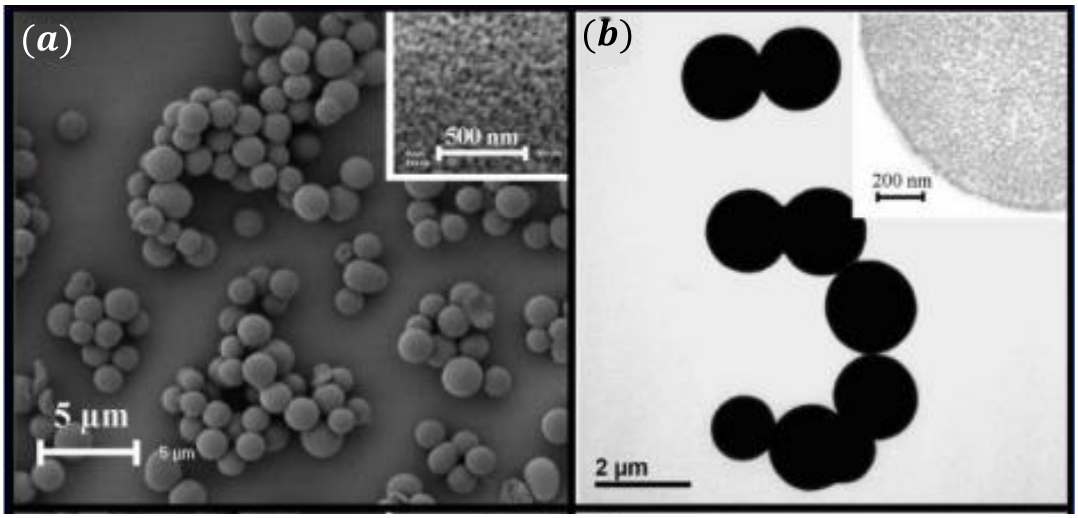

Figure 2.11. SEM (a) and TEM (b) images of cross-linked polyelectrolyte nanoporous spheres (NPS). Insets are higher magnification images. Inset in (b) is a microtomed thin section of the NPS. Adapted with permission.[200]

In addition to controlled drug release, LbL assembly has been used to create stimuli-responsive multilayer assemblies that undergo property changes from single or multiple signals for numerous applications such as sensing,[201-203] self-healing,[204] self-cleaning,[205] and switching of wetting.[206-207] A common strategy employed to create "smart coatings" is to incorporate non-covalent interactions within the assembly that can be stimulated through energetic or chemical changes. Rubner *et al.* showed that pH can be used to switch on sharp swelling and deswelling transitions of a thin film assembled from partially charged weak polyelectrolytes.[208] Nanopore sizes of 20-40 nm within the thin film produced after films, are immersed in pH 1.8, expand two orders of magnitude in diameter when exposed to pH 2.4 (Figure 2.12). Other stimuli responsive polymer thin films undergo structural change when subjected to stimulation such as light, heat, mechanical force, and temperature.[209] Lower critical solution temperature (LCST) polymers, such as poly(N-isopropylacrylamide) (PNIPAM), have been extensively used in biomedical applications to control cell adhesion to implant surfaces or trap and release small biomolecules.[210-213]

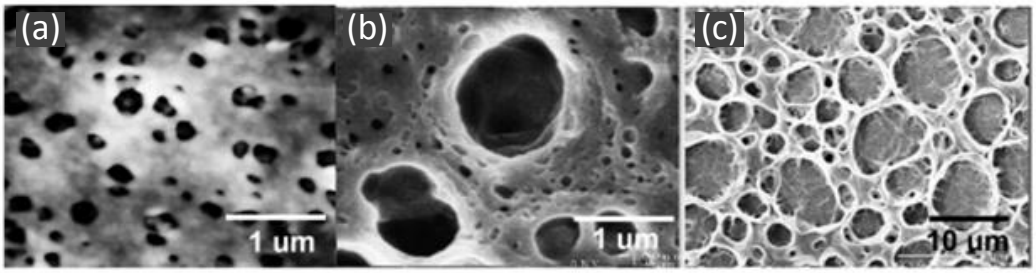

Figure 2.12. SEM images demonstrate pH-responsive properties of porous PAA-PAH thin films. Adapted with permission.[208]

Due to the high level of structural control, layer-by-layer assembly has become a popular technique used to fabricate clay-filled polymer multilayers for applications that require controlled transport and segregation of molecules.[214] The term 'nanobrick wall' was coined in 2010 for LbL-deposited polymer/clay nanocomposites because the microstructure was created through alternate adsorption of cationic polymeric mortar and highly oriented anionic clay platelets (i.e., nanobricks).[215] When deposited on a polyester substrate (Figure 2.13), a 51 nm film generates the lowest oxygen permeability ever reported for a polymer/clay composite ($\leq 5x10^{-22}$ $cm^3(STP)\cdot cm/(cm^2\cdot s\cdot Pa)$).[35] This barrier surpasses completely inorganic SiO_x (a commonly used barrier layer for plastic packaging films) by two orders of magnitude. As modeled by Cussler,[216] this layered structure creates a tortuous path through which gas molecules must travel. The diffusion path can be altered through precise tailoring of the thin film architecture (i.e., polymer mortar composition/thickness and clay spacing/packing/aspect ratio).[152, 217-218] Aside from their obvious promise for packaging applications, these polymer/silicate LbL multilayers are also being investigated for their mechanical properties[57, 219-221] and a variety of end-use applications such as diffusion barriers,[222-223] sensors,[224-225] drug delivery,[187, 226-228] and fire protection.[30, 229-231]

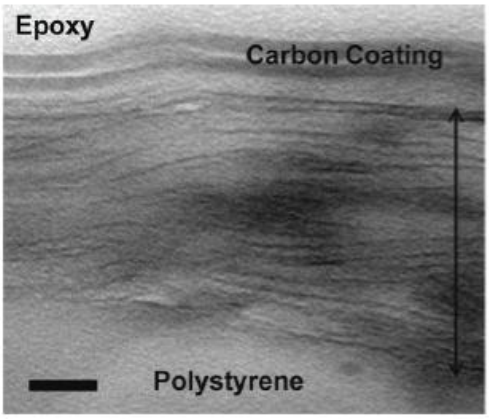

Figure 2.13. TEM cross-section image of a five QL thin film deposited on polystyrene. The scale bar is 20 nm and the double arrow spans the film's 80 nm thickness. Reprinted with permission.[35]

2.3.1 Layer-by-layer Flame Retardant Thin Films

Inspiration for applying these nanobrick walls as flame retardant (FR) coatings to polyurethane foam came from the final stage of a proposed flame suppression mechanism in melt-mixed ethylene-vinyl acetate (EVA) polymer-MMT clay,[28] which depicts a physical barrier created from the build-up of impermeable flakes and carbonized char. It is believed that ordered clay-polymer layers only on the surface can immediately act as a heat shield and interfere with the combustion cycle. This would simultaneously eliminate engineering concerns associated with silicate dispersion within the material that adversely affect mechanical behavior. Polymer-clay layer-by-layer assembled flame resistant coatings, which are capable of lowering the inherent flammability of cotton, were recently demonstrated as a novel alternative to conventional FR coating techniques.[30, 232] Upon degradation, 20 bilayers (BL) of this nanobrick wall multilayer (approximately 4.4 wt% addition to the original weight of the

fabric), composed of polymeric mortar that binds the clay platelets (or bricks) within the assembly, formed a thermal shielding residue, shown in Figure 2.14. This protective shell was primarily composed of montmorillonite (MMT) clay, pyrolyzed branched polyethyleneimine (PEI) and dehydrated cellulose, which retained the weave structure of the coated cotton fabric after vertical flame testing.

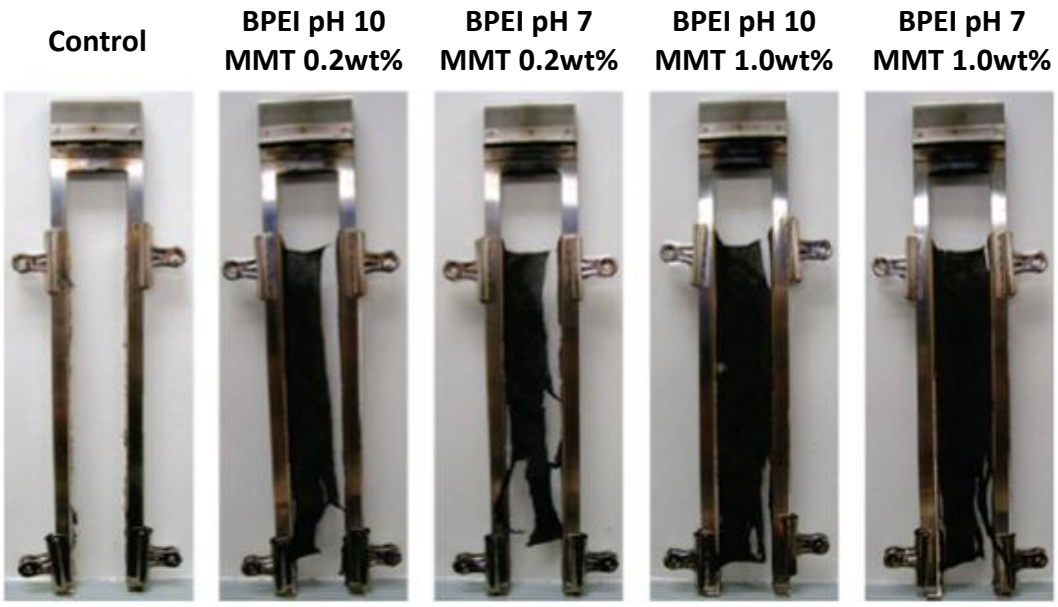

Figure 2.14. Images of uncoated and 20 BL-coated cotton fabrics following the vertical flame test. Adapted with permission.[30]

Shortly after this passive polymer-clay nanocoating was evaluated for improved cotton flame suppression, other fire retarding ingredients and mechanisms were investigated with this same concept for multiple substrates.[34, 58, 229, 231, 233-242] Intumescing nanocoatings deposited on fabric via layer-by-layer (LbL) assembly have recently demonstrated this protective bubbling phenomenon on the microscale.[234-235, 243]

Drawing inspiration from traditional intumescing systems,[244] these LbL-based flame retardant nanocoatings typically contain a carbon donor, an acid source, and a blowing agent. For example, 20 bilayers of polyallylamine/poly(phosphate sodium salt) (PAAm/PSP), deposited by alternately immersing the cotton fabric into oppositely charged solutions, resulted in a thin layer (~500 nm) that three dimensionally coats individual fibers and stops flame spread in a vertical flame test (Figure 2.15).[234] This work represents one of the most effective layer-by-layer coatings, and has led to the successful application of intumescing recipes on other fabric types (ramie,[243] polyethylene terephthalate,[236] polyethylene terephthalate-cotton blends,[239] nylon,[231] etc.). Numerous other LbL-applied flame retardant (non-intumescing) recipes, containing diverse building blocks, such as DNA[245] and carbon nanotubes,[16] have also shown good FR behavior by reducing the flammability of the base substrate (e.g., cotton fabric,[30, 232-233, 237, 240, 246-249] polylactic acid film,[229] polyurethane foam,[34, 58, 238, 241] polycarbonate film,[246] etc.).

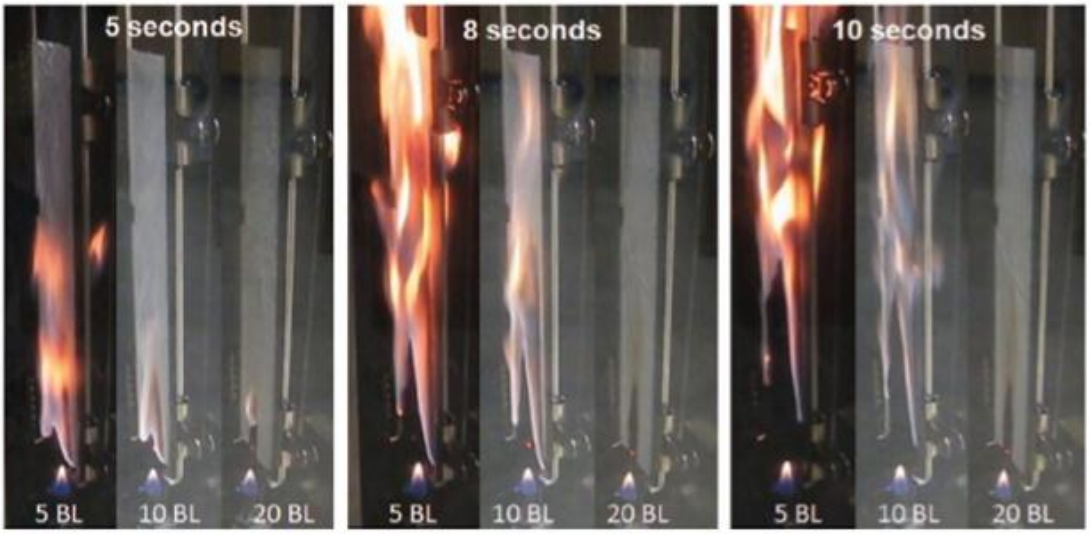

Figure 2.15. Images during vertical flame testing recorded at 5, 8, and 10 s. Reprinted with permission.[234]

CHAPTER III

PHOSPHOROUS-FILLED NANOBRICK WALL MULTILAYER THIN FILM ELIMINATE POLYURETHANE MELT DRIPPING AND REDUCES HEAT RELEASE ASSOCIATED WITH FIRE*

3.1 Introduction

In this chapter, the mortar that binds MMT clay bricks into the nanocoating deposited on polyurethane foam is composed of two polymers, poly(allylamine hydrochloride) (PAH) and PSP, in an effort to improve the heat barrier produced with MMT clay and a single polymer.[58] A PEI/MMT/poly(acrylic acid) trilayer system was previously shown to be an effective approach to rapidly deposit high clay-loaded nanocoatings on polyurethane, which reduced peak heat release rate, total heat release rate and total burning time.[34] In general, these nanobrick wall assemblies protect underlying substrates via the condensed phase mechanism.[250] Until a ceramic-like shell is constructed to break the pyrolysis cycle, polymeric mortar burns out between the platelets and refuels the fire. Using PSP/PAH as the mortar that binds MMT platelets should improve the thermally insulating physical barrier that forms when the heating source is applied. This concept is inspired by the intumescing all-polymer coatings used

*Reprinted with permission from Cain, A. A.; Murray, S.; Holder, K. M.; Nolen, C. R.; Grunlan, J. C., Phosphorous-filled Nanobrick Wall Multilayer Thin Film Eliminates Polyurethane Melt Dripping and Reduces Heat Release Associated with Fire. *Polymer Degradation and Stability* **2013**, *98*, 2645-2652**.** © 2013 Elsevier.

to arrest fire propagation on cotton fabric[234-235] and the synergistic interaction between phosphorous molecules and MMT.[229]

The PSP/PAH/MMT trilayer (TL) assembly produces a swollen protective shell structure around foam cell walls upon exposure to a butane torch. Unlike control polyurethane samples whose cellular structure combusts and flows into a flammable liquid, foam samples retain their shape, size and a large portion of pristine, unburned foam following this torch test. A 4 TL nanocoating, that is less than 20 nm thick and adds less than 3.0 wt% to open-celled polyurethane foam, reduces peak heat release rate (pkHRR) by more than a factor of two in a cone calorimeter test. This unique nanobrick wall coating system combines two common flame-retarding components (thermally shielding clay and phosphorous) into a single coating and offers an environmentally-benign alternative to FR treatments that are currently being scrutinized by various governmental agencies worldwide.

3.2 Experimental

3.2.1 Materials

Natural sodium montmorillonite (trade name Cloisite Na+) clay, provided by Southern Clay Products, Inc. (Gonzales, TX), was used as received. These layered silicates have an average aspect ratio of 200, a reported density of 2.86 g/cm^3,[251] an observed cationic exchange capacity of 0.926 meq/g,[252] and a negative surface charge in aqueous solution. Cationic poly(allylamine hydrochloride) (molecular weight, M =

120~200 kg/mol) was purchased from Polysciences, Inc. (Warrington, PA) and used as received. Poly(phosphate sodium salt) (also known as sodium hexametaphosphate; crystalline, +200 mesh, 96%), poly(acrylic acid) (PAA) solution (M = 100,000 g/mol, 35 wt% in water), sodium hydroxide pellets (anhydrous) (reagent grade, ≥ 98%), and nitric acid (red, fuming, HNO_3 > 90%) were purchased from Sigma-Aldrich (Milwaukee, WI). Polyethylene terephthalate (Melinex ST505 available at Tekra Corp., New Berlin, WI) film, with a thickness of 179 μm, was the substrate used for transmission electron microscopy imaging and oxygen transmission rate testing. Under dry conditions, this grade of PET film has an approximate OTR of 8.6 cc/(m^2 · day · atm). Layers were incrementally deposited on 5 MHz gold-electrode quartz crystals (Maxtek, Inc., Cypress, CA) to obtain mass deposited per layer using a quartz crystal microbalance. P-doped, single side polished (1 0 0) silicon wafers (University Wafer, South Boston, MA), with a thickness of 500 μm, were used as substrates for ellipsometric thickness measurements. Polyether-based polyurethane foams with densities of 1.75 lbs/ft were purchased from Future Foam (High Point, NC). Foam type 1850A contained 18.6 wt% flame-retardant additives, while 1850 did not.

3.2.2 Layer-by-Layer Deposition

All aqueous solutions were prepared with 18.2 MΩ deionized water (Direct-Q 5 Ultrapure Water System). Individual solutions containing 0.1 wt% PAH, 1.0 wt% PAH, 1.0 wt% PAA, 2.0 wt% PSP or 1.0 wt% MMT were rolled overnight to allow for full dissolution. MMT was used at an unaltered pH of approximately 9.9. Prior to deposition,

1.0 wt% PAA was altered from its natural pH of ~2.7 to a pH of 2.0 using 2.0 M HNO_3, while the pH of aqueous solutions of 0.1 wt% PAH (~3.5), 2.0 wt% PSP (~6.9), and 1.0 wt% PAH (~3.5) were adjusted to a pH of 7.0 using 1.0 M NaOH. LbL assemblies were fabricated on a given substrate in ambient conditions through an alternating deposition process in which the substrate was dipped into three aqueous solutions in the order of $(PSP/PAH/MMT)_n$, where n denotes the number trilayers deposited, as depicted in Figure 3.1.

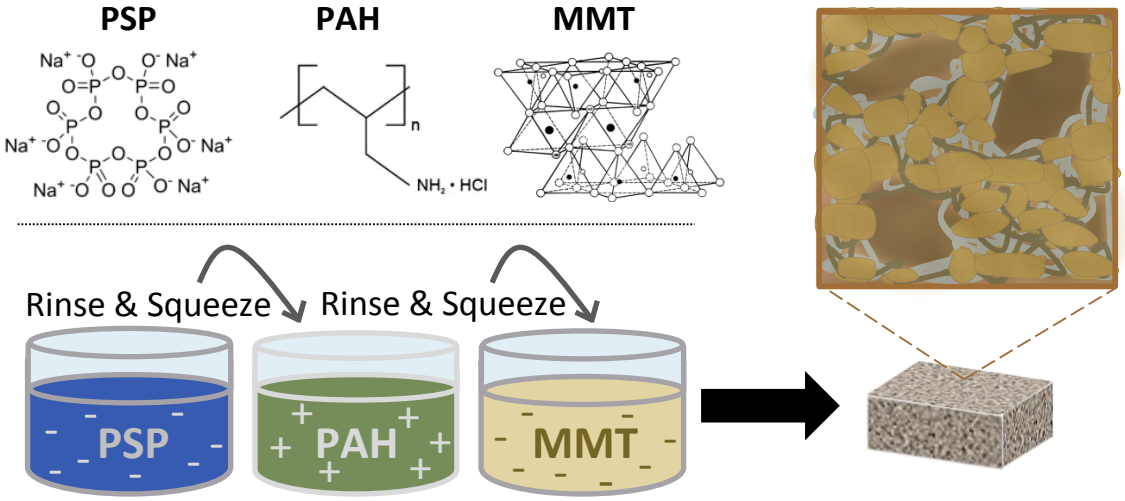

Figure 3.1. Schematic of the LbL deposition process and resulting nanobrick wall structure from the sequential adsorption of PSP, PAH, and MMT on flexible polyurethane foam.

In all cases, this TL nanocoating was deposited on a negatively-charged substrate, either due to an inherent negative charge or with surface manipulation by corona treatment (PET), plasma treatment (Ti/Al QCM crystal) or piranha solution

(silicon wafers). A negative charge was imparted on the PET surfaces with a BD-20C corona treater from Electro-Technic Products, Inc. (Chicago, IL). Prior to surface alteration, PET film substrates were cleaned with methanol and deionized water. QCM crystals were cleaned for 5 min in an enriched plasma environment with a Harrick Plasma treater (Ithaca, NY). Silicon wafers were cleaned for 30 min using bath sonication in a piranha solution,[253] and subsequently rinsed in deionized water, acetone and water, and dried with filtered air prior to use. ***Caution!*** *Piranha solution reacts violently with organic materials and should be handled with extreme caution.*

A primer layer of 0.1 wt% PAH readily adheres to the inherent negative charge on flat two-dimensional substrates. Polyurethane substrates were soaked in 1.0 wt% PAA for 30 s prior to the 0.1 wt% PAH primer to induce a negative surface charge on the foam. In acidic conditions (pH 2), the carboxylic acid groups on PAA polymer chains, which remain predominately protonated, attach to the PU surface through hydrogen bonding and deposit in a coiled, globular manner. The deposition time for the primer PAH and the first dip into PSP was 5 min, while all subsequent depositions were for 1 min. The difference in deposition time is to diminish island growth, a common issue found in the initial layers of LbL coatings. Each deposition was preceded by the substrate being rinsed with deionized water and wrung out (flat, two-dimensional substrates were dried with filtered air) to remove excess polymer and/or platelets, which typically establishes charge reversal on the surface and low surface roughness. All substrates were stored in a dry box for a minimum of 18 h prior to testing.

3.2.3 Characterization of Film Growth and Properties

Film thicknesses were measured using a Model alpha-SE Ellipsometer (J.A. Woollman Co., Inc., Lincoln, NE) with a 632.8 nm laser. Individual layers were deposited on Ti/Au crystals and the mass deposition was monitored using a QCM (Maxtexk Inc., Cypress, CA) in order to obtain the growth of individual layers within the thin film and to calculate total film density. Control and coated foams were exposed to the direct flame of a butane micro hand torch (Model ST2200, Benzomatic, Huntersville, NC) for 10 s (the approximate blue flame temperature is 2400 °F) to provide a visual demonstration of coating effectiveness. Cone calorimetry was performed at the National Institute of Standards and Technology (NIST), using a dual cone calorimeter at a heat flux of 35 kW/m^2, with an exhaust flow of 24 L/s, operating under ASTM standardized procedures (ASTM E-1354-07). The standard uncertainty is 5% in HRR and 2 s in time. A 10 x 10 x 2.5 cm sample was placed in a pan constructed from aluminum foil. Oxygen transmission rate (OTR) testing was performed by MOCON (Minneapolis, MN), in accordance with ASTM D-3985, using an Oxtran 2/21ML instrument at 0% RH. Films deposited on PET for OTR testing were placed in an oven at 70˚C for 15 min immediately following deposition to remove excess moisture in the film.

3.2.4 Microscopic Imaging

A 10 TL thin film deposited on a 179 μm PET substrate was coated with a protective layer of carbon and embedded in an epoxy resin of similar hardness. The epoxy resin is a 2:1:1 mole ratio of Araldite 502* (modified bisphenol A resin), Quetol

651* (ethylene glycol diglycidyl ether), and dodecenyl succinic anhydride hardener*. 0.25 mL of benxyldimethylamine accelerator* and 0.1 mL of Dow Corning Silane were added per 10 g of total epoxy weight. All "*" components were purchased from Electron Microscopy Sciences (Hatfield, PA). After curing overnight, thin gold sections were trimmed (< 100 nm) using a microtome and were picked up on Formvar-coated 150 mesh nickel grids. Thin film cross-sections were imaged with a JEOL 1200 EX TEM (JEOL USA Inc., Peabody, MA) at an operating voltage of 100 kV and calibrated magnifications. Coated thin films, deposited on PU substrates, were mounted on aluminum imaging stubs and thinly sputter coated with 5 nm of platinum/palladium (Pt/Pd) alloy in preparation for surface images that were acquired with a field-emission scanning electron microscope (FESEM) (Model JSM-7500F, JEOL; Tokyo, Japan). Energy-dispersive x-ray spectroscopy (EDX) digital images and elemental spectra were acquired on the FESEM, and samples were not sputter coated with Pt/Pd.

3.3 Results and Discussion

3.3.1 Film Growth and Microstructure

Figure 3.2 shows that sequential deposition of anionic poly(phosphate sodium salt), cationic poly(allylamine hydrochloride) and montmorillonite clay results in linear assembly growth. Deposition onto the substrates for these measurements was preceded

by a primer layer of cationic 0.1 wt% PAH to promote strong adhesion. The polymeric components of this trilayer system are similar to those that comprised the first intumescent all-polymer coating used to make anti-flammable cotton fabric.[234] The polyelectrolyte pair, PSP/PAAm, initially grows exponentially until islands coalesce (at ~10 BL) after which, linear growth is observed. PAH is the same water-soluble cationic polyelectrolyte, but it is in its salt form with chlorine counter ions. Both electrostatic attraction and hydrogen-bonding allow this trilayer assembly to grow, but it is notably thinner than the PSP/PAAm BL system because MMT interferes with polyelectrolyte build-up.[34, 234] Linear growth of this trilayer sequence is independently confirmed by both quartz crystal microbalance (QCM) and ellipsometry (Figure 3.2). The overall weight and weight of individual layers measured with QCM provides thin film density and composition. This novel trilayer sequence generates a thin film with a density of 1.82 g/cm^3 that is composed of 7.5 wt% PSP, 5.4 wt% PAH and 87.1 wt% MMT.

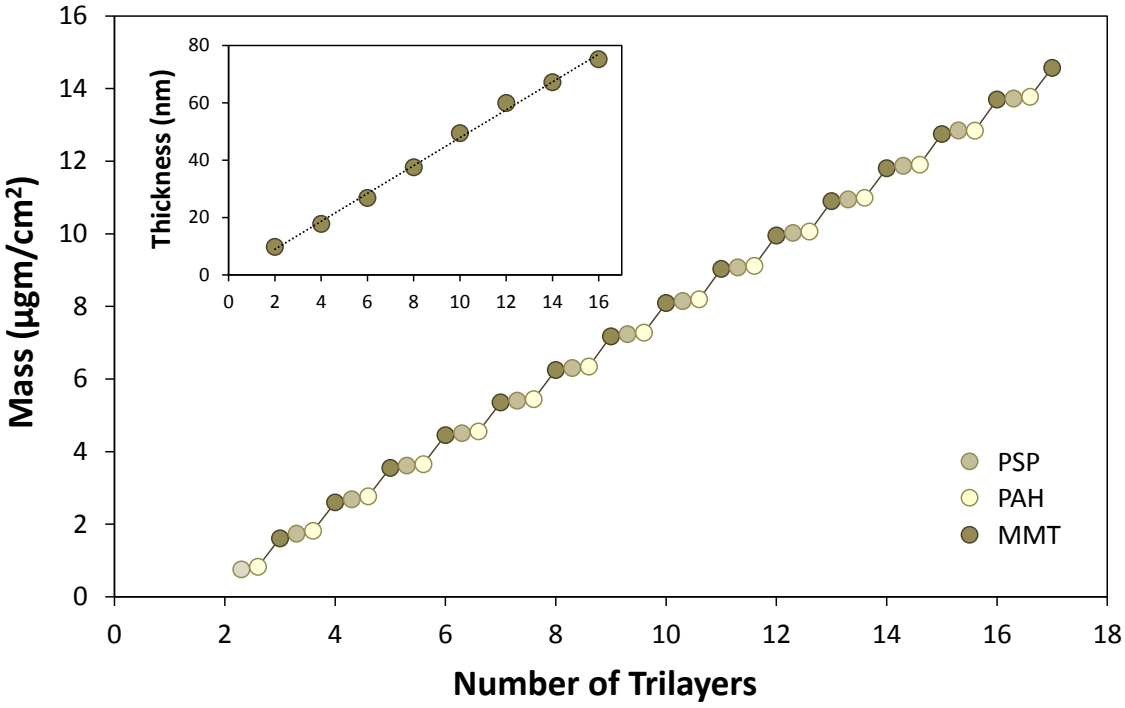

Figure 3.2. Mass as a function of the number of trilayers deposited. Individual layer mass is shown between 3 and 16 TL. The first layer deposited was PAH followed by sequential dips in PSP/PAH/MMT. The inset shows ellipsometric film thickness as a function of deposited TL.

TEM images of carbon coated 10 TL assemblies highlight the nanobrick wall architecture of these 56 nm fire protection coatings, as shown in Figure 3.3. Due to the difference in electron density between this thin film (dark lines represent clay platelets and lighter areas between are polymeric pairs), the cross section is able to highlight the assembly's unique ability to adsorb the largest dimension of the clay platelet parallel to the substrate. High clay loading and parallel plate adsorption are key parameters of this nanocoating's ability to retain the original foam shape and size after direct exposure to the flame from a butane torch for 10 s.

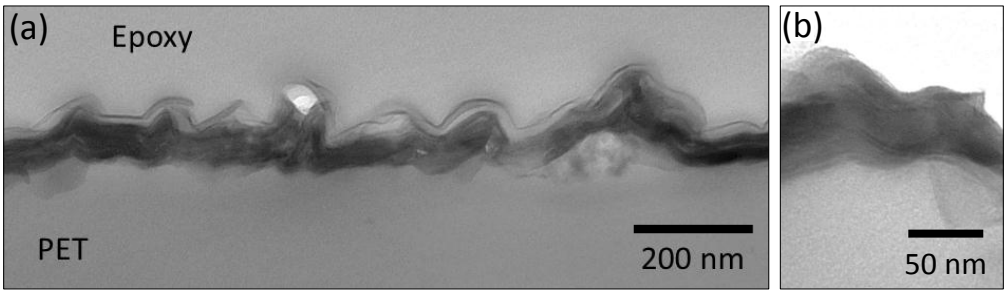

Figure 3.3. Transmission electron micrographs of cross-sections of a 10 TL assembly of PSP/PAH/MMT at low magnification (a) and high magnification (b).

3.3.2 Flame-retardant Behavior

Fire retardant behavior was evaluated as a function of trilayers deposited on open-celled flexible ether-based polyurethane foam. All foam samples were thoroughly rinsed in deionized water, dried in a 70°C oven and stored in a dry box prior to testing. Foams were weighed before and after coating to obtain weight addition from the nanocoating (reported as % add-on). The SEM images in Figure 3.4 reveal the complex, irregular architecture of control foams, which have a reported 50-70% open-celled structure. These micrographs also highlight the ability of the 10 TL coatings to conformally deposit onto polyurethane cell walls without altering the foam porosity. Imaged sections are cut from the center of coated foams. None of the coated foam contained FR additives in its inherent structure.

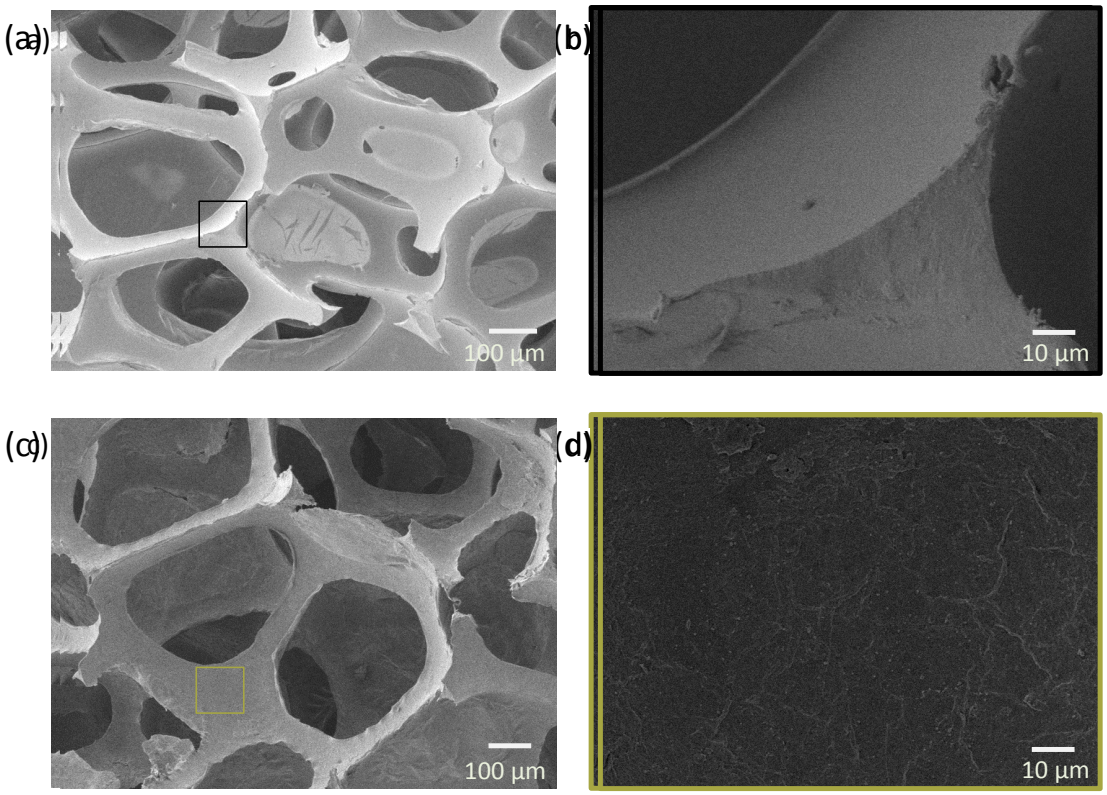

Figure 3.4. Scanning electron micrographs of uncoated polyurethane foam (a,b) and foam coated with 10 TL of PSP/PAH/MMT (c,d).

Coated and control PU foam samples were placed on top of a metal grating inside a hood, approximately 25.4 cm above other flammable materials (e.g., strips of paper towels, cotton, etc.), and ignited with a butane torch for 10 s. The flame of the torch was directed centrally and perpendicular to one of the sidewalls of the foam. Uncoated foams, with and without FR, withered away from the torch flame and melted instantly. Drips of melted polymer fell below the grating, forming a melted pool of ignitable material (flammable articles underneath ignited in some tests). Control foam with FR additives self-extinguished when the flame from the butane torch was removed.

All coated foams prevented melt dripping by forming a thin black and gray protective shell that shielded the underlying foam. Similar color variations have been observed in intumescing systems and are visual evidence of a heat gradient across the PU surface.[254]

All coated foams retained their original shape after flame exposure, but displayed a scorched area between pristine and charred foam, as shown in Figure 3.5. These yellow areas of discoloration are believed to be a consequence of both oxidative and thermal decomposition of the flexible foam.[80] Higher magnification reveals the effects of the thermal gradient on the PU foam samples. The protective armor is swollen and appears to have burst open in some areas (note the circled portion in the high magnification image of Figure 3.5), while white foam underneath the scorched area appears to have been unaffected. Individual clay platelets can easily be distinguished by their aspect ratio and grainy appearance. Energy-dispersive X-ray spectroscopy measurements (EDX) identified elemental phosphorous in the post-burn residue of 10 TL coated samples, as shown in Figure 3.6d. Phosphorous was not detected in control PU samples (Figure 3.6b), which indicates PSP was deposited in the coating and phosphorous acted in the condensed.[81] Coated polyurethane foam (post-burn) displayed additional peaks of sodium, aluminum and silica (representing MMT), and phosphorous (representing PSP), as shown in Figure 3.6d. Lower elemental identification peaks of phosphorous and platinum overlap, so sections of control and burned 10 TL coated foams were evaluated without the 5 nm conductive platinum/palladium sputter coating.

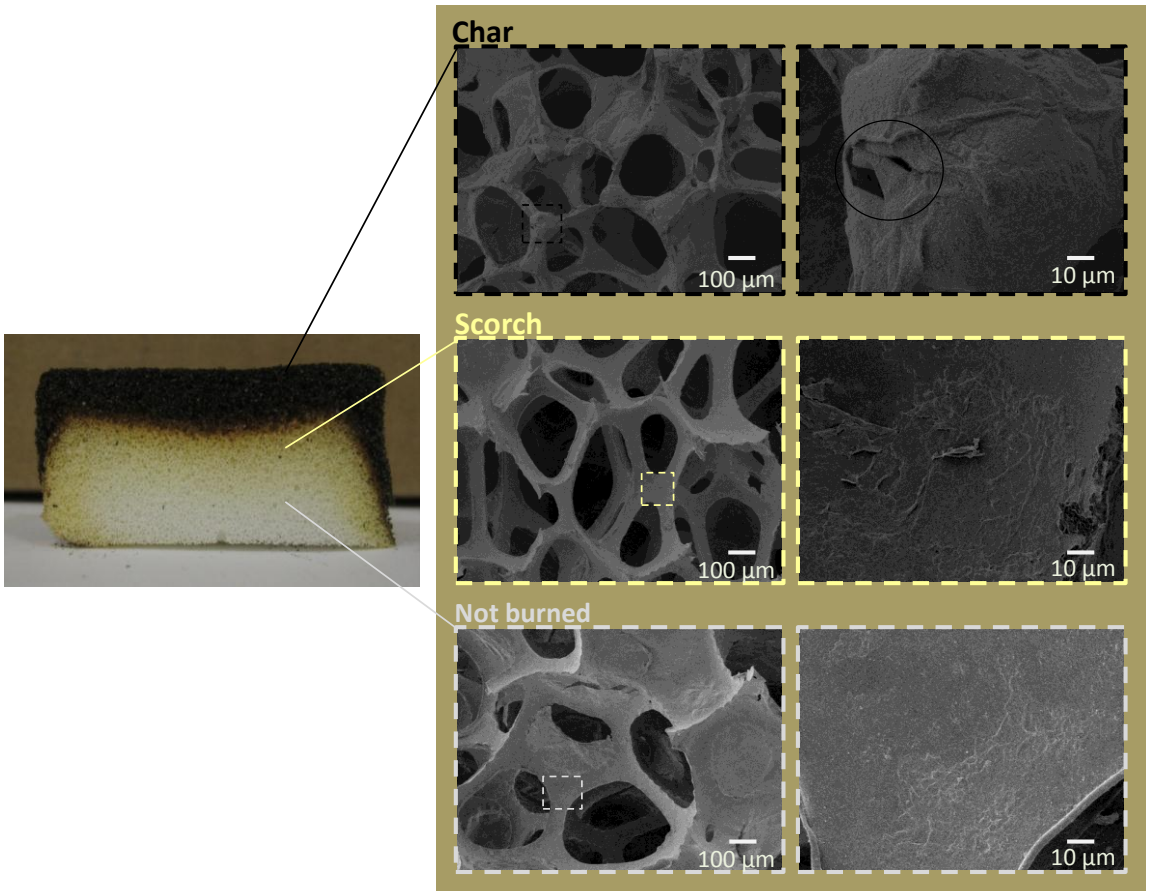

Figure 3.5. SEM micrographs highlight black/gray residue (black box), scorched (yellow box) and unburned/pristine (grey box) areas of foam coated with 10 TL of PSP/PAH/MMT following 10 s of direct exposure to the flame from a butane torch.

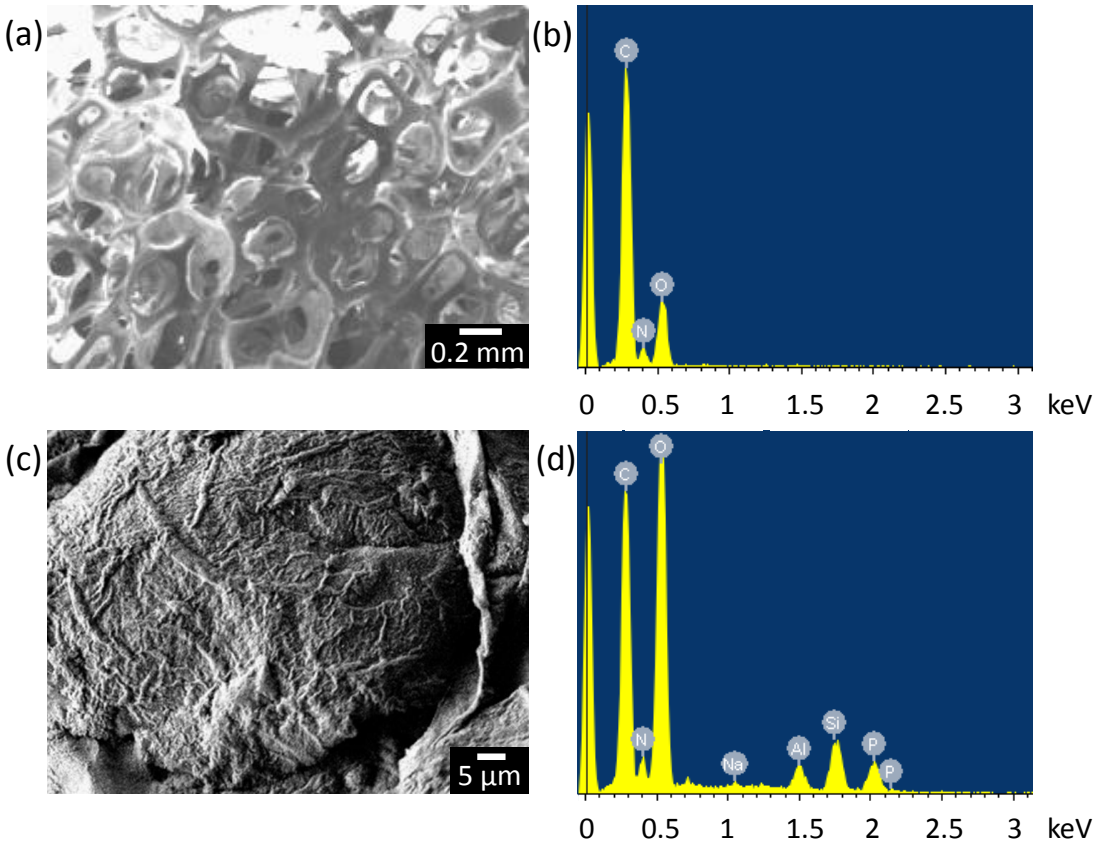

Figure 3.6. SEM images of control foam (a) and black/gray residue of 10 TL coated foam (c) with corresponding EDX elemental spectra (b and d, respectively).

Control and coated foam samples were also tested with standard cone calorimetry (ASTM E-1354-07) in an effort to quantitatively assess the thermal barrier properties of this nanobrick wall thin film.[255] 4, 6, 8, and 10 TL nanocoatings were evaluated and compared to control foams, with and without commercial FR additives, which contain a synergistic blend of solid and liquid FR (18.6 wt% of the foam). Cone calorimetry tests expose a horizontally oriented 100 cm-square specimen (2.5 cm thick) to a constant external heat flux of 35 kW/m^2. Heat release rate, which is a measure of a material's flammability,[256] is plotted as a function of time in effort to directly compare and

characterize the effect of the coatings on the foam. For clarity, data for 6 and 8 TL coated foams were not included in Figure 3.7.

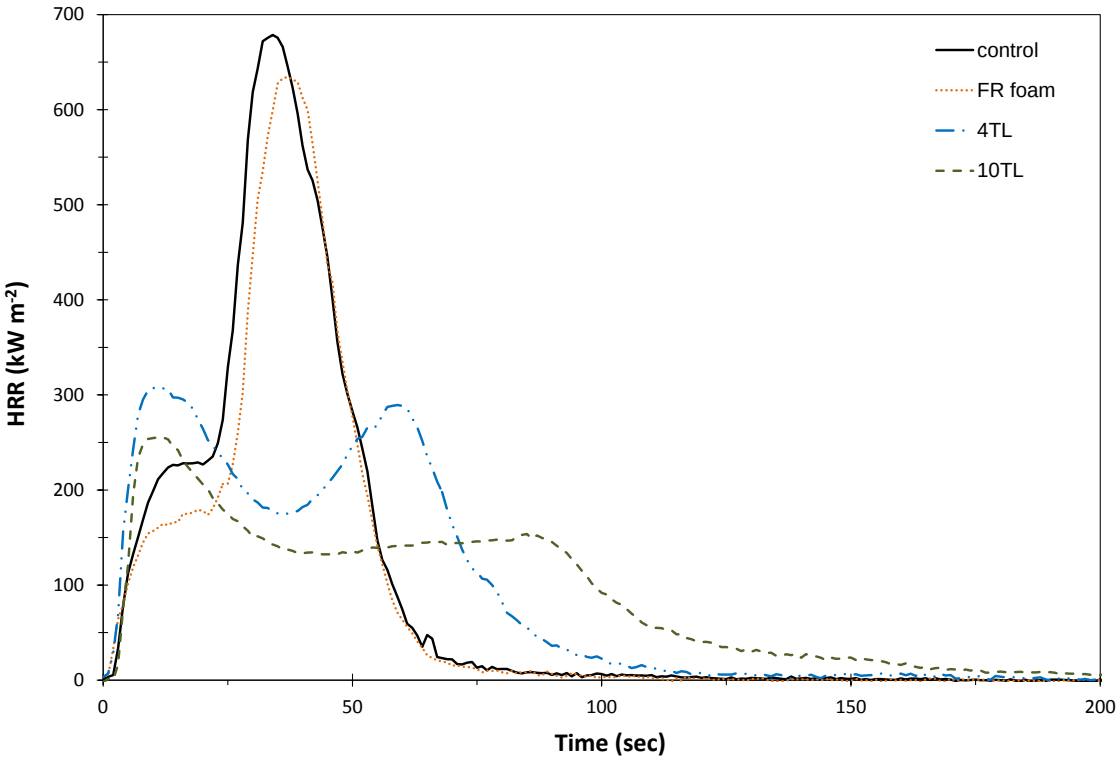

Figure 3.7. Heat release rate as a function of time (during cone calorimeter testing) for uncoated control foam with and without FR additives, and 4 and 10 TL coated foam without inherent FR additives.

After the control foam is ignited, heat quickly transfers and matures into a fully developed fire, which causes the foam matrix to collapse into a polymeric liquid. Heat release rate values are indicative of both isocyanate/polyol composition and the highly flammable nature of the components. After the rapid rise up to the second larger heat release peak for the control foam, decay of the curve swiftly ensues due to the material's quick transition into combustible volatiles. Coated foams generate a higher initial HRR

than both control foams due to the presence of polymer within the nanobrick wall. This increase in HR may also be a result of the high clay loading. It has been suggested that catalytic sites on MMT initially promote combustion until a protective shell is formed .[28] It is beneficial for the coating's degradation temperature to be below the PU substrate to create the insulating barrier. Minimizing the contribution of polyurethane to combustion will reduce the fire threat. Thermal shielding increases with additional coating layers. It should be noted that all coated foams exhibit reduced pkHRR of at least 54%, retain their shape, and do not exhibit the traditional two-step polyurethane decomposition behavior.[257] Whereas 4 TL are able to significantly diminish the second pkHRR, 10 TL coatings completely eliminate the peak and largely extend the time it takes for complete combustion to occur. Table 3.1 shows 10 TL coatings reduce both the pkHRR and avg HRR more than 62%, whereas the control foam with flame retardant additives only reduces the pkHRR and avg HRR by 6.5% and 10.9%, respectively. There is no statistical significance in the decrease of total heat evolved (i.e., area under the HR curve) for both additive and nanocoating FR systems.

Table 3.1. Cone calorimeter results for polyurethane foam samples.[a]

Sample	Weight Gain [%]	pkHRR [kW/m^2]	avg HRR [kW/m^2]	Total HR [MJ/m^2]	Eff Hc [MJ/kg]	Mass Loss [%]
control		679	301	19.6	28.1	95.3
FR foam		634	268	17.2	23.5	96.6
4TL	2.86	307	171	18.0	27.5	88.0
6TL	4.99	298	140	17.7	27.6	85.8
8TL	6.45	263	142	17.0	25.6	88.8
10TL	9.78	255	112	17.3	27.1	82.8

[a]HRR = heat release rate; pkHRR = peak heat release rate; Eff Hc = effective heat of combustion.

All foams were exposed to a constant external heat flux throughout the duration of cone calorimetry testing, which simulates a scenario in which a material's flammability can be evaluated based on radiant ignition. The resulting HRR data suggests that the flame retarding mechanisms of commercial FR additives and the trilayer nanocoating differ tremendously. The PU control foam with 18.6 wt% additive (an apparent blend of liquid brominated FR and unidentified solid FR) appears to operate predominately in the gas-phase. Flame inhibition in the gas-phase, in which halogen (or hydrogen halide) atoms interrupt chain branching by consuming free radicals,[89] can be indicated with a reduction of effective heat of combustion (Eff Hc), which is a measurement that only reflects the heat of combustion of the volatiles.[258] Though rarely demonstrated experimentally, several theories suggest that a physical effect of halogen-FRs can yield a reduced HRR.[259-260] Although both approaches complement each other, the 19.8% decrease in Eff Hc shown in the cone calorimetry data only provides evidence for radical trap theory. As previously noted, the additive-containing control foam did not effectively decrease pk- or avg HRR. Although halogen compounds affect the matrix material's propensity to ignite by inhibiting combustion of free radicals and diluting combustible products, their effectiveness depends on concentration and thermal stability.[81, 261] As shown in Figure 3.7, once the flame-retarding compounds are consumed, the heat release rate of commercial FR-containing foam is similar to that of the control thermoset foam without additives.

Layered-silicate polymer nanocomposites, on the other hand, traditionally create a physical barrier of inorganic and carbonaceous material that separates the heat source

from the object to be protected.[262] This trilayer nanocoating is a uniquely layered system that pairs thermally shielding MMT clay platelets with a salt that contains an average of 6 P atoms per oligomeric ring (the latter component can operate in multiple phases due to synergistic effects).[263] Motivation for this particular formula stems from the notion of engineering the polymeric mortar to actively participate in reducing polyurethane's fire hazard rather than simply binding clay bricks within the assembly. PSP/PAH polymeric mortar is analogous to the intumescing polyelectrolyte pair used to create the intumescent 20 BL coating of PAAm and PSP that extinguished the flame on cotton fabric during vertical flame testing.[234] PAH is used in place of PAAm in the present trilayer. It is reasonable to suppose that the nanobrick wall assembly on polyurethane cell walls transforms into a thermal shield upon the addition of heat. PSP acts as an acid source which breaks PAH down into smaller compounds. The amine groups degrade and form nitrogen gas that could serve as blowing agents to swell the P/MMT-based barrier. Due to the high loading of clay within the nanobrick wall assembly (> 87 wt%), it is likely that small gaseous bubbles become trapped within the barrier layers rather than migrating through the clay to the surface and coalescing to produce the larger bubbles often observed in intumescent char.[102, 234-235]

Butane torch and cone calorimetry burn scenarios differ greatly and thus yield different residue. Unlike torch testing, where PU foams are placed in direct contact with a butane torch for 10 s, cone calorimeter samples are horizontally situated under a cone heater ignited by a spark igniter) and irradiated at a desired heat flux.[264] Dehydration of the PU walls in combination with degradation of the polymeric components produces

gases in between the clay platelets that cause the coating to slightly swell when exposed to the butane torch (Figure 3.4). SEM micrographs of 4 and 10 TL coated foams following cone testing (Figure 3.8) reveal agglomerations scattered randomly over the cross-sections of P/MMT-based residues (composition is confirmed with an elemental analysis scan (see Figure 3.9). Elemental analysis reveals peaks of C, O, P, Si and Al across the surface (N peaks are present in most elemental spectra for both sample types; see Figure 3.6). It should be noted that some areas of the imaged cone calorimetry residue were not as densely populated with P/O agglomerations. In both scenarios, this protective barrier slows down PU pyrolysis and reduces evolution of mass into the gas-phase that would otherwise feed the fire.[103] Simultaneously, thermal penetration of heat is also diminished. Progressively diminished pkHRRs with increasing TL demonstrates this behavior for coated foam. The decrease in external heat flux and impedance of polymer pyrolysis during cone calorimetry testing suggests these protective layers could potentially reduce the production and escape of toxic, volatile gases.[250, 262]

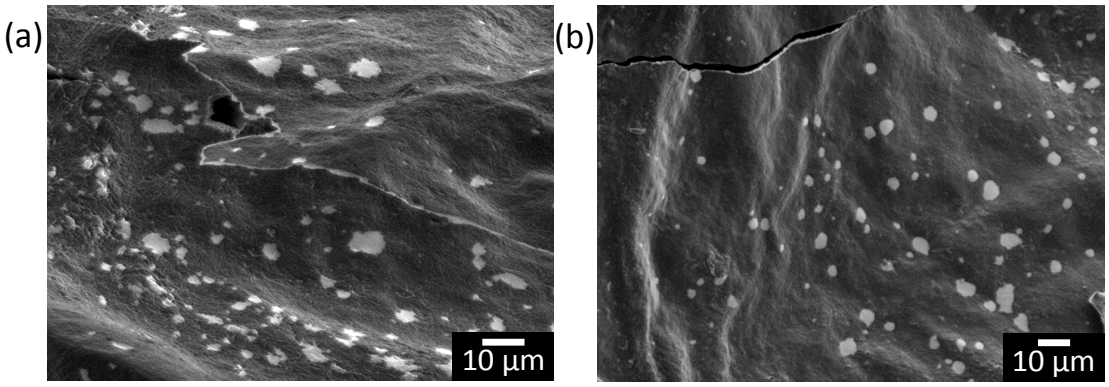

Figure 3.8. SEM micrographs of cross-sections of 4 TL (a) and 10 TL (b) coated foams post cone calorimetry testing. Note, lighter spots scattered across micrograph are P/O agglomerations.

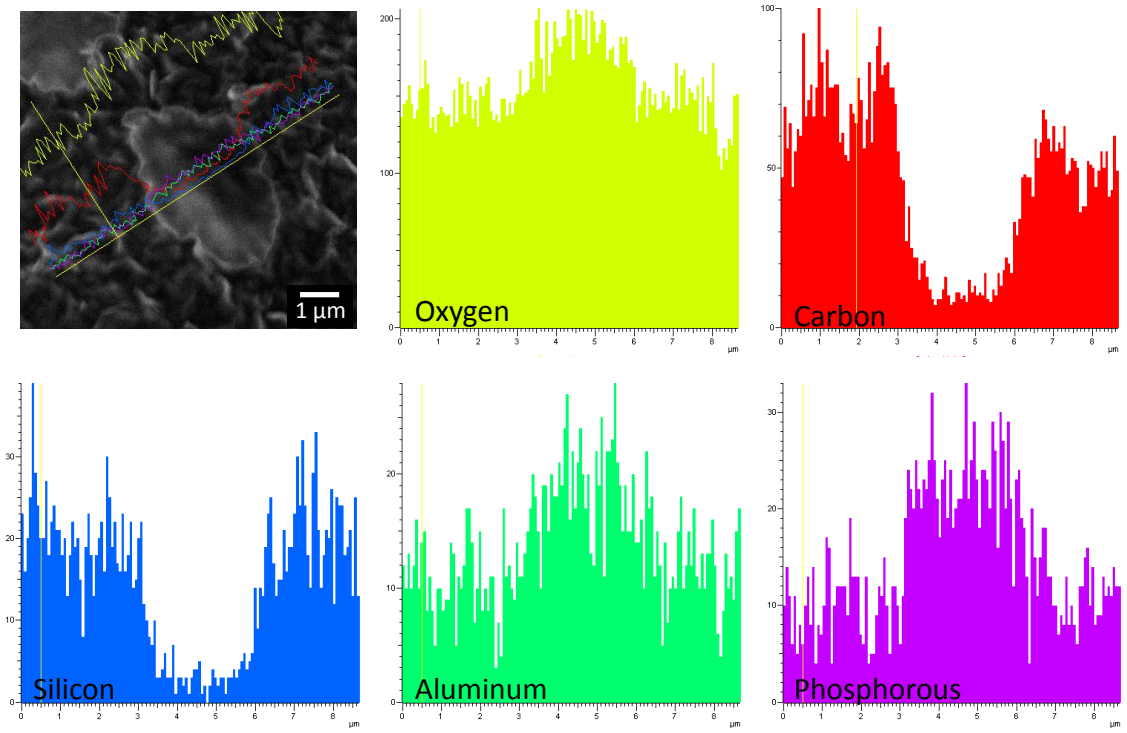

Figure 3.9. Individual elemental spectra peaks of oxygen, carbon, silicon, aluminum, and phosphorous are mapped across a portion of the 4 TL char obtained following cone calorimetry testing.

Cone calorimetry evaluates the flammability of a material by measuring oxygen consumption, which relates heat generated by combustion to the amount of oxygen present to facilitate it.[73, 261, 265] These nanobrick wall assemblies were deposited onto 179 μm PET film and then oxygen transmission rate (OTR) was tested at 23°C and 0% RH. By simply adding 10 TL, OTR decreases by one order of magnitude (see Supplemental Information for OTR of bare, 10 and 16 TL coated PET film). Unlike the coating formed on flat PET films, trilayer coatings three-dimensionally coat foam substrates by conformally covering the polyurethane cell walls. Oxygen is still able to flow through the porous structure post-deposition, but the architecture of the nanobrick wall restricts oxygen penetration to the underlying polyurethane by trapping molecules within the tortuous polymer-clay path. Once heat is applied and the nanobrick wall coating transforms into the protective shield, it is unclear if the tortuous path remains and/or contributes to the nanocoatings' flame retardant behavior.

A recent evaluation of the growth mechanism of $(PAH/PSP)_n$ BL assemblies provides some insight into the structure of these thin films.[266] It was suggested that islands formed during initial layers of film growth do not coalesce, even after 150 deposition steps, due to the dramatic difference in size of the polyelectrolytes. By adding clay into this deposition sequence, films form the conventional nanobrick wall structure, as shown in Figure 3.2. Clay bricks and polymeric mortar create the typical tortuous path demonstrated in previously reported LbL fabricated polymer-clay barrier layers.[35, 58, 215] Any differences in barrier are believed to be due to alternations in clay spacing and mortar chemistry.

3.4 Conclusions

Upon exposure to fire (or other forms of extreme heat), polyurethane decomposes into polyol and isocyanate components, which form highly flammable melt-pools and release volatile, toxic gases.[80] Typical layered-silicate polymer nanocomposites combat fire in the condensed phase,[250] where the MMT platelets strengthen the fire blocking residue and provide a shield heat.[262, 267] In prior work, 10 BL CH/MMT assemblies on polyester-based PU were able to reduce pkHRR by 52.4% with only 4 wt% coating addition.[58] Thermal shielding afforded by these ~30 nm thick films was solely provided by the presence of the inorganic clay platelets. This study demonstrates that it only takes 4 TL of the PSP/PAH/MMT nanobrick wall assembly (< 3 wt% coating addition) to cut the pkHRR of polyether-based PU by 54.8%. TL coatings (< 20 nm thick) provide comparable reduction in pkHRR with fewer total layers, suggesting synergistic interaction between components in the coating. The difference in performance is significant and points to the need for further investigation of these coatings on the same type of foam. It will be important to test the effectiveness of the nanocoating by further assessing the optical clarity and composition of any produced smoke (the cone calorimetry apparatus used here did not have this capability). Most thin films prepared via layer-by-layer assembly use an even number of deposited layers, which adds to the uniqueness of the present three-component nanocoating. This trilayer deposition sequence allows the polymeric component to play a more active role in the FR behavior of the traditional nanobrick wall architecture. There is now additional ability to tailor the properties of this new class of environmentally-benign FR treatment.

These thin, water-based nanocoatings proved a tremendous opportunity to protect the complex substrates found in upholstered furniture, clothing and the transportation industry.

CHAPTER IV

IRON-CONTAINING, HIGH ASPECT RATIO CLAY AS NANOARMOR THAT IMPARTS SUBSTANTIAL THERMAL/FLAME PROTECTION TO POLYURETHANE WITH A SINGLE ELECTROSTATICALLY-DEPOSITED BILAYER*

4.1 Introduction

Nanobrick wall coatings have recently been developed to thwart the two key problems of polyurethane foam exposed to a heating source:[32, 34, 58, 179] melt dripping and heat release.[268] In one case, a nine-layer system (three trilayers of PAA/PEI/MMT), resulted in a 4.8 wt% nanocoating on foam, reduced peak heat release rate (pkHRR) by 70%.[33] This system is a condensed phase flame retardant, which means the pyrolysis process and mass loss rate are slowed through the formation of carbonaceous-silicate char. Despite their promise, the numerous layers required to impart sufficient flame retardant behavior is daunting for practical use.

In an effort to create a flame retardant nanocoating for polyurethane foam with relatively few layers, montmorillonite (MMT) clay and vermiculite (VMT) clay were chosen as building blocks for nanobrick wall assemblies. The influence of clay aspect

---

*Cain, A. A.; Plummer, M. G. B.; Murray, S. E.; Bolling, L.; Regev, O.; Grunlan, J. C., Iron-containing, High Aspect Ratio Clay as Nanoarmor that Imparts Substantial Thermal/Flame Protection to Polyurethane with a Single Electrostatically-deposited Bilayer. *Journal of Materials Chemistry A* **2014**, *in review.* – Reproduced by permission of The Royal Society of Chemistry.

ratio and composition on fire behavior was studied as a function of layers deposited and nanocoating weight addition. It was found that a single PEI/VMT bilayer (BL) can achieve a 54% reduction in pkHRR and a 31% reduction in total smoke release (TSR), in comparison to uncoated polyurethane foam. Adding a second bilayer further reduces pkHRR and cuts in half the amount of smoke released. Four nanobrick wall bilayers made with standard MMT clay are needed to match the weight gain and performance of a single vermiculite-based bilayer, which is attributed to complex interfacial interactions that occur between the components during thin film construction and to insulating properties of the phosphorous-formulated VMT platelets during combustion. Although vermiculite has been previously used in bulk polymer matrices, or layered into nanobrick walls to reduce gas permeation,[21, 269-272] this is the first report of VMT being used in LbL multilayer thin films for anti-flammable purposes. This ability to cut peak heat release rate in half with a single bilayer (just 3.2 wt% added to the foam), using environmentally-benign ingredients, is a tremendous breakthrough. It is likely that this nanocoating technology could be used to protect many household items (e.g., upholstered furniture) in a safe, cost-effective manner.

4.2 Experimental

4.2.1 Materials

Poly(acrylic acid) (PAA, M = 100 kg/mol, 35 wt% in water) and branched polyethylenimine (PEI, M = 25 kg/mol) were purchased from Sigma-Aldrich

(Milwaukee, WI), while chitosan (CH, M = 60 kg/mol, deacelylation 95%) was purchased from G.T.C. Union Group Ltd. (Qingdao, China). Sodium montmorillonite clay (MMT, trade name Cloisite Na+) was provided by Southern Clay Products, Inc. (Gonzales, TX) and formulated vermiculite HTS-SE (VMT, 15-16 wt% in water) was purchased from Specialty Vermiculite (Cambridge, MA). This type of VMT has 60% of particles ≤20 μm (≤25% particles are larger than 45 μm). Aqueous solutions of 1 wt% PAA, 0.1 wt% PEI, 0.1 wt% CH, 1.0 wt% MMT, and 1.0 wt% VMT were prepared using deionized (DI) water and rolled for 12 h. Prior to deposition, the pH of each PAA and PEI solution was altered to 2 (using 2 M HNO_3) and 10 (using 1 M HCl), respectively. CH was solubilized in acidic deionized water (pH 1.5), and then the pH of the cationic solution was raised to 6 prior to deposition (using 1M NaOH). Both MMT and VMT clay suspensions were used at their natural pH (9.7 and 7.8, respectively).

4.2.2 Substrates

P-doped, single side polished (1 0 0) silicon wafers (University Wafer, South Boston, MA), with a thickness of 500 mm, were used as substrates for ellipsometric thickness measurements. Layers were incrementally deposited on 5 MHz gold-electrode quartz crystals (Maxtek, Inc., Cypress, CA) to obtain mass deposited per layer using a quartz crystal microbalance. Polyether-based polyurethane foams with densities of 1.75 lbs/ft were purchased from Future Foam (type 1850, High Point, NC).

4.2.3 Layer-by-layer Deposition

Fabrication of the multilayer FR nanocoatings on two-dimensional substrates (silicon wafers and Au/Ti crystals) for thin film characterization was carried out using a home-built dipping system, where flat, 2D substrates were immersed in solutions for reported times and rinsed with deionized water (blade rinsing) and dried with filtered air.[273] Fabrication of the multilayer thin films for 3D substrates was carried out by fully compressing foam in solutions three times with a thin sheet of acrylic in an effort to achieve a more uniform compression across the surface. Excess solution (or rinse water) was removed from the foam with hand crank wringers. This coating technique significantly improved the consistency in weight addition of the nanocoating (relative to squeezing foam by hand). Polyurethane was first submerged in PAA for 30 sec to enhance the adhesion between the foam surface and the nanocoating. In these acidic conditions (i.e., PAA at pH 2), carboxylic acid groups on the polyion hydrogen bond with the polyurethane surface. Treated substrates were then dipped in the PEI solution for 5 min, rinsed in deionized water and wrung out. When the PAA-coated surface was exposed to pH 10 solution, the charge density of the weak polyelectrolyte increased and caused PAA chains to attract PEI to the surface via hydrogen bonding (and possibly electrostatic attraction). This deposition procedure was followed by an identical dipping, rinsing and wringing dry for the clay suspension. If subsequent polymer/clay layers were deposited, the same coating procedure was followed with 1-min CH/clay dip times, until the desired number of layers was deposited, as shown in Figure 4.1. Foam samples were dried in an oven at 70 °C for 3 h immediately following deposition.

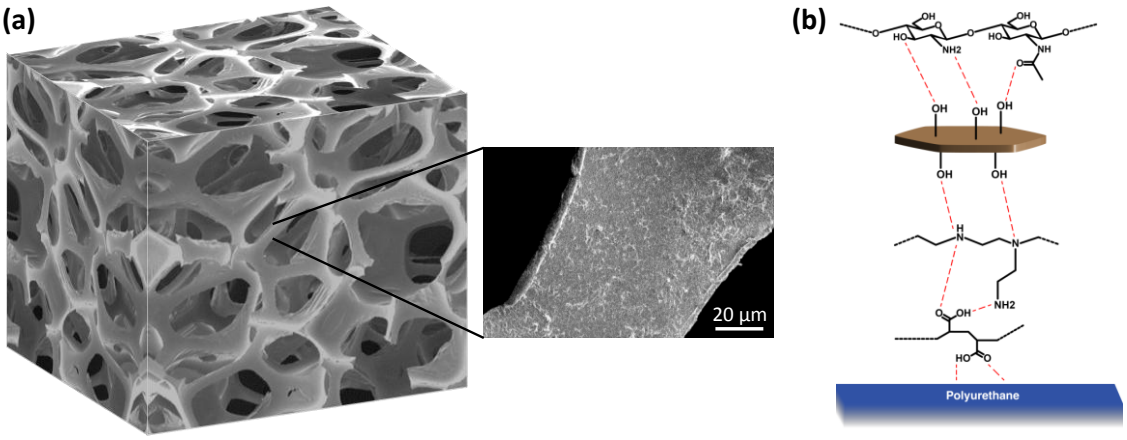

Figure 4.1. Schematic of the coated foam (inset: SEM image of 4 BL MMT-based nanobrick wall on polyurethane). b) Chemical structures in the nanobrick wall after depositing the primer, clay, and chitosan.

4.2.4 Thin Film Characterization

An alpha-SE Ellipsometer (J.A. Woollman Co., Inc., Lincoln, NE) with a 632.8 nm laser was used to measure film thicknesses on polished silicon wafers. A Maxtek Research Quartz Crystal Microbalance (QCM, Cypress, CA) was used to monitor mass deposition of individual layers deposited on Ti/Au crystals in order to calculate total film density. Small slices taken from single bilayer coated foam (PEI/MMT and PEI/VMT) were embedded in Epofix (EMS, Hatfield, PA) and left to cure overnight at room temperature. Thin gold sections were trimmed (< 90 nm) using a microtome and were picked up on lacey Formvar-coated 300 mesh copper grids. Thin film cross-sections were imaged with a Tecnai G2 F-20 TEM (FEI, Hillsboro, OR) at an operating voltage of 200 kV and calibrated magnifications. Coated thin films, deposited on PU substrates, were mounted on aluminum imaging stubs and thinly sputter coated with 5 nm of platinum/palladium (Pt/Pd) alloy in preparation for surface images that were acquired

with a field-emission scanning electron microscope (FESEM) (Model JSM-7500F, JEOL; Tokyo, Japan). Energy-dispersive X-ray spectroscopy (EDX) samples were not sputter coated with Pt/Pd (elemental spectra in Figure S3 were acquired on the FESEM).

4.2.5 Thermal Stability, Flammability, and Combustibility of Foam

Fire behavior of the nanocoating was qualitatively screened with the direct flame of a butane micro hand torch (MT-76K, Master Appliance Corp., Racine, WI) for 10 s (the approximate blue flame temperature is 2500 °F). A Q50 Thermogravimetric Analyzer (TA Instruments, New Castle, DE) was used to measure the thermal stability of control and coated polyurethane foam. Each sample was approximately 10 mg and was tested in an air atmosphere from room temperature up to 640 °C, with a heating rate of 10 °C/min. Cone calorimetry was operated according to standardized procedures (ASTM E-1354-11) at the University of Dayton Research Institute using a FTT Dual Cone Calorimeter (exhaust flow of 24 L/s). Samples (10 x 10 x 2.5 cm) were placed in a pan constructed from aluminum foil and exposed to at a heat flux of 35 kW/m^2, with an uncertainty of 5% in HRR and 2 s in time.

4.3 Results and Discussion

4.3.1 Film Growth on 2D and 3D Surfaces and Thin Film Microstructure

Chitosan (CH)/clay bilayers were initially deposited on silicon wafers, using branched polyethylenimine as the initial layer to improve adhesion, to measure thickness

as a function of bilayers, as shown in Figure 4.2. Films grew linearly as a function of the number of layers deposited for both clay systems, with VMT having a greater growth rate (~6.2 nm/2 BL) than MMT (~ 2.8 nm/2 BL). Not only do these thicknesses suggest deposited clay nanoplatelets are oriented parallel to the substrate, the data implies that clays adsorbed to the surface are well exfoliated (platelets are ~1 nm thick), which has previously been observed.[274] The same linear growth was observed when a quartz crystal microbalance was used to measure growth as a function of weight deposited, with VMT-based recipes generating heavier layers. VMT-based films also have higher clay loading (87 wt%), which results in a more dense thin film (MMT-based thin films are composed of 78 wt% clay).

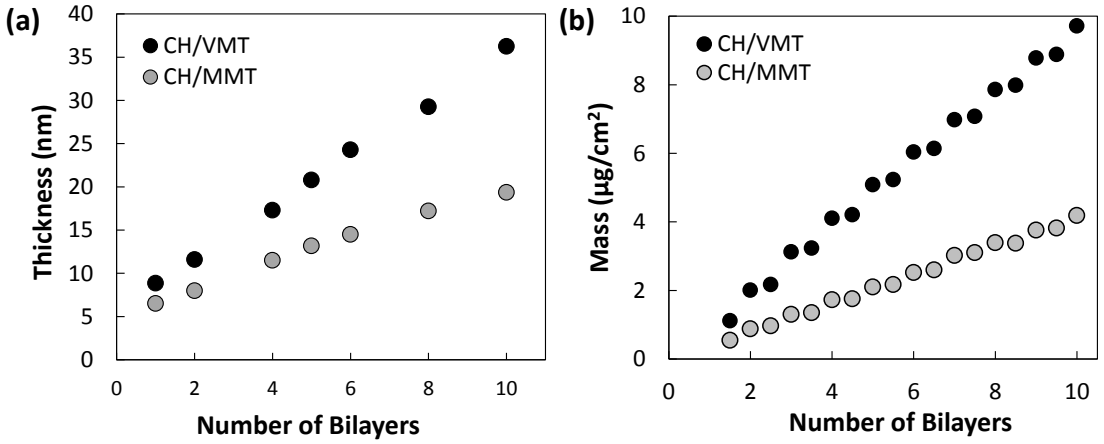

Figure 4.2. a) Film thickness and b) mass as a function of bilayers deposited for polymer/clay assemblies. Ellipsometry was used to measure thickness, while QCM measured mass.

Coating three-dimensional, porous polyurethane required submersion into a poly(acrylic acid) (PAA) solution, whose pH was adjusted to 2 with nitric acid. This deposition step functions as a primer treatment that promotes nanocoating adhesion to the otherwise hydrophobic foam. It is believed that dissociated nitric acid ions increase the charge density of the PU. The carboxylic acid pendant groups present on PAA have the ability to hydrogen-bond through partial charge attraction with other polar groups on polyurethane. One and two bilayers of both clay-based recipes were then deposited on the foam, with PEI substituting for CH in the first cationic polyelectrolyte deposition. The MMT-based system was also evaluated at 4 BL to match the weight gain of 1 BL of the VMT-based system. Figure 4.3 shows SEM micrographs of the surface of uncoated foam, foam coated with a single layer of PEI, a single PEI/VMT BL, a single PEI/MMT BL, and 4 MMT-based BL. Uncoated polyurethane has a smooth surface (Figure 4.3a), while several cracks can be seen in the PAA/PEI-primed foam (Figure 4.3b) due to the glassy nature of this polyelectrolyte film.[217] The single polymer/clay bilayer coatings reveal excellent clay coverage over the PU surface. Aspect ratios of the observed clusters are much larger than the reported aspect ratios for both VMT (1100) and MMT (200),[251, 274] providing good evidence of aggregated clay platelets adhering well to the porous foam surface. Individual MMT platelets are not distinguishable in the 4 BL MMT-based coating systems (Figure 4.3e).

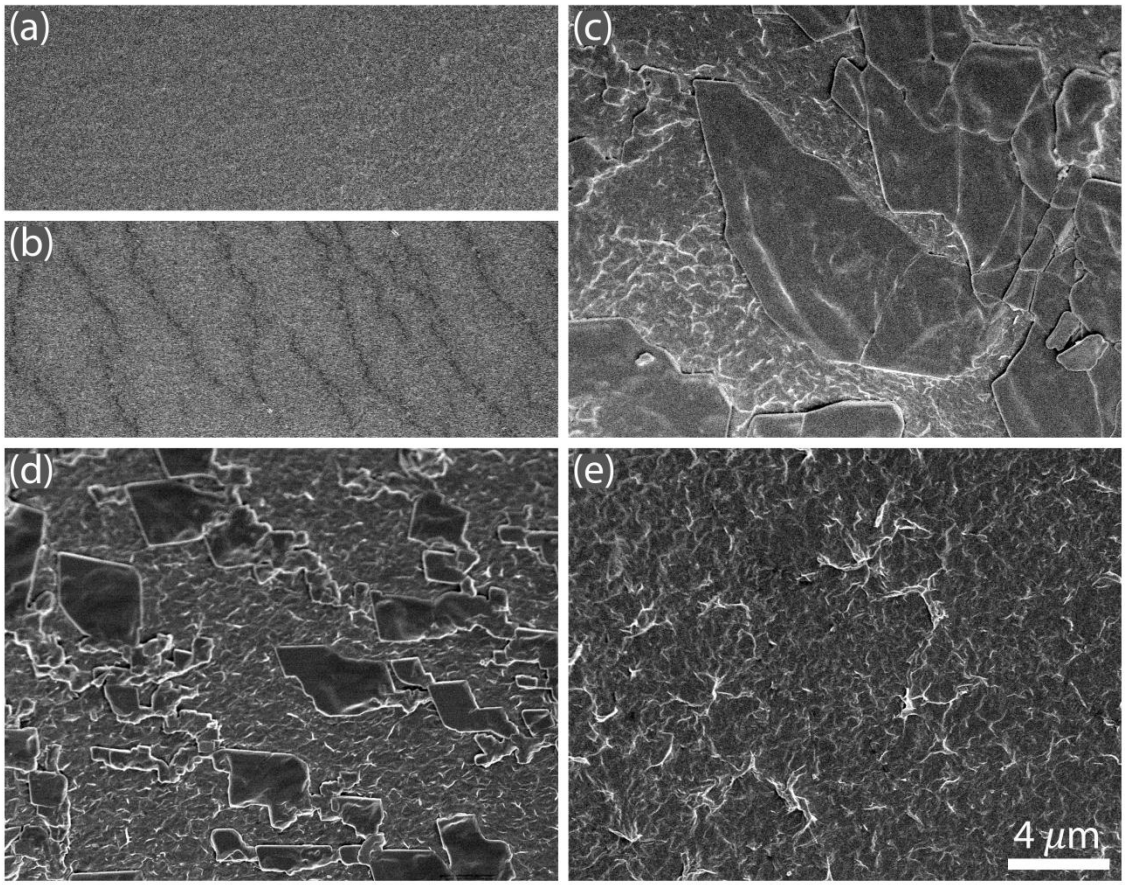

Figure 4.3. SEM images of a) control foam, foam coated with b) a single layer of PEI, c) a single PEI/VMT, d) a single PEI/MMT, and e) 4 BL MMT-based coating.

Figure 4.4 shows SEM images of freeze-fractured samples that highlight the complex, irregular polyurethane matrix fully coated with both clay-based recipes at 1 BL and confirm the presence of clay aggregates within the coating. Figures 3c and 3f show high magnification TEM cross-sectional micrographs of these same single bilayer coatings deposited on the flexible foam. The source of contrast in these TEM micrographs is electron density, where materials with higher electron density (clay) appear darker than lower electron dense materials (polymer). The image of the ordered

layers also highlights that the largest dimension of the clay deposits parallel to the surface. As shown in Figure 3c, several vermiculite platelets are deposited after a single deposition in the aqueous clay suspension, suggesting VMT clay is only partially exfoliated in solution and that stacks of clay deposit in the thin film. The same trend holds for the MMT-based recipe in Figures 4.4d, e, and f. Figure 4.4 also shows that the nanocoatings deposit much thicker on polyurethane than what was measured on flat silicon wafers. The observed differences are attributed to several factors: the influence of the PAA deposition on the deposited multilayers, the effects of the different coating procedures for 2D and 3D substrates, and the chemical nature of the substrates themselves. Thickness of a deposited multilayer containing weak polyelectrolytes is strongly dependent upon the degree of ionization and conformation of both absorbed polymer and that of the previous layer.[156] When PAA-coated PU surfaces are immersed into PEI solutions at pH 10, there is an increase in surface charge density. It is well documented that PEI chains diffuse into deposited PAA layers when both polymers have a low degree of ionization.[275] The PAA surface treatment step added to the foam coating procedure not only enhances adhesion between the polyurethane and subsequent layers, it promotes thick PEI deposition. The observed surface roughness is attributed to the rigorous coating process (involving full compression of the foam and multiple wringing steps). The complex, porous structure of the polyurethane hinders thorough rinsing, where weakly bound polyelectrolytes and clay become trapped within the matrix, contributing to thicker deposition and rougher deposited layers.

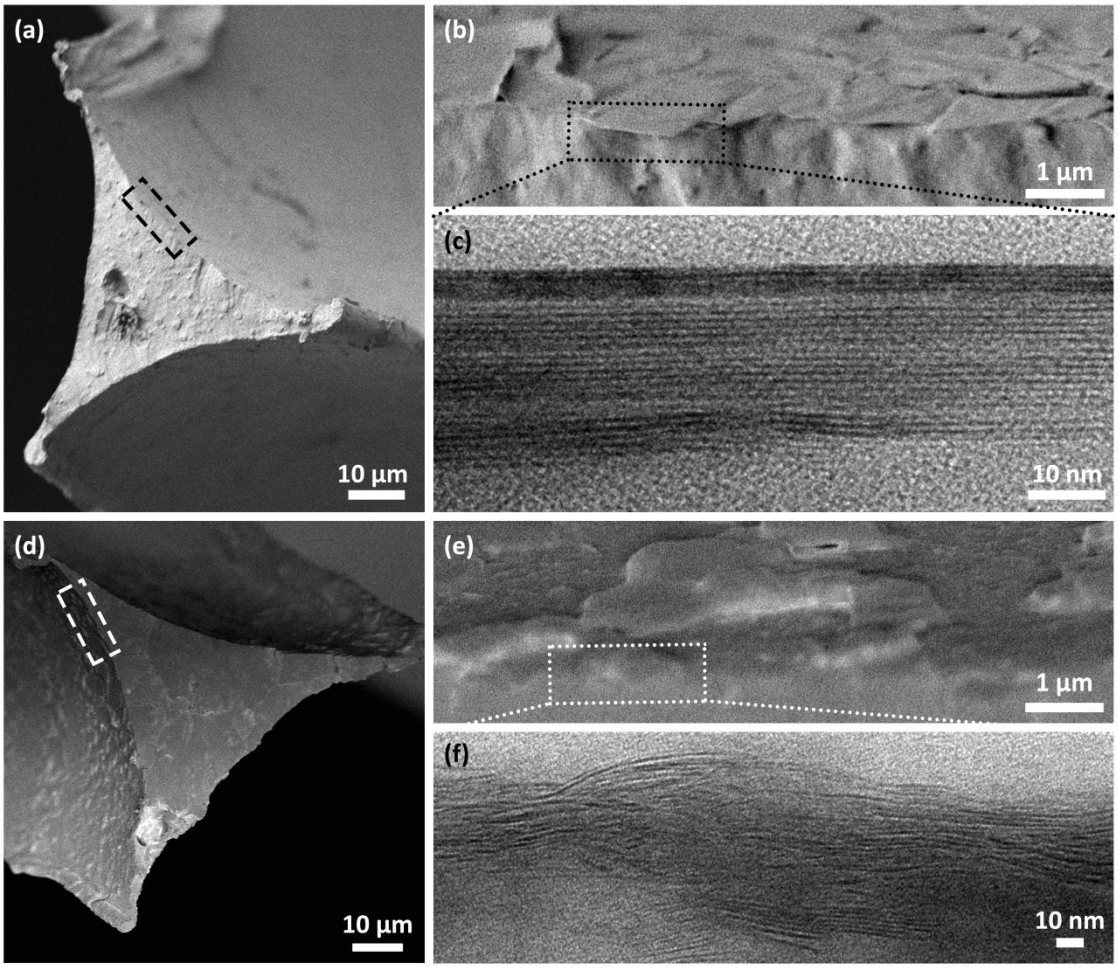

Figure 4.4. SEM images of freeze-fractured polyurethane foam coated with 1 BL of a-b) polymer/VMT and d-e) polymer/MMT. TEM micrographs of polyurethane foam coated with 1 BL of c) polymer/VMT and f) polymer/MMT.

4.3.2 Butane Torch Testing

Nanobrick walls (i.e., polymer/clay LbL thin films) composed of either MMT or VMT bricks were deposited on open-celled, flexible foam to evaluate the influence of nanoplatelet composition and aspect ratio on thermal stability. Nanocoating weight gain was determined by dividing the difference in weight of the foam before and after the

coating was applied by the original weight of the PU. Foam flammability was qualitatively screened by applying a butane torch to one side of a (5 x 5 x 2.54 cm) foam sample suspended in the air on a metal grating. Immediately upon contact with the flame, polyurethane melts away and the cellular structure is completely lost, forming liquid tar that melt drips and ignites paper placed directly below the grating.

All nanocoatings eliminated melt dripping. The flame from the butane torch burrowed a hole in both clay systems at 1 and 2 BL, while the 4 BL MMT-based coating fully maintained the foam's cellular structure and shape. Figure 4.5 shows images of foam coated with both nanobrick wall thin films before (top row) and after torch testing (2nd row: top-down, 3rd row: torch side, 4th row: bottom, 5th row: cross-section). As a function of layers deposited, VMT-based coatings protected the underlying polyurethane better than MMT, with 2 BL VMT providing enough thermal shielding that undamaged foam was preserved under a thick char layer. When fire behavior is qualitatively compared as a function of nanocoating weight addition, 4 BL MMT-coated samples (~3.3 wt%) left more pristine foam remaining after torch testing than 1 BL VMT-coated samples (~3.2 wt%). Pyrolysis molecules and heat have more gaps to breach and permeate through single BL MMT-based nanobrick walls because the bricks are an order of magnitude smaller. The additional polymer/clay layers necessary to normalize weight gain adds multiple MMT platelets with each additional BL. It is possible these additional layers not only significantly increase the thermal stability of the MMT-based nanobrick walls but also increase the tortuous path for combustion products to escape and feed the flame.

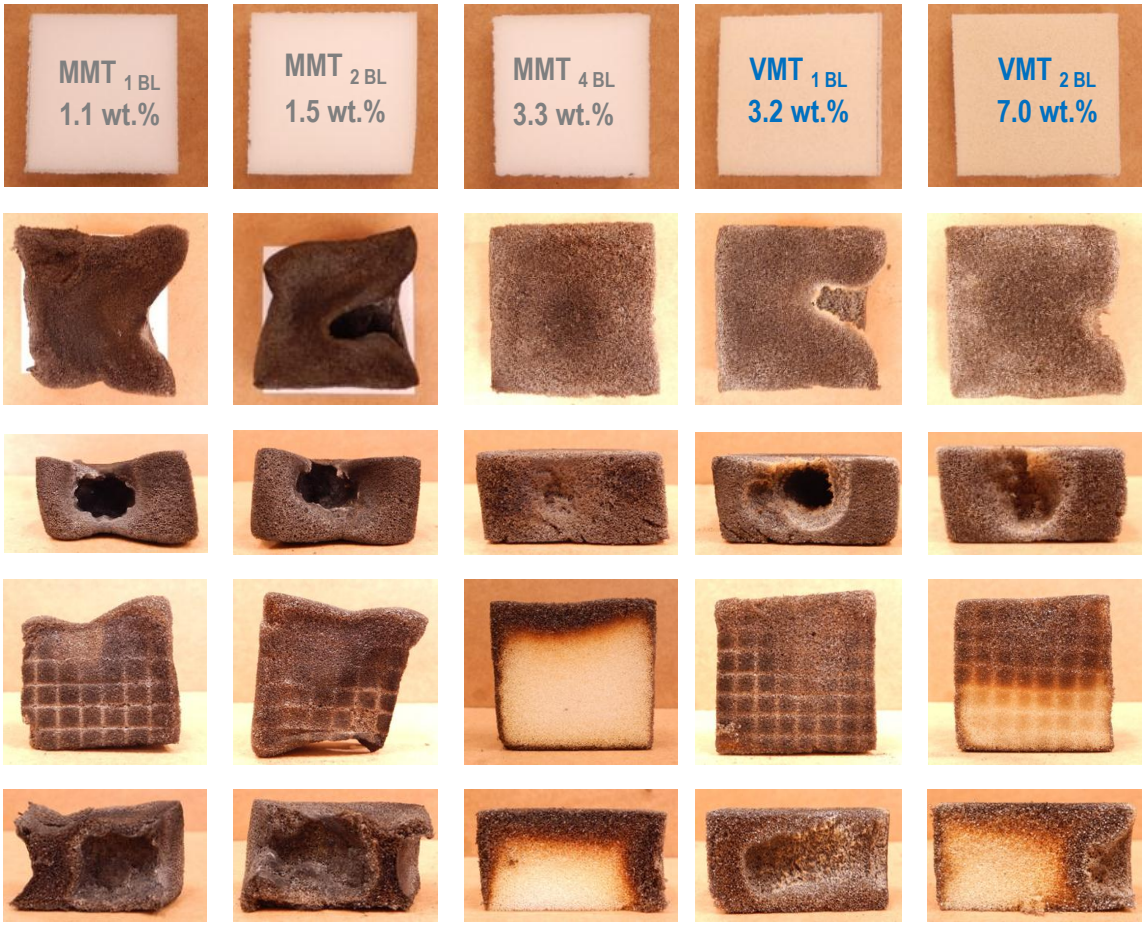

Figure 4.5. Images of nanobrick wall coated polyurethane before (top row) and after 10 s of direct exposure to a flame from a butane torch.

4.3.3 Cone Calorimetry and Thermal Analysis of Fire Behavior

In an effort to quantitatively evaluate the thermal barrier properties of these polymer/clay thin films, control and coated (1, 2, and 4 MMT-BL; 1 and 2 VMT-BL) polyurethane foam was tested with standard cone calorimetry (ASTM E-1354-07). All samples were exposed to an external heat flux of 35 kW/m^2. While samples were subjected to this controlled radiant heat, heat and smoke release rates, production of toxic gas species, and mass loss data were collected as a function of time with an oxygen

sensor, a laser photometer beam, a CO_2/CO detection system, and a load cell. Figure 4.6 shows heat release rate (HRR) and flammability data for six sample sets plotted as a function of the number of layers deposited (Figure 4a) and as a function of coating weight addition (Figure 4b). Control specimens ignited rapidly, and underwent polyurethane's characteristic two-step combustion process (i.e., thermosetting polymer boils, liquefies, and cellular structure collapses releasing large amounts of heat), which produces two distinct peak heat release rates (pkHRRs). The first peak is associated with the combustion of the isocyanate peak and the second higher peak is associated with the combustion of the polyol components.[257] As expected, immediately following high pkHRR, the remaining combustible material volatilizes and very little residue remains.

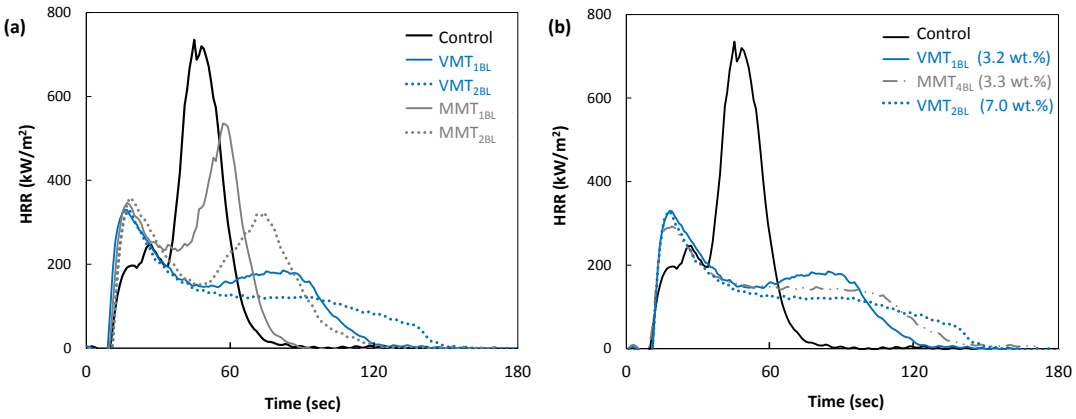

Figure 4.6. Heat release rate plotted versus time for control foam and foam coated with nanobrick wall thin films as a function of a) the number of layers deposited and b) coating weight addition.

The most significant predictor of a fire hazard is heat release rate.[256] For both clay coating systems, increasing the number of bilayers deposited resulted in greater

reductions in peak heat release rate and maximum average rate of heat emission (MARHE). pkHRR reports the highest rate of heat release, as determined via oxygen consumption calorimetry, and indicates the propensity of the flame to self-propagate and/or spread to other materials in the absence of an external heating source. MARHE is a fire engineering parameter, defined as the total heat release normalized by time, which can be used to rank materials in terms of their ability to spread fire to other objects. In all cases, char yield and total heat release (THR) appear to be inversely related (**Table 4.1**). Higher char yield signifies that more of the sample is converted into less flammable solid residue, which diminishes the amount of specimen available as fuel. For both clay systems, increasing the number of bilayers deposited yielded greater reductions in total smoke release, which is noteworthy because deaths related to fire incidents commonly result from inhalation of toxic combustion products.[276]

Table 4.1. Cone calorimeter results for coated and uncoated polyurethane foam.[a]

Sample [units]	Wt. Gain [%]	pkHRR[a)] [kW m^{-2}]	THR[b)] [MJ m^{-2}]	Wt. Lost [%]	TSR[c)] [m^2 m^{-2}]	MARHE[d)] [kW m^{-2}]
Control		735 ± 11	19.5 ± 0.2	100	146 ± 4	318 ± 5
$(PEI/MMT)_1$	1.1 ± 0.2	531 ± 33	18.7 ± 0.6	94 ± 1	157 ± 14	273 ± 16
$(PEI/MMT)_2$	1.5 ± 0.1	343 ± 15	19.2 ± 0.8	96 ± 1	130 ± 3	207 ± 6
$(PEI/MMT)_4$	3.3 ± 0.3	298 ± 6	17.2 ± 0.5	92 ± 1	72 ± 7	170 ± 6
$(PEI/VMT)_1$	3.2 ± 0.2	339 ± 12	17.9 ± 0.6	87 ± 7	101 ± 12	195 ± 11
$(PEI/VMT)_2$	7.0 ± 0.4	322 ± 7	17.1 ± 0.5	89 ± 1	61 ± 1	178 ± 4

[a] pkHRR = peak heat release rate; Total HR = total heat release; Total SR = total smoke release; MARHE = maximum average rate of heat emission

After exposure to the cone heater, both 1 and 2 BL MMT-based systems rapidly smoked and ignited, but no liquefaction occurred. Surface char that formed from 1 BL

MMT samples shrank during burning, leaving a final stiff char of approximately 0.25 inches thick. Although 2 BL MMT nanocoated samples did not shrink during burning, as much as single bilayer MMT systems, the second pkHRR curve shape suggests char formed was not sufficient to prevent underlying fuel from being converted into heat. 1 and 2 BL VMT and 4 BL MMT samples also smoked and ignited quickly after exposure to the cone heater, but these nanocoatings rapidly formed a thermally thick residue that prevented collapse and flow during burning. For these three systems, the first peak has the highest heat release rate, which is why the time from ignition to the pkHRR decreases from 40 sec (uncoated, control PU) down to 13 sec (coated PU). Although it is meaningful to understand how fast the sample reaches its maximum energy release after ignition, all three of these coating systems effectively decrease the flammability of the open-celled foam by decreasing the pkHRR and avg HRR by at least 54%. 1 BL VMT sufficiently reduced the second pkHRR, but the other two systems (2 BL VMT and 4 BL MMT recipes) completely eliminated the peak and greatly extended the time the total heat was released. One bilayer MMT-based systems exhibited the highest overall flammability, whereas 4 BL MMT had the lowest overall pkHRR value (298 kW/m^2) and MARHE rating (170 kW/m^2) of the systems studied.

In a direct comparison of polymer/clay thin films at 1 BL, VMT-based coatings reduce the pkHRR of polyurethane 36% more than MMT-based coatings (with respect to uncoated polyurethane). Although there is only a 6% reduction in pkHRR of 2 BL VMT-based thin films relative to 2 BL MMT-based films, VMT bilayers suppress the second pkHRR and significantly extend the time it takes for total heat to be released. MMT

bilayers simply alter the polyurethane decomposition cycle. In addition to having less thermally shielding material present in these 1 BL thin films, the average aspect ratio of montmorillonite platelets is an order of magnitude smaller than vermiculite, which generates more gaps for heat to permeate through and pyrolysis products to propagate out of the thin film. Increasing platelet aspect ratio in these thin film assemblies is known to impart improved gas barrier.[53, 165, 277] When nanocoating weight addition was normalized between the two clay systems, both 1 BL VMT and 4 BL MMT based coatings had similar HRR curves, whose shape represents the typical thermally thick charring sample, but the montmorillonite system has the lowest pkHRR, THR, and TSR. Of all polymer/clay systems evaluated with cone calorimetry, the 2 BL VMT-based nanocoating has the greatest reduction in smoke release.

Polymer nanocomposites typically fight fire through the condensed phase mechanism, interfering with a polymer's combustion cycle by forming a thermal shield of ceramic armor that prevents melt dripping when a heating source is applied.[4] As more MMT layers are deposited, the protective nature of the nanobrick wall coating increases suggesting the effect of aspect ratio of clay diminishes. TGA analysis reveals this thermally shielding residue at 400 °C, 500 °C, and 600 °C is equivalent for both a 1 BL VMT coating and 4 BL MMT (see Figure 4.7a, b). It should be noted that the percent residue at each of the specified temperatures is greater than the amount of coating deposited on the polyurethane, signifying some of the foam has been converted to carbonized residue.

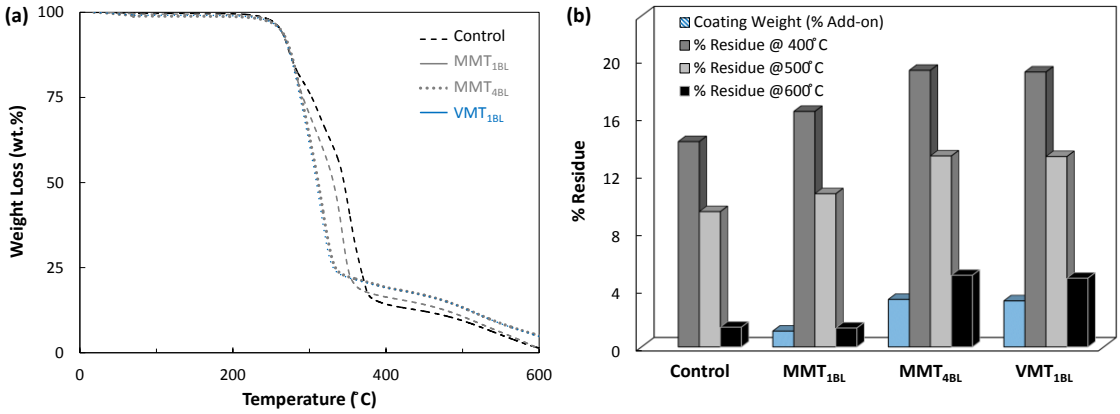

Figure 4.7. a) Weight loss as a function of temperature in air atmosphere for control foam and foam coated with nanobrick wall thin films. b) Percent residue of control and coated polyurethane foam samples at 400, 500, and 600 °C.

Both montmorillonite and vermiculite are 2:1 phyllosilicate minerals (i.e., their crystal structures have 1 octahedral hydroxide sheet between 2 tetrahedral silicate sheets) and have high cationic exchange capacity.[252, 278] Despite their similarity, there are key differences between these clays that explain why MMT-based coatings require 4 bilayers to match the fire performance of a single polymer/vermiculite bilayer. VMT has an order of magnitude larger aspect ratio than MMT and this reduces the number of interfaces pyrolysis products can escape through and/or heat can be transferred past the insulating barrier. Partial clay exfoliation in solution, which results in platelet stacks depositing in the nanocoating, is another parameter that enhances fire retarding performance, as VMT itself intumesces.[279] Upon the addition of heat, bound water molecules (and possibly other combustion gases) expand and thermally exfoliate the vermiculite in the direction perpendicular to the platelet's longest dimension.[280] It has been suggested that iron

present within vermiculite's tetrahedral layers could enhance the clay's thermal stability by acting as a radical trap and/or char catalyst site.[281-284]

The particular VMT chosen for this study was modified with phosphorous-based molecules that are reported to increase thermal stability. It is well known that phosphorous compounds (depending on their chemical structure and their interaction with polymer and/or added synergists) can interfere in the combustion cycle in both vapor and condensed phases by either volatilizing into the gas phase (HPO_2•, PO•, PO_2•, and HPO•)[96] and scavenging H• and OH• radicals or decomposing in the condensed phase, catalyzing char accumulation on the polymer surface.[4, 81, 97] Figure 4.8 shows top-down and cross-sectional SEM micrographs of both 1 BL nanobrick wall systems and 4 BL MMT-coated samples after cone calorimetry testing, along with corresponding energy-dispersive X-ray spectroscopy (EDX). SEM images highlight how the single bilayer MMT-coated foams shrank during burning. It is unlikely that the phosphorous played a large role (if any) in enhancing the barrier because the amount of the compound in the single bilayer VMT-coated foam was too low to be detected by EDX both prior to and after cone calorimetry testing. The residue of VMT-coated samples contained iron (in addition to expected carbon, nitrogen, oxygen, magnesium, aluminum, and silicon elemental peaks found in both clay sample sets) suggesting this element did participate in the condensed phase mechanism. If the metal ions did promote char formation (i.e., Lewis acid mechanism),[285] reduction of smoke release could also be attributed, in part, to the iron.

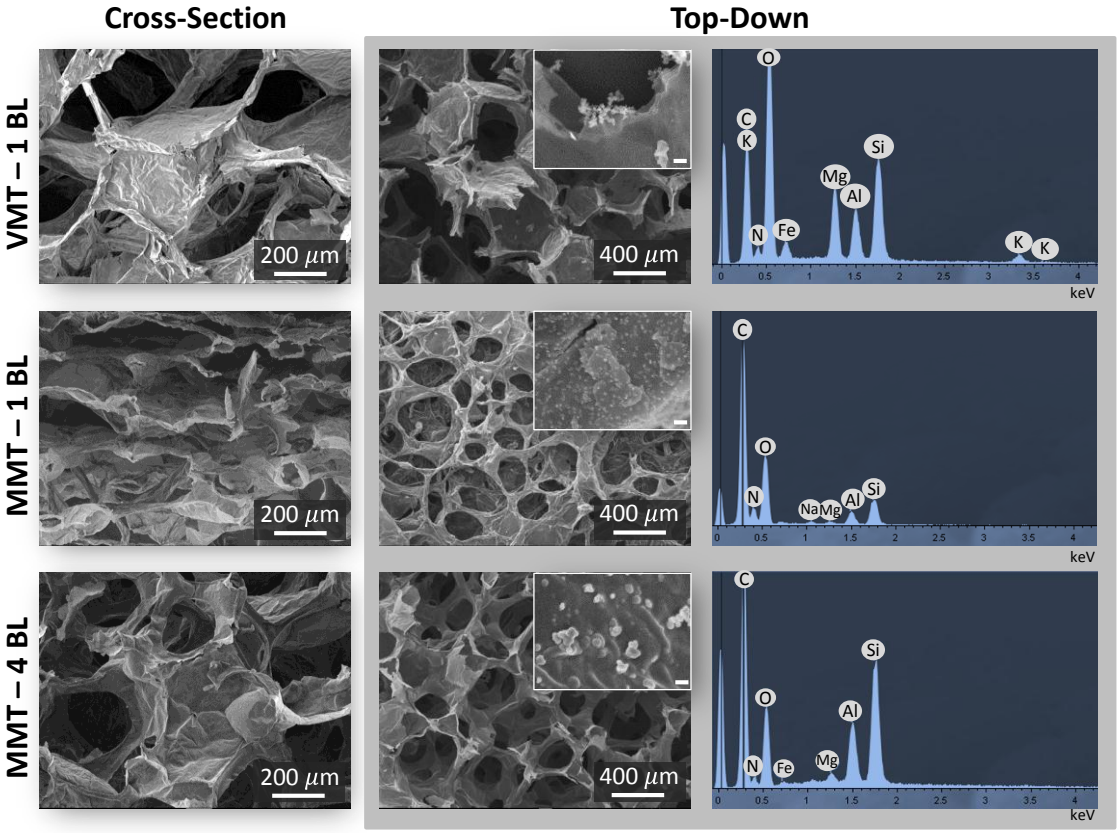

Figure 4.8. a) SEM images of foam coated with a single VMT layer, a single MMT layer, and a 4 BL MMT-based coating. The scale bar in the inset is 200 nm. b) EDX spectra of nanobrick wall coated foam after cone calorimetry testing.

4.4 Conclusions

Flame retardant thin films deposited on open-celled, flexible polyurethane foam, using layer-by-layer assembly of polymeric mortar and vermiculite clay platelets, were shown to dramatically improve fire performance through the condensed phase mechanism. A single bilayer of PEI and formulated-vermiculite clay, which adds only 3.2 wt% to the foam, successfully prevented formation of a melt pool of burning polymer and reduced peak heat release rate and total smoke release by 54% and 31%,

respectively. Four polymer/MMT bilayers are needed to surpass the fire protection properties of VMT's single bilayer barrier. These exceptional fire protection properties are largely attributed to the self-intumescing and heat-shielding characteristics of this high aspect ratio clay. The effect of the added phosphorous on flammability performance is negligible. This first ever report of vermiculite in a LbL-constructed nanobrick wall for fire protection provides an exciting opportunity for imparting environmentally-benign anti-flammability to complex polymer substrates. In some instances, just one or two bilayers may be necessary to impart adequate protection, making this relatively fast and simple.

CHAPTER V

INTUMESCENT NANOCOATING EXTINGUISHES FLAME ON FABRIC USING AQUEOUS POLYELECTROLYTE COMPLEX DEPOSITED IN SINGLE STEP*

5.1 Introduction

Layer-by-layer processing now appears to be a viable method to impart flame resistance to textiles, with comparable or improved performance relative to well-established approaches such as fiber blending, surface treatment, FR additives engineered into the backbone of synthetic fibers, and nanocomposite based-coatings.[286-292] Despite being able to use techniques commonly employed in textile processing, layer-by-layer assembly requires multiple layers to obtain the required amount of intumescent coating to produce a thermally insulating, foamed char. Reducing the number of layers needed could dramatically lower cost by minimizing processing steps and the time necessary to deposit the nanocoating. In this chapter, a two-component, aqueous polyelectrolyte complex system is described, which results in a tunable intumescing nanocoating in one deposition step. This weak polyelectrolyte complex of poly(phosphate sodium salt) and branched polyethylenimine (PEI) is applied by soaking a piece of cotton fabric into this 'OnePot' mixture. This nickname was adopted in reference to the need for only a single solution and a single coating step to produce an

*Reprinted with permission from Cain, A. A.; Murray, S.; Holder, K. M.; Nolen, C. R.; Grunlan, J. C., Intumescent Nanocoating Extinguishes Flame on Fabric Using Aqueous Polyelectrolyte Complex Deposited in Single Step. *Macromolecular Materials and Engineering* **2014**, *in press***.** © 2014WILEY-VCH.

effective flame retardant coating. A 10 minute soak produces a 23.0 wt% addition to cotton, and this coated fabric self-extinguishes during a vertical burn test and reduces heat release by 77.0%. This OnePot concept provides a powerful new framework for imparting flame resistance to textiles in an efficient and environmentally-benign manner.

5.2 Experimental

5.2.1 Materials

Bleached, desized cotton print cloth (i.e., fabric) with an approximate weight of 100 g/m^2 (3 oz/yd^2) was purchased from Testfabrics, Inc. (West Pittston, PA). Poly(phosphate sodium salt) (crystalline, +200 mesh, 96%) and branched polyethylenimine (molecular weight, Mw ~ 25 kg/mol) were used to create the OnePot system and were used as received. NaOH (made from sodium hydroxide pellets, anhydrous; reagent grade, ≥ 98%) and HCl (ACS reagent, 37%) were used to adjust the pH of the deposition solutions. All chemicals were purchased from Sigma-Aldrich (Milwaukee, WI).

5.2.2 Microscopic Imaging

Coated thin films, deposited on cotton substrates, were mounted on aluminum imaging stubs and thinly sputter coated with 5 nm of platinum/palladium alloy in preparation for surface images that were acquired with a field-emission scanning electron microscope (FESEM, Model JSM-7500F, JEOL; Tokyo, Japan).

5.2.3 OnePot Deposition

All individual solutions were prepared with 18.2 MΩ deionized water and were rolled overnight to ensure complete dissolution. The pH of 2.0 wt% PSP and 1.0 wt% PEI aqueous solutions were altered to 7 using NaOH and HCl, respectively. Cotton fabric was coated in a pan large enough for the fabric to lay flat. The OnePot mixture was created by pouring 1 kg of prepared PEI solution into the coating basin that already contained 1 kg of prepared PSP solution. It should be noted that 2.0 wt% PSP solution is clear and 1.0 wt% PEI solution is transparent, with a slight yellow hue. When mixed, the solution immediately turns turbid (cloudy white), suggesting that complexation has occurred. As soon as PEI is poured into the basin, the timer count for the pot life begins from zero. In each case, the solution is 30 min old at the end of soaking. The term 'soak time' denotes the time that the fabric is in the PSP/PEI mixture. To determine the pot life at which the fabric was submerged into the mixture, the reported soak time is subtracted from 30 min. After being submerged in pH 2 water for 5 min, the fabric is removed, wrung out, stretched over the coating holder, and is put into the OnePot complex at the specified time (see Figure 5.1 for soak time diagram). The purpose of the holder is to keep the fabric parallel to the coating basin. The 2 kg mixture completely covers the submerged fabric. At the conclusion of the soak time, which always occurred when the mixture was 30 min old, the fabric was removed, wrung out, and rinsed in deionized water. Fabrics were hung to dry in a 70 °C oven for 3 hours and stored in dry box prior to further testing.

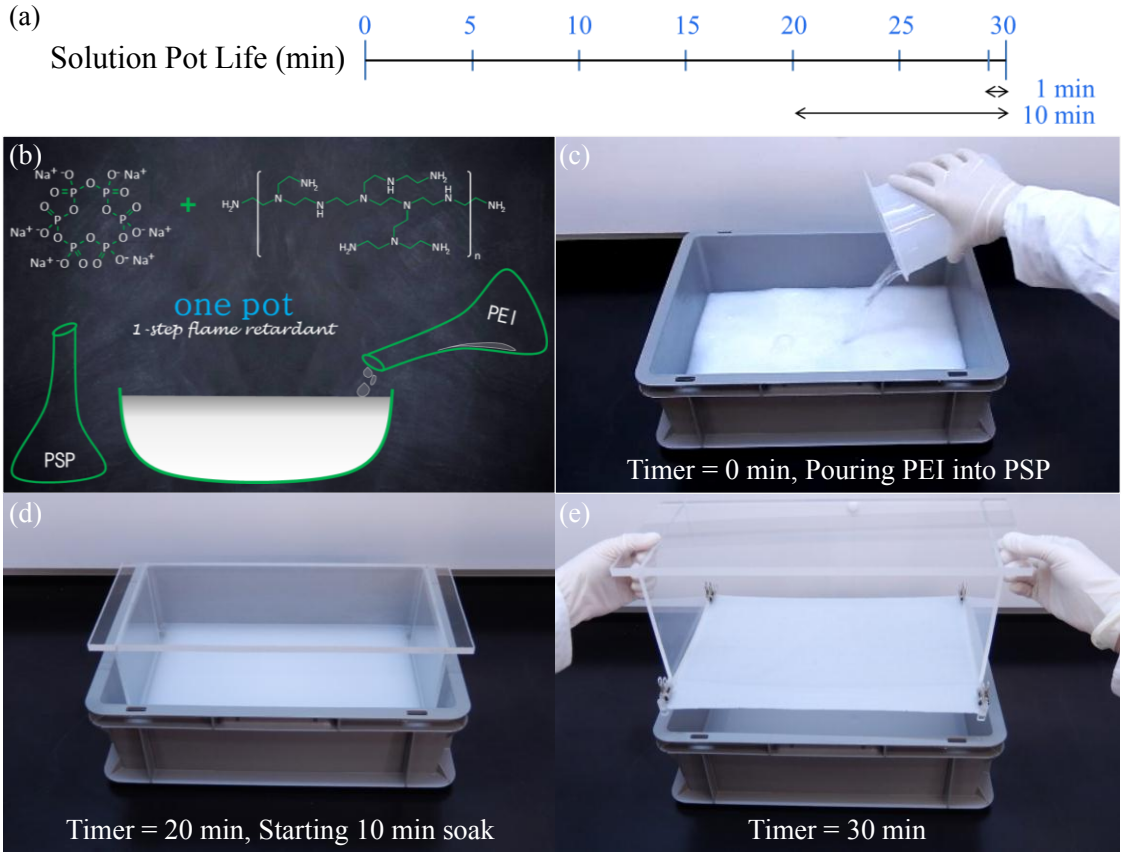

Figure 5.1. a) Time line for OnePot solution life and example immersion times for fabrics. b) Schematic of OnePot assembly procedure. c-e) Still shots of the OnePot coating process. Upon pouring branched polyethylenimine into poly(phosphate sodium salt), a turbid-white solution forms illustrating polyion complexation. Fabrics are submerged for various times in the mixture.

5.2.4 Thermal Stability, Flammability, and Combustibility of Fabric

Thermal stability of control fabric and OnePot coated cotton samples (approximately 30 mg) were evaluated in triplicate using a Q-50 thermogravimetric analyzer (TA Instruments, New Castle, DE) under a controlled heating ramp of 20 °C/min, from ambient temperature up to 600 °C. Coated and control samples were cut into 3 x 12 in. strips, and vertically hung in a metal clamp within a model VC-2 vertical

flame cabinet (Govmark, Farmingdale, NY). Samples were exposed to a small direct flame of a Bunsen burner (situated 40 mm below fabric sample) for 12 sec to measure time to ignition, time after-flame and after-glow times. Control cotton and fabric soaked for 1, 5, 10, and 15 min were run in triplicate for micro combustion calorimetry testing at a 1 °C/sec heating rate, from 150-550 °C, using method A of ASTM D7309 (pyrolysis under nitrogen) at the University of Dayton Research Institute.

5.3 Results and Discussion

5.3.1 OnePot Polyelectrolyte Complex Coating

Complex coacervation occurs when oppositely charged polyelectrolytes are drawn toward one another through ionic interaction, in an aqueous environment, and agglomerate into a network. This complex formation is governed by a number of parameters including polymer concentration, mixing ratio, ionic strength, charge density, and composition.[293] pH is a key factor that affects the formation and stability of polyelectrolyte complexes (PECs), especially in weak polyelectrolyte systems where the ionic groups are pH dependent.[294-295] When binding between the oppositely charged species is moderate, the PECs can agglomerate into soluble complexes, which are homogeneous, colloidal systems.[294] Turbid systems appear cloudy-white due to liquid-like polymer-rich and poor phases. Turbidity results when there is a strong interaction between polyanion and cation. It is possible to constrain aggregate growth to colloidal levels by limiting the number of polyion pairs through control of concentration.[296]

Improved complex stability has been observed when uncomplexed negative charges remain, especially in polyelectrolyte systems containing phosphates or polybases.[297] As the size of the coacervate complex grows, such that the corresponding weight is greater than repulsive Coulombic forces, flocculation and macroscopic phase separation occurs.

Combining a branched polyethylenimine (PEI) solution with that of poly(phosphate sodium salt) (PSP) immediately results in turbidity due to the spontaneous formation of macroscopic PSP + PEI complexes. This turbid solution quickly transitions (< 1 min) from its cloudy appearance to one that is uniformly white, suggesting the charged groups in the mixture are kinetically trapped (e.g., more energy is necessary for an equilibrium to be reached), as shown in Figure 5.1. Over time, macroscopic phase separation slowly develops. A clear, water-like supernatant continues to grow as the solution sits. The basin is not agitated during this process in an effort to allow diffusion to control the complex formation. When this mixture is vigorously stirred, the viscous polymer-rich phase abruptly precipitates to the bottom of the container. Due to the varied and irregular structure of the branched PEI (containing an assortment of primary, secondary and tertiary amine groups), the configuration of the polyelectrolyte complex is not stoichiometrically defined here. Electrostatic attraction and entropy drive the PEC formation, and result in the release of sodium counterions from PSP in exchange for stronger ionic bonding with protonated amine groups on PEI. As the polyelectrolyte complex domains grow, charged sites are neutralized and gravity overcomes electrostatic and/or steric stabilization that results in macroscopic phase separation.

The polyethylenimine/poly(phosphate sodium salt) system has two variables that strongly influence its deposition onto a fabric: solution pot life and soak time. Soaking fabric in longer standing mixtures allows greater coating pickup to be attained in a shorter time due to increasing viscosity. In this study, solution pot life was limited to 30 min. By submerging fabrics at the latter end of the solution life, the soak time necessary to obtain sufficient coating weight gain was reduced. Fabrics were immersed in the mixture at 15, 20, 25 and 29 min after the OnePot system was created, which means they were soaked in the flame retarding solution for 15, 10, 5 and 1 min, respectively (see Figure 5.1 for the submersion time diagram and a sequence of pictures demonstrating the coating process). Weight gain of the PSP/PEI complex on the fabric increases linearly as a function of soak time, as shown in Figure 5.2. The cotton fabric was presoaked in pH 2 deionized water to increase the positive surface charge on the cellulose.[298] Five swatches of fabric (9.5 in. x 16.5 in.) were coated at each soak time, with each piece wide enough for two vertical flame test panels (3 in. x 12 in.). Coating weight on fabric increased from 2.0 – 35.0 wt% as a function of soak time (1-15 min). The fabric with weight gain closest to the median coating addition was chosen for micro combustion calorimetry (MCC), scanning electron microscopy (SEM), and thermogravimetric analysis (TGA). SEM micrographs of the control and coated fabric, shown in Figure 5.3, illustrate the weave structure is maintained, even with 35.0 wt% coating addition. The coating appears to adhere conformally around individual fibers, although some fiber bridging is observed at higher weight additions. For 1, 5, and 10 min soak times, increased coating weight directly corresponds to improved flame retardancy.

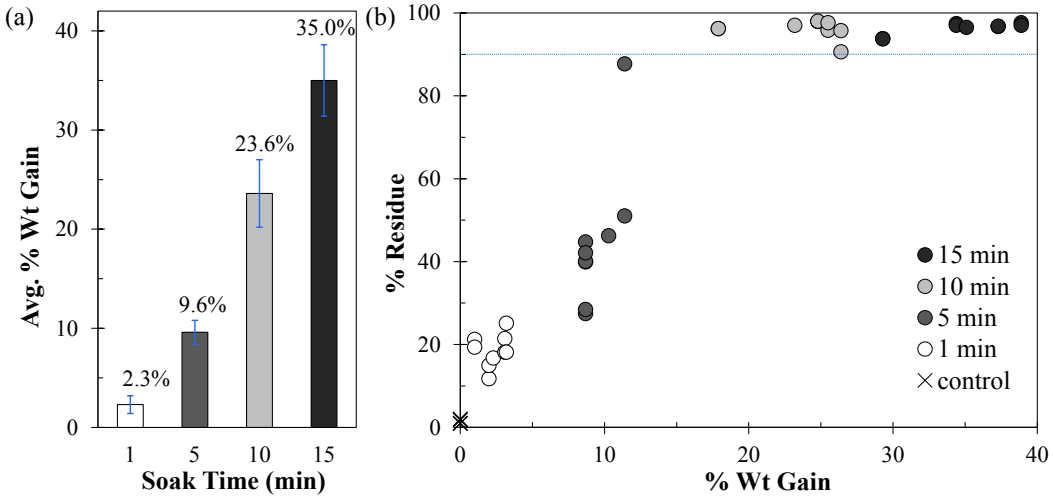

Figure 5.2. a) PSP/PEI weight gain (average weight of five coated fabrics) as a function of soak time. b) Residue remaining after vertical flame testing as a function of PSP/PEI weight gain (expressed as percent of total coated fabric weight). Nine VFT samples are plotted for each soak time.

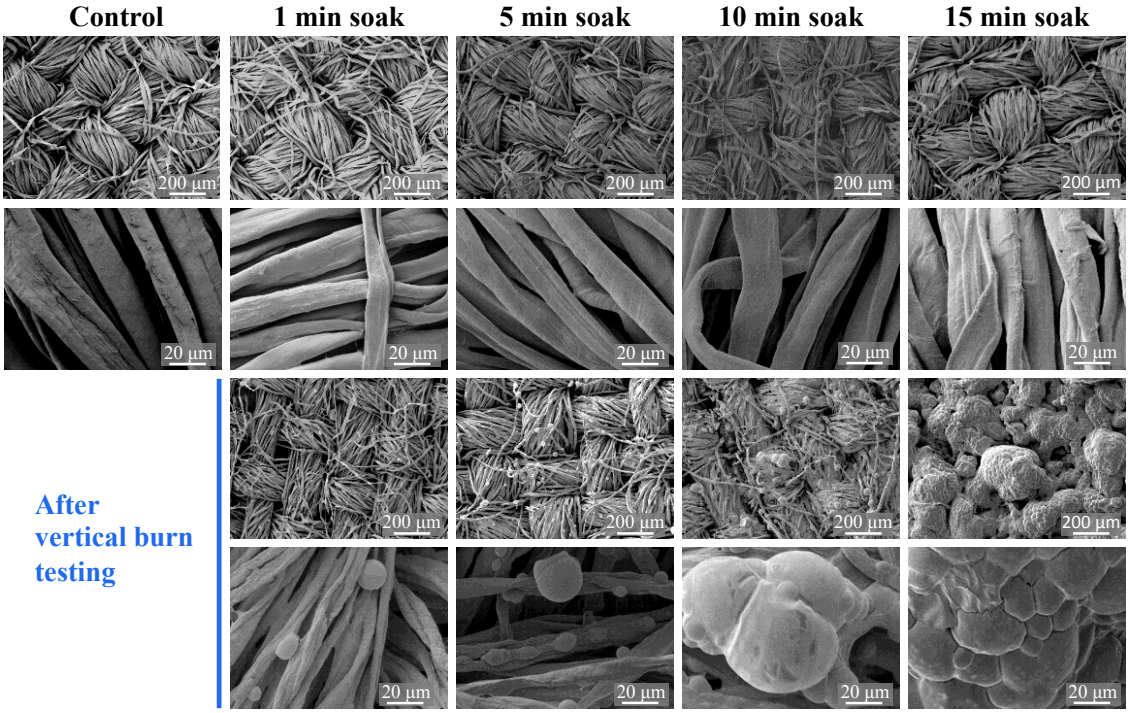

Figure 5.3. SEM images of uncoated cotton fabric and fabric soaked in the PSP/PEI OnePot solution for 1, 5, 10 and 15 min before (top) and after (bottom) vertical flame testing. There is no image for the control fabric after VFT because no material remained (i.e., cotton is completely consumed by fire during testing).

5.3.2 Flame Retardant Behavior of OnePot Nanocoating

Control fabric and PSP/PEI coated cotton samples were heated from ambient temperature up to 600 °C in oxidizing conditions using a thermogravimetric analyzer at a controlled heating ramp of 20 °C/min. The decreasing slopes on the overlaid thermal curves in Figure 5.4a indicate mass is lost as a function of temperature. In comparison to the uncoated cotton, coated fabric exhibits an earlier onset degradation temperature. The OnePot nanocoating is designed to alter the combustion cycle of cellulose through the condensed phase mechanism, known as intumescence. Since heat initiates this phenomenon and transforms the nanocoating into a swollen, insulating barrier, it is

expected (and desired)[234-235] that the onset degradation temperature of the coated fabric occurs prior to that of untreated cotton. At 550 °C, the control fabric is completely consumed. Percent residue retained for coated fabrics increases with coating weight, and is greater than the amount of FR nanocoating applied (see Figure 5.5). These results suggest this combination of intumescent coating and cellulose were converted to a less combustible material upon heating.

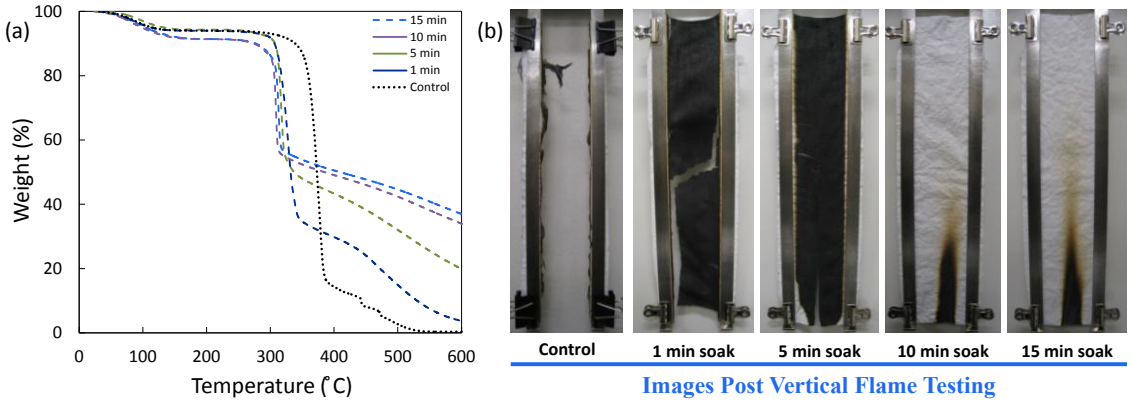

Figure 5.4. a) Weight loss as a function of temperature for uncoated (control) fabric and fabric soaked for various times in the PSP/PEI complex, measured in an oxidizing atmosphere. b) Images of control and coated fabrics after vertical flame testing.

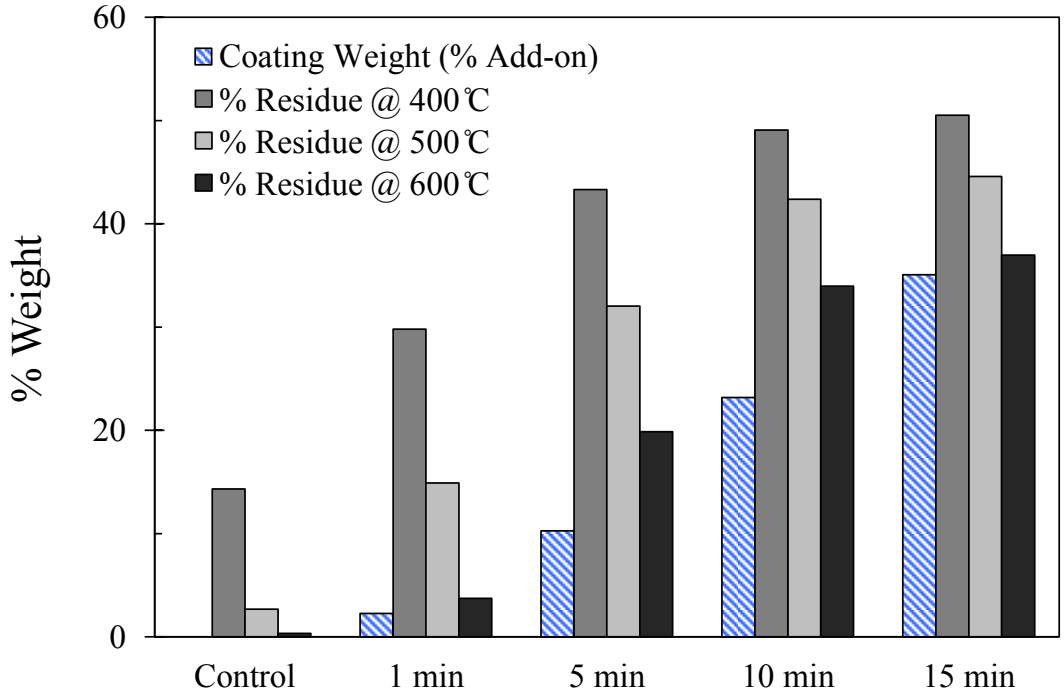

Figure 5.5. Blue striped bars represent the % add-on of coating and grayscale bars represent the % residue remaining at 400°C, 500°C, and 600°C (from TGA testing).

During vertical flame testing (VFT), uncoated cotton ignites, is engulfed in flame, and is completely consumed (see post-test image in Figure 4b). Ashes along holder edges radiate with afterglow for an average of 21 sec. None of the coated fabrics exhibited afterglow when the flame was removed. The % residue of VFT samples (9 per soak time) are plotted against % weight gain of the nanocoatings in Figure 2b. Fabric soaked for 1 min (2.3 wt% average coating) has 18.5 wt% residue that indicates cotton is incorporated into the char. Figure 5.2 also shows that 5 min soaked fabric, with an average of 9.6 wt% coating, displays a large standard deviation (~17.7 %) for residue, which ranges from 27.4% - 87.7%, suggesting this coating weight is near the threshold of passing the standard vertical flame test. Increasing coating weight on fabric

corresponds to increasing fire resistance, with maximum benefit occurring with a 10 min soak time (~23.6 wt% coating addition). Flames self-extinguished (i.e., fire propagation is halted) before the test flame was removed on all 10 and 15 min soaked VFT samples. On average, the char lengths for 10 and 15 min soak times are 3.2 ± 1.2 in. and 2.7 ± 0.9 in., respectively (see images in Figure 5.6). **Table 5.1** summarizes coating weight for the various samples tested.

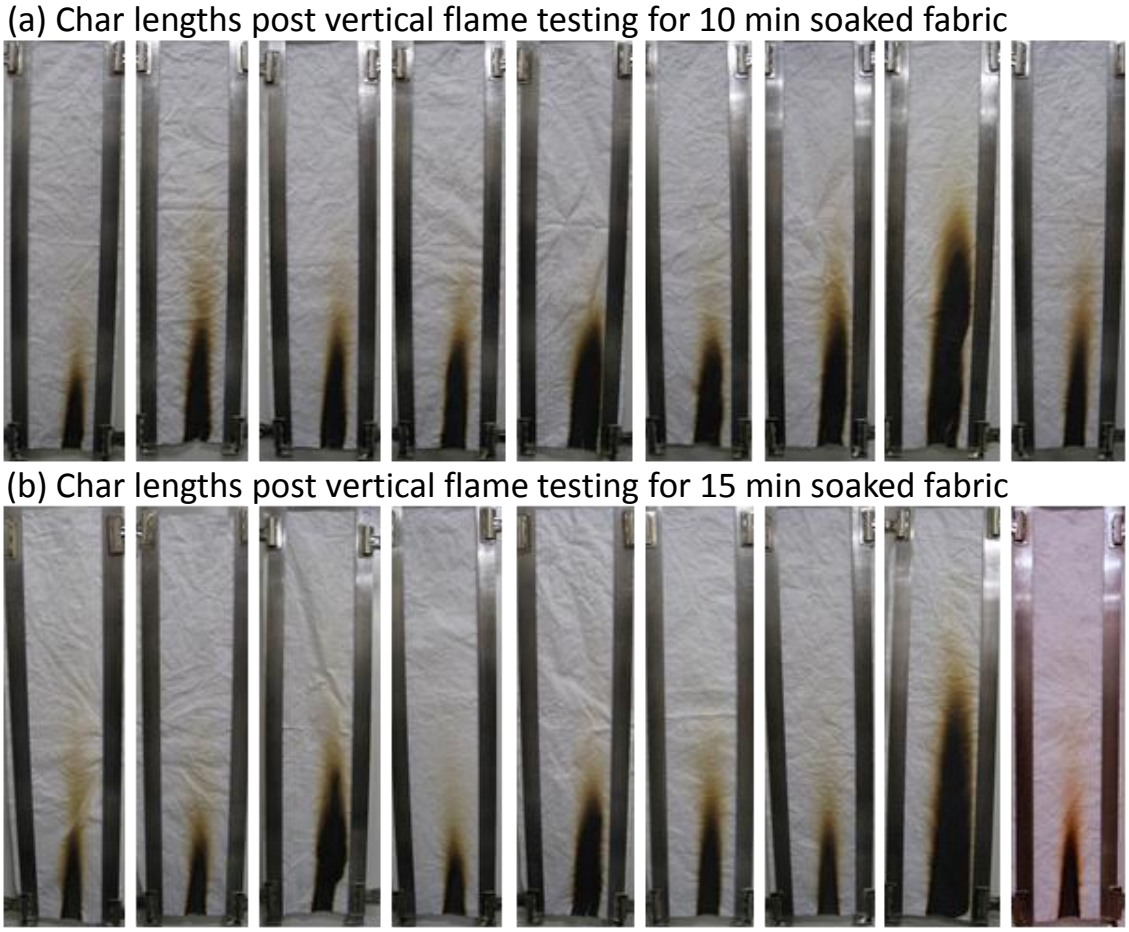

Figure 5.6. Images of OnePot coated samples following vertical flame testing, for cotton fabric soaked in PSP/PEI for a) 10 and b) 15 minutes.

Table 5.1. MCC Results for Uncoated Control and OnePot Coated Cotton Fabric.

OnePot	Wt Gain	Char Yield	pkHRR		pkHRR T	Total HR	Total HR Reduction
	[%]	[wt%]	[W/g]		[°C]	[kJ/g]	[%]
Control	---	7.0 ± 0.2	---	279 ± 5.7	383 ± 0.8	12.3 ± 0	---
1 min soak	2.3	26.5 ± 1.4	---	231 ± 2.6	324 ± 1.0	5.8 ± 0.1	52.7 ± 1.0
5 min soak	10.3	41.1 ± 1.1	9 ± 0	181 ± 3.5	317 ± 0.6	3.1 ± 0	74.8 ± 0
10 min soak	23.2	45.0 ± 0.7	18 ± 1.2	118 ± 2.9	315 ± 2.0	2.7 ± 0.1	77.8 ± 0.5
15 min soak	35.1	44.3 ± 1.2	22 ± 2.0	120 ± 11.2	315 ± 1.0	2.9 ± 0.1	76.2 ± 0.9
PAAm/PSP	Wt Gain	Char Yield	pkHRR		pkHRR T	Total HR	Total HR Reduction
	[%]	[wt%]	[W g^{-1}]		[°C]	[kJ/g]	[%]
Control	---	9.59 ± 0.61	253 ± 8.2		400 ± 1.3	11.7 ± 0.23	---
5 BL	1.6	23.83 ± 1.96	146 ± 14.5		306 ± 2.7	5.8 ± 0.4	54.4
10 BL	6.0	31.43 ± 0.06	97 ± 7.1		303 ± 4.7	2.9 ± 0.12	75.2
20 BL	17.5	31.07 ± 0.38	92 ± 16.2		307 ± 4.7	3.8 ± 0.17	67.5
			17 ± 2.1		415 ± 1.2		
PA/CH	Wt Gain	Char Yield	pkHRR		pkHRR T	Total HR	Total HR Reduction
[pH 4]	[%]	[wt%]	[W/g]		[°C]	[kJ/g]	[%]
Control	---	5.6 ± 0.1	259 ± 6.7		382 ± 2.1	12.0 ± 0.1	---
32 BL	18.0	42.4 ± 0.3	100 ± 1.8		313 ± 0.8	2.8 ± 0.1	76.7

Figure 5.3 shows high resolution micrographs of these fabric samples before and after vertical flame testing, which provide information about how heat and/or direct flame alter the nanocoating. Despite flames propagating up the entire length of OnePot-coated fabrics with weight addition less than or equal to 11.4 wt%, weave structure is maintained for all coated fabrics post burn. Bubbles are present even at the lowest evaluated soak time (1 min with ~2.3 wt% coating addition). Post burn images of 10 min soaked fabric reveal how the coating intumesces around the fibers to form a protective thermal barrier. The weave structure of fabric prepared with 15 min soak times is indistinguishable as the excess coating swells, expands, and coalesces over fibers.

Uncoated cotton and fabric soaked for 1, 5, 10, and 15 min were tested with a micro combustion calorimeter to evaluate heat release rates. Flammability describes a material's propensity to ignite and/or combust and is evaluated using 'reaction-to-fire

tests' under specific heat fluxes.[256] Heat release describes the liberation of heat that is a driving force for fire. The rate at which this exothermic chemical reaction is produced is defined as the heat release rate (HRR) and is used to predict fire hazards of specific materials. Fire spreads across cotton fabric very quickly, largely reducing the wearers ability to remove a clothing item before injury occurs.[299] Just like with TGA (Figure 4a), MCC data reveals that OnePot nanocoatings, regardless of amount, decrease the onset degradation temperature of the fabric relative to uncoated cotton. Figure 5.7 shows heat release rates as a function of temperature for various cotton samples. Even though the ignition temperature is decreased, all coated fabric reduced peak heat release rates and total heat release, which suggests disruption and alteration of cellulose's combustion cycle. A 1 min soaked sample, with only 2.3 wt% coating, dramatically reduces the total heat release (52.7%) in comparison to uncoated cotton. Reductions in peak and total heat release lower the risk of other combustible items being ignited and add time for escape from a hazardous situation. Whereas 5 min soaked fabrics (10.3 wt% add-on) reduce pkHRR temperatures by 35.0%, 10 min soaked fabrics (23.3 wt% add-on) reduce pkHRR more than 57.0%. The extra coating achieved by increasing soak time from 5 to 10 min yields only nominal increases in char yield (9.5%) and total heat release reduction (4.0%), but significantly drops the pkHRR (by an additional 34.8%) down to 118 W/g. Although 10 and 15 min soak times have the lowest peak heat release rate temperatures, a shoulder in the HRR curve can be seen in the temperature range of 250-300 °C (shown as a second pkHRR in Table 5.1). This shoulder indicates pyrolysis and suggests coating and/or cotton is burning. The extra coating addition for 15 min soaked

fabric actually results in a slight worsening of overall performance. Fabrics soaked for 5 min in the OnePot solution yield the best performance in an inert atmosphere when evaluations couple processing time and added weight with burn behavior.

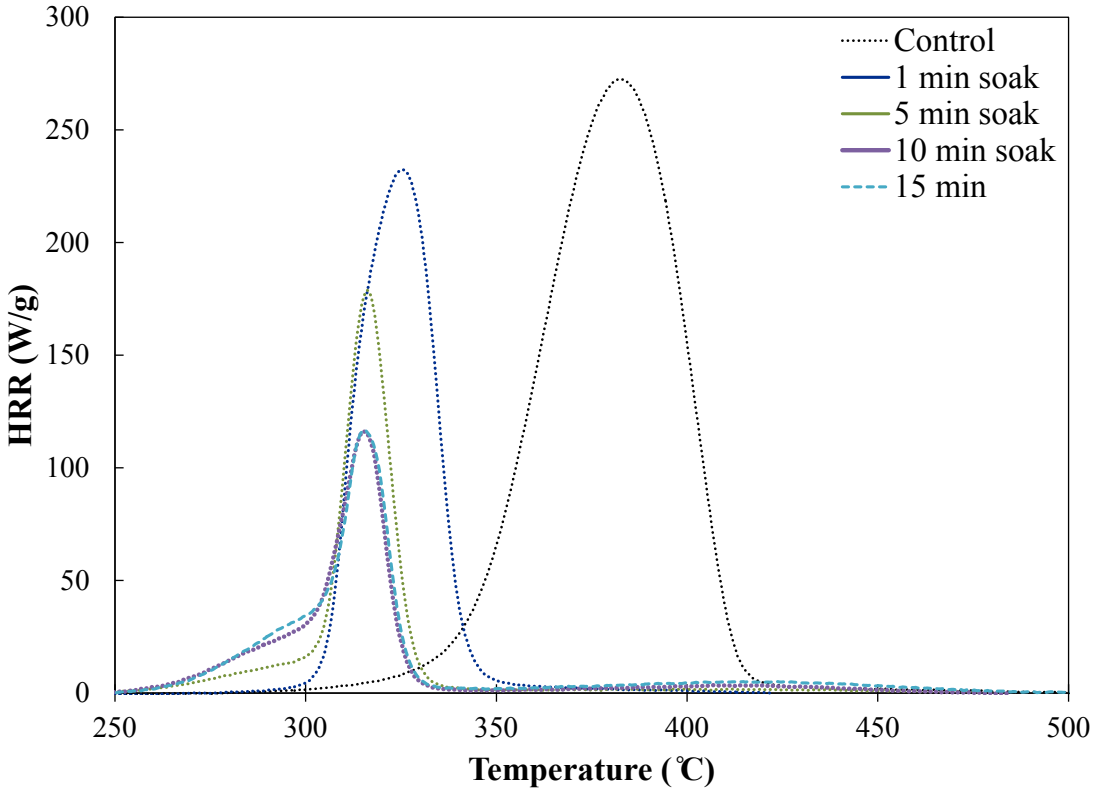

Figure 5.7. Heat release rate as a function of temperature, measured with a micro combustion cone calorimeter, for control and OnePot coated cotton fabric.

Cotton fabric, as depicted in vertical flame and calorimetry testing, is very flammable. Cellulose degrades into a heavy tar in a temperature range of 280-340 °C and then further decomposes into combustible volatiles and char.[300] Vertical flame tests are run in ambient conditions, which allows for organic materials to be oxidized (i.e.,

oxygen catalyzes cellulose decomposition). Control fabric subjected to MCC testing, which is performed in an inert atmosphere, is able to retain an average of 7.0 wt% char that is noticeably shrunken. Residues of all fabrics post VFT and MCC testing are shown in Figures 5.6 and Figure 5.8 for visual comparison. Coating weight additions up to 23.6 wt% retain more char (45.0%) and reduce peak heat release rates and total heat release by 57.7% and 77.8%, respectively. Upon the application of heat, this intumescent coating transforms into a swollen and expanded thermal barrier of phosphorocarbonaceous cellular material. Elemental analysis of coated fabric post vertical flame testing, confirmed the presence of phosphorous, oxygen, and carbon (nitrogen was detected in some areas) in the residues. This protection mechanism functions in the condensed phase as it promotes char formation that locks the fuel source into a non-pyrolyzable thermal insulation.[81] It is believed that the acid source (PSP) degrades the carbon donor (PEI and/or cotton) and induces crosslinking. Amine pendant groups on polyethylenimine decompose into nitrogen-containing gas and act as the blowing agent that foams the forming char.[81, 301] Evidence of swelling and foamed char is clearly observed in SEM micrographs of coated fabric after vertical flame testing (Figure 3). Increases in char yield in MCC testing quantitatively demonstrate modification of the cellulose degradation pathway and provide evidence of an enhanced thermal barrier upon increasing addition of this nanocoating.

A comparison of published intumescent nanocoatings on cotton (OnePot, PAAm/PSP, and PA/CH) is shown in Table 5.1. Due to differing test temperature ranges (150-550 °C, 200-600 °C, 200-700 °C, respectively), char yield between sample sets is

not directly comparable. With that said, all of these systems achieve heat release rates near zero at high temperature, which validates the comparison of pkHRR and THR between the present polyelectrolyte complex (OnePot) and the layer-by-layer coated assemblies (PAAm/PSP and PA/CH). Fabrics coated with 20 BL of PAAm/PSP (the first all-polymer intumescing system created via LbL) reduced pkHRR to ~92 W/g (63.6% reduction) and THR to ~3.8 kJ/g (67.5% reduction) with 17.5 wt% coating. Fabrics coated with 32 BL of PA/CH (the first renewable polyelectrolyte intumescing multilayer system) are able to achieve similar reduction in pkHRR (~100 W/g, 61.4% reduction) and THR (2.8 kJ/g, 76.7% reduction) with ~ 18% coating addition. If coated by hand, it would take approximately 68 min to coat 20 BL and 104 min to coat 32 BL using the procedure described in these studies. Fabric soaked for 10 min in the OnePot polyelectrolyte complex reduces the pkHRR down to 118 W/g (57.7% reduction) and THR to 2.7 kJ/g (78.0% reduction) with 23.6 wt% coating addition.

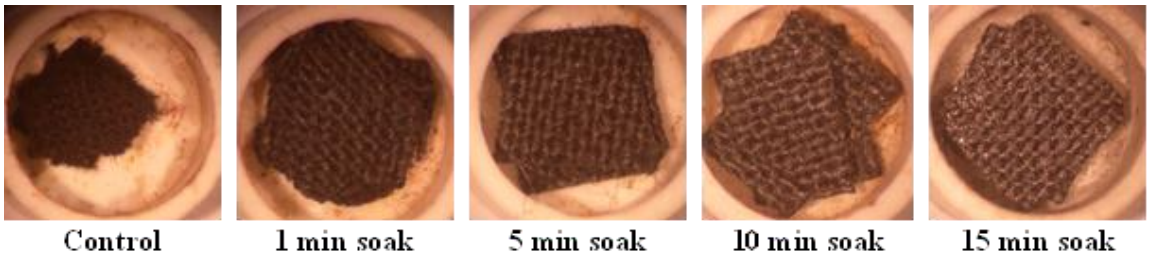

Figure 5.8. Char/residue of control and OnePot coated fabric following micro combustion calorimetry testing.

5.4 Conclusions

An aqueous polyelectrolyte complex comprised of branched polyethylenimine and poly(phosphate sodium salt), was deposited on cotton fabric, in an effort to impart flame retardant behavior in a single deposition step. Fabric soaked in this aqueous complex for 1, 5, 10, and 15 min generated nanocoatings with average weight additions of 2.3, 10.3, 23.2, and 35.1%, respectively. Flame retarding behavior of these OnePot-treated fabric swatches was evaluated with TGA, VFT, and MCC testing. SEM images taken prior to flame testing indicate the polyelectrolyte complex conformally coats individual fibers, maintaining the weave structure of the textile, while post-burn images confirm the intumescent action of these coatings. Cotton soaked for 1 min obtained a 2.3 wt% coating addition, which resulted in a 16.7% residue after vertical flame testing and a 52.7% reduction in total heat release in comparison to uncoated cotton in MCC. Nanocoatings produced from a 10 min immersion result in fabric capable of self-extinguishing during vertical flame testing. This environmentally-benign PSP/PEI complex deposits on fabric in one simple step, to impart exceptional FR performance. There is ample opportunity to expand the types of electrolytes and textiles used to demonstrate the universality of this approach in future studies.

CHAPTER VI

CONCLUSIONS AND FUTURE WORK

6.1 Flame Retardant Thin Film Assemblies

It has increasingly become more challenging to develop effective and safe flame retarding solutions as industries phase out halogen-containing flame retardants, such as decabromodiphenyl ether. The ultimate goal of this dissertation was to explore suitable materials to build nanostructured thin films that impart anti-flammable behavior to polyurethane foam and cotton fabric. The layer-by-layer assembly technique was used to control composition and tune thin film architectures, deposited directly on to complex polymeric substrates, to reduce heat and smoke release. Aqueous polyelectrolyte coacervation was also explored as a 'OnePot' coating technique to deposit an intumescing nanocoating around fibers in one quick processing step. This work provides unprecedented new approaches for imparting flame resistance using environmentally-benign components in an efficient manner that minimizes processing steps and the time necessary to deposit the nanocoating.

6.1.1 Phosphorous-filled Nanobrick Wall Assemblies

Intumescing nanobrick wall assemblies comprised of nitrogen and phosphorus-containing polymers (mortar) and clay platelets (bricks) were deposited on a silicon wafer and polyurethane foam using layer-by-layer assembly. When exposed to 10 s of direct contact with a butane torch, the coating swells around the polyurethane cell walls

and smothers the flame. With only 4 TL (~20 nm thick and ~3 wt% added to foam), foam samples retain their shape, melt dripping is eliminated, and heat release rate is reduced by 54% (compared to uncoated foam). Not only does this protective coating distinguish itself from traditional nanobrick wall films by being comprised of three deposited layers (comprised of repeating 'trilayers'), it also transforms the passive nature of the polymeric mortar into an active intumescing polyelectrolyte pair. These results demonstrate a viable, non-halogenated and environmentally-benign flame retarding solution that combines two flame-retarding mechanisms into a single nanocoating system.

6.1.2 Few Clay Layer Nanocoatings

Nanobrick wall thin films comprised of polymeric mortar and montmorillonite or vermiculite clay bricks were deposited as a continuous coating on porous polyurethane to investigate the effect of nanoplatelet aspect ratio and elemental composition on multilayer growth and structural composition. Clay-filled polymer nanocomposites are traditionally condensed phase flame retardants, meaning carbonaceous-silicate char forms to insulate the underlying material and slow mass loss rate. When comparing fire behavior as a function of layers deposited, superior fire protection of VMT-based thin films over MMT-systems is primarily attributed to a higher content of larger aspect ratio nanoplatelets. When weight of the nanocoating is normalized, 4BL MMT-based walls better suppress peak, total and average heat release rate, and total heat and smoke release of control polyurethane relative to a 1 BL VMT-based nanobrick wall. This result

suggests that the effect of aspect ratio diminishes as the number of MMT clay platelets within the nanocoating increases. A particularly unique aspect of the development of this single bilayer flame retarding solution, that cuts peak HRR of polyurethane in half with only 3.2% mass addition, is that the number of processing steps to create the halogen-free, fire protective coating is commercially feasible.

6.1.3 OnePot Intumescent Nanocoating

Aqueous coacervation was investigated as a single step process to quickly deposit flame retardant nanocoatings on textiles. Fabric was soaked in a phosphorous- and nitrogen-rich polyelectrolyte complex comprised of PSP and PEI as a function of time (1, 5, 10, and 15 min) and solution pot life. Nanocoating weight addition increased with increasing time in the 'OnePot' flame retarding complex. Upon the application of heat, the nanocoating around the fibers intumesces into a multicellular, phosphorocarbonaceous heat shield. Micro calorimetry data demonstrates cotton fabric soaked for only 1 minute exhibits a 52.7% reduction in total heat release, with only 2.3 wt% coating added. Flames self-extinguished (i.e., fire propagation is halted) before the test flame was removed on all 10 min soaked samples during vertical flame testing. This OnePot concept provides an unprecedented new approach for imparting flame resistance to textiles using environmentally-benign components in a way that minimizes processing steps and the time necessary to deposit the nanocoating.

6.2 Future Research Direction

Chapters III and IV demonstrated thin films uniquely constructed (by changing the polymeric mortar chemistry and clay brick type) to work via the condensed phase flame retarding mechanism. The flame retardant thin films conformally coated porous polyurethane surfaces and trapped polymeric material within a ceramic shell and eliminated melt dripping. The ability to impart a similar heat barrier to thermoset fabric, which typically has a higher onset degradation temperature than cotton fabric, and degrades and melt drips when heated to a critical temperature, could be achieved by coating fabrics with a system that intumesces and traps the melting polymer within an insulating char. Nanofibrillated cellulose is an interesting building block material that could be used to create a self-extinguishing, swollen system from renewable resources. Additionally, there is significant interest in carbon-based materials to produce highly conductive networks due to the delocalized electrons in sp^2 hybridized bonds. Understanding how thin, percolated networks could be used as a flame retardant that transfers and conducts away heat also needs to be investigated. It would be interesting to develop a non-halogenated and environmentally-benign flame retarding solution that combines flame retardant and antistatic properties into a single nanocoating system. Finally, increasing the durability of these nanocoatings to survive repeated washings cycles would improve the prospect of commercialization of these layer-by-layer assembled thin films on fabric. These areas of future research are described in more detail below.

6.2.1 Cationic-nanofibrillated Cellulose/Phosphorous Nanocoatings

Wood pulp fibers, which are 1-3 mm in length and 10-50 μm in width,[302] are an important natural resource used in the paper and packaging industries. Recent investigations have incorporated these fibers into a composite to enhance mechanical properties using low density materials. Cellulose fibers have a multi-level organization of microfibrils (structures with dimensions less than 1 μm),[303] which can be chemically processed and/or mechanically separated down to smaller dimensions (e.g., cellulose whiskers, cellulose nanocrystals, nanofibrillated cellulose, etc.). Pairing surface functionality with cellulose's abundance, durability, and good mechanical properties, makes this biomass an attractive resource to be incorporated into thin films for a variety of applications (e.g., gas barriers, thermo-responsive nanocontainers, and antimicrobial multilayers).[302, 304] In a future study, the cationic nanofibrillated cellulose (NFC) dispersion will be prepared from a slurry of bleached, softwood sulfite dissolving pulp, which will be modified with N-(2,3 epoxypropyl)trimethylammonium chloride (EPTMAC) (as shown in Figure 6.1), homogenized, and exfoliated into individual nanofibrils at the Royal Institute of Technology in Sweden (KTH) by Dr. Lars Wagberg's group. These amine-modified NFC will be paired with poly(phosphate sodium salt), and applied on blended polyester/cotton fabric via layer-by-layer assembly. Weight gain and fire behavior of the nanocoatings can be evaluated as a function of the number of bilayers deposited (from 5-20 BLs). These thin, water-based nanocoatings have the potential to protect complex substrates that melt drip when exposed to high heat using environmentally-friendly components.

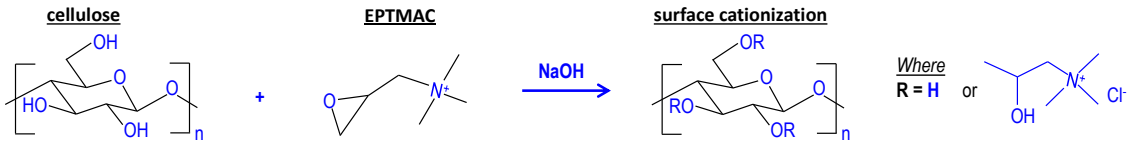

Figure 6.1. Schematic of nucleophilic addition of the alkali-activated cellulose hydroxyl groups to the epoxy moiety of EPTMAC.

6.2.2 Pyrene-modified Polyelectrolytes/MWNT Assemblies

Chapter III and IV demonstrated that LbL assembled polymer-clay thin films, deposited along the surface of the substrate, combat fire in the condensed phase.[250] In this case, the platelets strengthen the fire blocking residue and provide a heat shield.[262, 267] Although concentrating inorganic platelets to the outer surface of polymeric substrates significantly reduces heat in cone calorimetry testing,[32] when a torch is applied, flame propagation is not immediately halted. A flame flashes over the surface and burns away polymer mortar in the nanocoating and the underlying substrate until the inorganic shield begins reducing heat and suffocates the flame. Several studies have reported a decrease in heat release when a small volume fraction of sp^2-hybridized material is added within the polymer matrix or in a polymer nanocoating.[16, 238, 305] Reductions in flammability are attributed to char reinforcement and reduction in crack formation within the char. With a simple reductive amination reaction, pyrene groups can be added to polyethylenimine, as shown in Figure 6.2, to enhance dispersion of CNTs (through stronger interaction) and increase char formation during combustion.[306-307] Nanocoating combinations of PEI-pyrene and PAA, in which one, both, or neither of the polyion solutions have multi-walled carbon nanotubes (MWNTs) dispersed, could be

evaluated with horizontal and vertical flame testing, cone calorimetry, and TGA to determine fire behavior, and their effect on heat release, smoke density, and smoke toxicity.

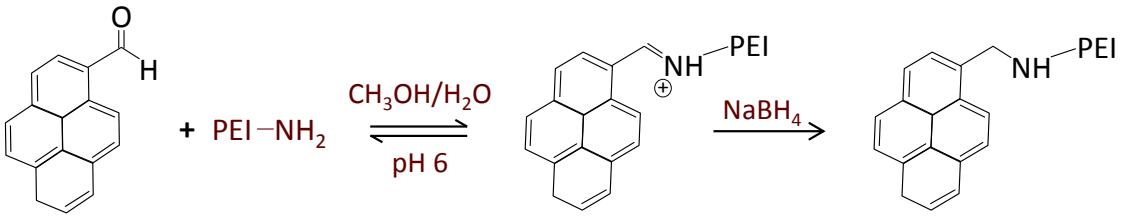

Figure 6.2. Schematic representation of the synthesis of PEI-pyrene.

Preliminary data suggests CNT-based assemblies provide superior fire protection to polyurethane foam in comparison to MMT-based nanobrick wall thin films. Carbon nanotube-containing recipes reduce the pkHRR by at least 67% ± 1.9% and the TSR by at least 76% ± 2.2%, relative to uncoated foam. Normalized cone data reveals recipes containing carbon nanotubes (PEI-py+MWNT/PAA+MWNT, PEI-py+MWNT/PAA, and PEI-py/PAA+MWNT) also have the same performance/g. Normalized data is defined as the fire performance quantity (i.e., pkHRR, avg HRR, THR, TSR, and avg. Eff Hc) divided by the weight of the individual sample before testing. Further flammability testing should be made with PEI-pyrene/PAA+MWNT because it has the lowest weight percent addition of the carbon nanotube-containing thin films. These non-halogenated nanocoatings would be highly marketable if, in addition to effectively reducing heat release in cone calorimetry testing, they are able to pass vertical flame testing.

6.2.3 Wash Durability of Nanocoating on Cotton Fabric

It was previously discovered that a LbL multilayer of poly(diallyldimethyl ammonium chloride) (PDDA) and multi-walled carbon nanotubes stabilized with sodium deoxycholate (DOC), deposited on PET film, creates a thin nanocoating with sheet resistance of 104 Ω/□ and visible light transmittance of 84%.[48] When applied to a complex, 3D substrate such as cotton fabric, this conductive nanocoating improves conductivity by 5 orders of magnitude relative to uncoated cotton, which is suitable for antistatic applications.[308] The decrease in sheet resistance indicates that the network formed around the individual fibers is at or above the percolation threshold (see Appendix A for more details regarding this conductive recipe and an important proof of concept for commercial-scale, continuous processing of LbL nanocoatings). In order for this nanocoating to be implemented as an antistatic coating, the applied thin film needs to be mechanically robust.

The pyrene-modified polyelectrolyte-MWNT recipe (see Section 6.2.2) as a novel flame retardant nanocoating, also forms a conductive network. Unlike the first conductive thin film, functional groups (i.e., amine pendant groups on PEI and carboxylic acid groups on PAA) present on both the anionic and cationic components within this thin film could be crosslinked to create covalent linkages between polymer chains, which enhances mechanical robustness.[309-310] Schiff base linkages (N=C) between uncharged primary amine groups could be created.[311] It is also possible to form amide bonds between primary amines and carboxyl groups with chemical (i.e., carbodiimide chemistry)[312] or thermal crosslinking.[313] In addition to evaluating the effect

of various temperatures or the chemical crosslinking agent type, exposure time, and concentration of the crosslinking agent need to be considered. One method to evaluate the durability of the crosslinked coatings is to measure fire performance and electrical conductivity before and after being laundered in a washing machine for 5, 10, and 20 cycles, relative to a set of coated samples that were not crosslinked. Wash durability testing can be performed according to American Association of Textile Chemists and Colorists, Test Method 124-2006.[314] LbL thin films with covalent bonds are more robust and less susceptible to being destroyed when exposed to detergent. Clothing that provides electrostatic shielding from non-lethal weapons such as Tasers and stun guns, and outdoor camping equipment are two distinct applications for which there is significant importance for a thin film with both antistatic and anti-flammable properties to remain unaffected after washing.

REFERENCES

1. Quintiere, J. G., The Evolution of Fire Science. In *Principles of Fire Behavior*, Huth, M.; Mesick, J.; Daugherty, D., Eds. Delmar: Albany, NY, 1998; pp 2-23.

2. Gharehbagh, A.; Ahmadi, Z., Polyurethane Flexible Foam Fire Behavior. In *Polyurethane*, Zafar, F.; Sharmin, E., Eds. InTech: 2012; pp 101-120. http://www.intechopen.com/books/polyurethane/polyurethane-flexible-foam-fire-behavior.

3. Hull, T. R.; Stec, A. A., Polymers and Fire: Chemical and Physical Processes. In *Fire Retardancy of Polymers: New Strategies and Mechanisms*, Hull, T. R.; Kandola, B. K., Eds. RCS: Cambridge, U.K., 2009; pp 1-14.

4. Laoutid, F.; Bonnaud, L.; Alexandre, M.; Lopez-Cuesta, J.-M.; Dubois, P., New Prospects in Flame Retardant Polymer Materials: From Fundamentals to Nanocomposites. *Materials Science and Engineering: R: Reports* **2009,** *63*, 100-125.

5. Buser, H. R., Polybrominated Dibenzofurans and Dibenzo-p-dioxins: Thermal Reaction Products of Polybrominated Diphenyl Ether Flame Retardants. *Environmental Science & Technology* **1986,** *20*, 404-408.

6. Jansson, B.; Asplund, L.; Olsson, M., Brominated Flame Retardants — Ubiquitous Environmental Pollutants? *Chemosphere* **1987,** *16*, 2343-2349.

7. Rahman, F.; Langford, K. H.; Scrimshaw, M. D.; Lester, J. N., Polybrominated Diphenyl Ether (PBDE) Flame Retardants. *Science of the Total Environment* **2001,** *275*, 1-17.

8. Bonati, A.; Merusi, F.; Bochicchio, G.; Tessadri, B.; Polacco, G.; Filippi, S.; Giuliani, F., Effect of Nanoclay and Conventional Flame Retardants on Asphalt Mixtures Fire Reaction. *Construction and Building Materials* **2013,** *47*, 990-1000.

9. Witkowski, A.; Stec, A. A.; Richard Hull, T., The Influence of Metal Hydroxide Fire Retardants and Nanoclay on the Thermal Decomposition of EVA. *Polymer Degradation and Stability* **2012,** *97*, 2231-2240.

10. Laoutid, F.; Lorgouilloux, M.; Lesueur, D.; Bonnaud, L.; Dubois, P., Calcium-based Hydrated Minerals: Promising Halogen-free Flame Retardant and Fire Resistant Additives for Polyethylene and Ethylene Vinyl Acetate Copolymers. *Polymer Degradation and Stability* **2013,** *98*, 1617-1625.

11. Hull, T. R.; Witkowski, A.; Hollingbery, L., Fire retardant action of mineral fillers. *Polymer Degradation and Stability* **2011,** *96*, 1462-1469.

12. Hamdani, S.; Longuet, C.; Perrin, D.; Lopez-cuesta, J.-M.; Ganachaud, F., Flame Retardancy of Silicone-based Materials. *Polymer Degradation and Stability* **2009,** *94*, 465-495.

13. Kashiwagi, T.; Morgan, A. B.; Antonucci, J. M.; VanLandingham, M. R.; Harris, R. H.; Awad, W. H.; Shields, J. R., Thermal and Flammability Properties of a Silica–Poly(methylmethacrylate) Nanocomposite. *Journal of Applied Polymer Science* **2003,** *89*, 2072-2078.

14. Periadurai, T.; Vijayakumar, C. T.; Balasubramanian, M., Thermal Decomposition and Flame Retardant Behaviour of SiO2-phenolic Nanocomposite. *Journal of Analytical and Applied Pyrolysis* **2010,** *89*, 244-249.

15. Chattopadhyay, D. K.; Webster, D. C., Thermal Stability and Flame Retardancy of Polyurethanes. *Progress in Polymer Science* **2009,** *34*, 1068-1133.

16. Kashiwagi, T.; Grulke, E.; Hilding, J.; Harris, R.; Awad, W.; Douglas, J., Thermal Degradation and Flammability Properties of Poly(propylene)/Carbon Nanotube Composites. *Macromolecular Rapid Communications* **2002,** *23*, 761-765.

17. Kashiwagi, T.; Du, F.; Douglas, J.; Winey, K.; Harris, R.; Shields, J., Nanoparticle Networks Reduce the Flammability of Polymer Nanocomposites. *Nat Mater* **2005,** *4*, 928-933.

18. Hapuarachchi, T. D.; Peijs, T.; Bilotti, E., Thermal Degradation and Flammability Behavior of Polypropylene/Clay/Carbon Nanotube Composite Systems. *Polymers for Advanced Technologies* **2013,** *24*, 331-338.

19. Lecouvet, B.; Sclavons, M.; Bourbigot, S.; Bailly, C., Highly Loaded Nanocomposite Films as Fire Protective Coating for Polymeric Substrates. *Journal of Fire Sciences* **2014,** *32*, 145-164.

20. Chen, S.; Sun, B.; Huang, G.; Guo, H.; Wang, S., Effects of an (Intumescent Flame Retardant)-Montmorillonite Combination on the Thermal Stability and Fire-retardant Properties of LDPE/EVA Nanocomposites. *Journal of Vinyl and Additive Technology* **2013,** *19*, 285-292.

21. Park, Y. T.; Qian, Y.; Lindsay, C. I.; Nijs, C.; Camargo, R. E.; Stein, A.; Macosko, C. W., Polyol-assisted Vermiculite Dispersion in Polyurethane Nanocomposites. *Acs Appl Mater Inter* **2013,** *5*, 3054-3062.

22. Isitman, N. A.; Kaynak, C., Nanoclay and Carbon Nanotubes as Potential Synergists of an Organophosphorus Flame-retardant in Poly(methyl methacrylate). *Polymer Degradation and Stability* **2010,** *95*, 1523-1532.

23. Winey, K. I.; Vaia, R. A., Polymer Nanocomposites. *MRS Bulletin* **2007,** *32*, 314-322.

24. Morgan, A. B., Flame Retarded Polymer Layered Silicate Nanocomposites: A Review of Commercial and Open Literature Systems. *Polymers for Advanced Technologies* **2006,** *17*, 206-217.

25. Leszczynska, A.; Njuguna, J.; Pielichowski, K.; Banerjee, J. R.; Leszczyńska, A., Polymer/Montmorillonite Nanocomposites with Improved Thermal Properties. *Thermochimica Acta* **2007,** *454*, 1-22.

26. Tang, Y.; Hu, Y.; Wang, S.; Gui, Z.; Chen, Z.; Fan, W., Intumescent Flame Retardant–Montmorillonite Synergism in Polypropylene-Layered Silicate Nanocomposites. *Polymer International* **2003,** *52*, 1396-1400.

27. Hu, Y.; Wang, S.; Ling, Z.; Zhuang, Y.; Chen, Z.; Fan, W., Preparation and Combustion Properties of Flame Retardant Nylon 6/Montmorillonite Nanocomposite. *Macromolecular Materials and Engineering* **2003,** *288*, 272-276.

28. Zanetti, M.; Kashiwagi, T.; Falqui, L.; Camino, G., Cone Calorimeter Combustion and Gasification Studies of Polymer Layered Silicate Nanocomposites. *Chem Mater* **2002,** *14*, 881-887.

29. Qin, H. L.; Zhang, S. M.; Zhao, C. G.; Hu, G. J.; Yang, M. S., Flame Retardant Mechanism of Polymer/Clay Nanocomposites Based on Polypropylene. *Polymer* **2005,** *46*, 8386-8395.

30. Li, Y.-C.; Schulz, J.; Mannen, S.; Delhom, C.; Condon, B.; Chang, S.; Zammarano, M.; Grunlan, J. C., Flame Retardant Behavior of Polyelectrolyte−Clay Thin Film Assemblies on Cotton Fabric. *Acs Nano* **2010,** *4*, 3325-3337.

31. Decher, G., Polyelectrolyte Multilayers, an Overview. In *Multilayer Thin Films: Sequential Assembly of Nanocomposite Materials*, 2nd ed.; Decher, G.; Schlenoff, J., Eds. Wiley-VCH: Weinheim, Germany, 2012; Vol. 1.

32. Cain, A. A.; Nolen, C. R.; Li, Y.-C.; Davis, R.; Grunlan, J. C., Phosphorous-filled Nanobrick Wall Multilayer Thin Film Eliminates Polyurethane Melt Dripping and Reduces Heat Release Associated with Fire. *Polymer Degradation and Stability* **2013,** *98*, 2645-2652.

33. Li, Y.; Kim, J.; Shields, R.; Davis, Controlling Polyurethane Foam Flammability and Mechanical Behaviour by Tailoring the Composition of Clay-based Multilayer Nanocoatings. *Journal of Materials Chemistry A: Materials for Energy and Sustainability* **2013,** *1*, 12987.

34. Kim, Y. S.; Harris, R.; Davis, R., Innovative Approach to Rapid Growth of Highly Clay-filled Coatings on Porous Polyurethane Foam. *ACS Macro Letters* **2012,** *1*, 820-824.

35. Priolo, M. A.; Gamboa, D.; Holder, K. M.; Grunlan, J. C., Super Gas Barrier of Transparent Polymer−Clay Multilayer Ultrathin Films. *Nano Letters* **2010,** *10*, 4970-4974.

36. Erel, I.; Zhu, Z.; Zhuk, A.; Sukhishvili, S. A., Hydrogen-bonded Layer-by-Layer Films of Block Copolymer Micelles with pH-responsive Cores. *Journal of Colloid and Interface Science* **2011,** *355*, 61-69.

37. Zhuk, A.; Pavlukhina, S.; Sukhishvili, S., Hydrogen-bonded Layer-by-Layer Temperature-triggered Release Films. *Langmuir* **2009,** *25*, 14025-14029.

38. Sung, C.; Vidyasagar, A.; Hearn, K.; Lutkenhaus, J., Effect of Thickness on the Thermal Properties of Hydrogen-bonded LbL Assemblies. *Langmuir* **2012,** *28*, 8100-8109.

39. Kurapati, R.; Raichur, A., Composite Cyclodextrin–Calcium Carbonate Porous Microparticles and Modified Multilayer Capsules: Novel Carriers for Encapsulation of Hydrophobic Drugs. *Journal of Materials Chemistry B: Materials for Biology and Medicine* **2013,** *1*, 3175-3184.

40. Adamczyk, Z.; Zembala, M.; Kolasinska, M.; Warszynski, P.; Kolasińska, M.; Warszyński, P., Characterization of Polyelectrolyte Multilayers on Mica and Oxidized Titanium by Streaming Potential and Wetting Angle Measurements. *Colloids and surfaces. A, Physicochemical and engineering aspects* **2007,** *302*, 455-460.

41. Castelnovo, M.; Joanny, J.-F., Formation of Polyelectrolyte Multilayers. *Langmuir* **2000,** *16*, 7524-7532.

42. Ariga, K.; Hill, J. P.; Ji, Q. M., Layer-by-layer assembly as a versatile bottom-up nanofabrication technique for exploratory research and realistic application. *Phys Chem Chem Phys* **2007,** *9*, 2319-2340.

43. Decher, G., Fuzzy Nanoassemblies: Toward Layered Polymeric Multicomposites. *Science* **1997,** *277*, 1232-1237.

44. Zhang, L.; Qiao, Z.-A.; Zheng, M.; Huo, Q.; Sun, J., Rapid and Substrate-independent Layer-by-Layer Fabrication of Antireflection- and Antifogging-integrated Coatings. *Journal of Materials Chemistry* **2010,** *20*, 6125-6130.

45. Hiller, J.; Mendelsohn, J. D.; Rubner, M. F., Reversibly Erasable Nanoporous Anti-reflection Coatings from Polyelectrolyte Multilayers. *Nat Mater* **2002,** *1*, 59-63.

46. Park, J. S.; Cho, S. M.; Kim, W. J.; Park, J.; Yoo, P. J., Fabrication of Graphene Thin Films Based on Layer-by-Layer Self-assembly of Functionalized Graphene Nanosheets. *Acs Appl Mater Inter* **2011,** *3*, 360-368.

47. Park, Y. T.; Ham, A. Y.; Grunlan, J. C., Heating and Acid Doping Thin Film Carbon Nanotube Assemblies for High Transparency and Low Sheet Resistance. *Journal of Materials Chemistry* **2011,** *21*, 363-368.

48. Park, Y. T.; Ham, A. Y.; Yang, Y. H.; Grunlan, J. C., Fully Organic ITO Replacement through Acid Doping of Double-walled Carbon Nanotube Thin Film Assemblies. *RSC Advances* **2011,** *1*, 662-671.

49. Ou, J. F.; Liu, L.; Wang, J. Q.; Wang, F. J.; Xue, M. S.; Li, W., Fabrication and Tribological Investigation of a Novel Hydrophobic Polydopamine/Graphene Oxide Multilayer Film. *Tribol. Lett.* **2012,** *48*, 407-415.

50. Kim, J. H.; Lee, M. J.; Kim, S.; Hwang, J.; Lim, T. Y.; Kim, S. H., Fabrication of Patterned TiO2 Thin Film by a Wet Process. *Met. Mater.-Int.* **2012,** *18*, 833-837.

51. Wang, L.; Zhang, X.; Li, B.; Sun, P.; Yang, J.; Xu, H.; Liu, Y., Superhydrophobic and Ultraviolet-blocking Cotton Textiles. *Acs Appl Mater Inter* **2011,** *3*, 1277-1281.

52. Plackett, D. V.; Holm, V. K.; Johansen, P.; Ndoni, S.; Nielsen, P. V.; Sipilainen-Malm, T.; Sodergard, A.; Verstichel, S., Characterization of L-polylactide and L-polylactide-polycaprolactone Copolymer Films for Use in Cheese Packaging Applications. *Packaging Technology and Science* **2006,** *19*, 1-24.

53. Yang, Y.-H.; Bolling, L.; Priolo, M. A.; Grunlan, J. C., Super Gas Barrier and Selectivity of Graphene Oxide-Polymer Multilayer Thin Films. *Advanced Materials* **2013,** *25*, 503-508.

54. Li, H.; Fu, S. Y.; Peng, L. C.; Zhan, H. Y., Photocatalytic Nanocomposite Films Fabricated by Layer-by-Layer Self-assembly of TiO2 Nanoparticles and Lignosulfonates. *Chin. J. Chem.* **2012,** *30*, 1605-1610.

55. Lee, J. A.; Nam, Y. S.; Rutledge, G. C.; Hammond, P. T., Enhanced Photocatalytic Activity using Layer-by-Layer Electrospun Constructs for Water Remediation. *Adv Funct Mater* **2010,** *20*, 2424-2429.

56. Priolo, M. A.; Holder, K. M.; Gamboa, D.; Grunlan, J. C., Influence of Clay Concentration on the Gas Barrier of Clay-Polymer Nanobrick Wall Thin Film Assemblies. *Langmuir* **2011,** *27*, 12106-12114.

57. Podsiadlo, P.; Kaushik, A. K.; Arruda, E. M.; Waas, A. M.; Shim, B. S.; Xu, J.; Nandivada, H.; Pumplin, B. G.; Lahann, J.; Ramamoorthy, A.; Kotov, N. A., Ultrastrong and Stiff Layered Polymer Nanocomposites. *Science* **2007,** *318*, 80-83.

58. Laufer, G.; Kirkland, C.; Cain, A. A.; Grunlan, J. C., Clay–Chitosan Nanobrick Walls: Completely Renewable Gas Barrier and Flame-retardant Nanocoatings. *Acs Appl Mater Inter* **2012,** *4*, 1643-1649.

59. Park, Y. T.; Ham, A. Y.; Grunlan, J. C., High Electrical Conductivity and Transparency in Deoxycholate-stabilized Carbon Nanotube Thin Films. *Journal of Physical Chemistry C* **2010,** *114*, 6325-6333.

60. Loh, K. J.; Kim, J.; Lynch, J. P.; Kam, N. W. S.; Kotov, N. A., Multifunctional Layer-by-Layer Carbon Nanotube-Polyelectrolyte Thin Films for Strain and Corrosion Sensing. *Smart Materials & Structures* **2007,** *16*, 429-438.

61. Shah, N. J.; Macdonald, M. L.; Beben, Y. M.; Padera, R. F.; Samuel, R. E.; Hammond, P. T., Tunable Dual Growth Factor Delivery from Polyelectrolyte Multilayer Films. *Biomaterials* **2011,** *32*, 6183-6193.

62. Saurer, E. M.; Flessner, R. M.; Sullivan, S. P.; Prausnitz, M. R.; Lynn, D. M., Layer-by-Layer Assembly of DNA- and Protein-containing Films on Microneedles for Drug Delivery to the Skin. *Biomacromolecules* **2010,** *11*, 3136-3143.

63. Dai, J. H.; Bruening, M. L., Catalytic Nanoparticles Formed by Reduction of Metal Ions in Multilayered Polyelectrolyte Films. *Nano Letters* **2002,** *2*, 497-501.

64. Yoon, M.; Kim, Y.; Cho, J., Multifunctional Colloids with Optical, Magnetic, and Superhydrophobic Properties Derived from Nucleophilic Substitution-induced Layer-by-Layer Assembly in Organic Media. *Acs Nano* **2011,** *5*, 5417-5426.

65. Sperling, L. H., *Introduction to Physical Polymer Science*. fourth ed.; John Wiley and Sons INC.: Hoboken, 2006.

66. Price, D.; Horrocks, A. R., Polymer Degradation and the Matching of FR Chemistry to Degradation. In *Fire Retardancy of Polymeric Materials*, Second ed.; Wilkie, C. A.; Morgan, A. B., Eds. CRC Press Boca Raton, FL, 2010; pp 15-42.

67. Jellinek, H. H. G., The Combustion of Organic Polymers, C. F. Cullis and M. M. Hirschler, Eds., Oxford University Press, London, 1981. Price: $59.00. *Journal of Polymer Science: Polymer Letters Edition* **1982,** *20*, 606.

68. Madorsky, S. L., *Thermal Degradation of Organic Polymers*. Interscience New York, 1964.

69. Hergenrother, P. M., The Use, Design, Synthesis, and Properties of High Performance/High Temperature Polymers: An Overview. *High Performance Polymers* **2003,** *15*, 3-45.

70. Hiemenz, P. C.; Lodge, T. P., *Polymer Chemistry*. second ed.; CRC Press: Boca Baton, 2007.

71. Lin, H.; Han, L.; Dong, L., Thermal Degradation Behavior and Gas Phase Flame-retardant Mechanism of Polylactide/PCPP Blends. *Journal of Applied Polymer Science* **2014,** *131*.

72. Alam, M. K.; Islam, M. T.; Mina, M. F.; Gafur, M. A., Structural, Mechanical, Thermal, and Electrical Properties of Carbon Black Reinforced Polyester Resin Composites. *Journal of Applied Polymer Science* **2014,** *131*.

73. Babrauskas, V. In *Ten years of heat release research with the cone calorimeter*, Japan Symposium on Heat Release and Fire Hazard, First (1st) Proceedings. Session 3. Scope for Next-Generation Fire Safety Testing Technology, Tsukuba Building Test Laboratory, Center for Better Living, Tsukuba Building Test Laboratory, Center for Better Living, 1993.

74. Bolland, J. L.; Gee, G., Trans. A Review of the Role of Basic Iron (III) Oxide Acting as a Char Forming/Smoke Suppressing/Flame Retarding Additive in Halogenated Polymers and Halogenated Polymer Blends. *Faraday Society* **1946,** *42*, 1946.

75. Mark, H. F.; Atlas, S. M.; Shalaby, S. W.; Pearce, E. M., Combustion of Polymers and its Retardation. In *Flame-retardant Polymeric Materials*, Lewin, M.; Atlas, S. M.; Pearce, E. M., Eds. Plenum Press: New York, 1975; pp 1-17.

76. Lyon, R. E.; Janssens, M. L. *Polymer Flammability*; DOT/FAA/AR-05/14; Southwest Research Institute: Springfield, Virginia, 2005.

77. Milnes, G. J.; Eling, B.; Price, D.; Gao, F.; John Milnes, G.; Lindsay, C. I.; McGrail, P. T., Laser Pyrolysis/Time-of-flight Mass Spectrometry Studies Pertinent to the Behaviour of Flame-retarded Polymers in Real Fire Situations. *Polymer Degradation and Stability* **1999,** *64*, 403-410.

78. Camino, G.; Costa, L.; Luda di Cortemiglia, M. P., Overview of Fire Retardant Mechanisms. *Polymer Degradation and Stability* **1991,** *33*, 131-154.

79. Woolley, W. D., Nitrogen-containing Products from the Thermal Decomposition of Flexible Polyurethane Foams. *British Polymer Journal* **1972,** *4*, 27-43.

80. Levchik, S. V.; Weil, E. D., Thermal Decomposition, Combustion and Fire-retardancy of Polyurethanes - A Review of the Recent Literature. *Polymer International* **2004,** *53*, 1585-1610.

81. Morgan, A. B.; Gilman, J. W., An Overview of Flame Retardancy of Polymeric Materials: Application, Technology, and Future Directions. *Fire and Materials* **2012,** *37*, 259-279.

82. Mouritz, A. P.; Gibson, A. G., Flame Retardant Composites. In *Fire Properties of Polymer Composite Materials*, Gladwell, G. M. L., Ed. Springer: London, 2006; pp 237-286.

83. Edward, D. W.; Sergei, V. L., Overview of Modes of Action and Interaction of Flame Retardants. In *Flame Retardants for Plastics and Textiles*, Carl Hanser Verlag GmbH & Co. KG: 2009; pp 241-251.

84. Liang, S.; Neisius, N. M.; Gaan, S., Recent Developments in Flame Retardant Polymeric Coatings. *Progress in Organic Coatings* **2013,** *76*, 1642-1665.

85. Troitzsch, J. H., Overview of Flame Retardants. *Chemistry Today* **1998,** *16*, 1-19.

86. Hollingbery, L. A.; Hull, T. R., The Fire Retardant Behaviour of Huntite and Hydromagnesite – A Review. *Polymer Degradation and Stability* **2010,** *95*, 2213-2225.

87. Aseeva, R.; Zaikov, G., Flammability of polymeric materials. In *Key Polymers Properties and Performance*, Springer Berlin Heidelberg: Berlin, Germany, 1985; Vol. 70, pp 171-229.

88. Lyons, J. W., *The Chemistry and Uses of Fire-retardants*. John Wiley and Sons: New York, 1970.

89. Wilson, W. E.; O'Donovan, J. T.; Fristrom, R. M., Flame Inhibition by Halogen Compounds. *Symposium (International) on Combustion* **1969,** *12*, 929-942.

90. Shen, K. K.; Kochesfahani, S.; Jouffret, F., Zinc Borates as Multifunctional Polymer Additives. *Polymers for Advanced Technologies* **2008,** *19*, 469-474.

91. Weil, E. D.; Levchik, S. V., Flame Retardants in Commercial Use or Development for Polyolefins. *Journal of Fire Sciences* **2008,** *26*, 5-43.

92. Church, J. M.; Little, R. W.; Coppick, S., Evaluation of Flame-Resistant Fabrics. *Industrial & Engineering Chemistry* **1950,** *42*, 418-427.

93. de Wit, C. A., An Overview of Brominated Flame Retardants in the Environment. *Chemosphere* **2002,** *46*, 583-624.

94. Bocchini, S.; Camino, G., Halogen-Containing Flame Retardants. In *Fire Retardancy of Polymeric Materials*, Second ed.; Wilkie, C. A.; Morgan, A. B., Eds. CRC Press: 2009; pp 75-105.

95. Birnbaum, K. S.; Staskal, D. F., Brominated Flame Retardants: Cause for Concern? *Environ. Health Perspect.* **2004,** *112*, 9-17.

96. Babushok, V.; Tsang, W., Inhibitor Rankings for Alkane Combustion. *Combustion and Flame* **2000,** *123*, 488-506.

97. Weil, E. D., Phosphorous-based Flame Retardants. In *Flame-Retardant Polymeric Materials*, Lewin, M.; Atlas, S. M.; Pearce, E. M., Eds. Plenum Press: New York, 1978; Vol. 2, pp 103-128.

98. Bradbury, A. G. W.; Sakai, Y.; Shafizadeh, F., A Kinetic Model for Pyrolysis of Cellulose. *Journal of Applied Polymer Science* **1979,** *23*, 3271-3280.

99. van der Veen, I.; de Boer, J., Phosphorus Flame Retardants: Properties, Production, Environmental Occurrence, Toxicity and Analysis. *Chemosphere* **2012,** *88*, 1119-1153.

100. Price, D.; Bullett, K. J.; Cunliffe, L. K.; Hull, T. R.; Milnes, G. J.; Ebdon, J. R.; Hunt, B. J.; Joseph, P., Cone Calorimetry Studies of Polymer Systems Flame Retarded by Chemically Bonded Phosphorus. *Polymer Degradation and Stability* **2005,** *88*, 74-79.

101. Vandersall, H. L., Intumescent Coating Systems, their Development and Chemistry. *The Journal of Fire and Flammability* **1971,** *2*, 97-140.

102. Camino, G.; Lomakin, S., Intumescent Materials. In *Fire Retardant Materials*, Horrocks, A. R.; Price, D., Eds. Woodhead Publishing Ltd: Boca Raton, FL, 2001; pp 319-335.

103. Bourbigot, S.; Le Bras, M.; Duquesne, S.; Rochery, M., Recent Advances for Intumescent Polymers. *Macromolecular Materials and Engineering* **2004,** *289*, 499-511.

104. Chen, S.; Wang, B.; Kang, J.; Chen, J.; Gai, J.; Yang, L.; Cao, Y., Synergistic Effect of Organic Vermiculite on the Flame Retardancy and Thermal Stability of Intumescent Polypropylene Composites. *Journal of Macromolecular Science, Part B* **2013,** *52*, 1212-1225.

105. Fang, K. Y.; Li, J. A.; Ke, C. H.; Hu, Q. L.; Tao, K.; Zhu, J.; Yan, Q., Intumescent Flame Retardation of Melamine-Modified Montmorillonite on Polyamide 6: Enhancement of Condense Phase and Flame Retardance. *Polymer Engineering and Science* **2011,** *51*, 377-385.

106. Butler, K. M.; Baum, H. R.; Kashiwagi, T., Heat Transfer in an Intumescent Material Using a Three-Dimensional Lagrangian Model. In *International Conference of Fire Research and Engineering*, Lund, M. A.; Angell, D. P., Eds. Orlando, FL, 1995; pp 261-266.

107. Rhys, J. A., Intumescent Coatings and their Uses. *Fire and Materials* **1980,** *4*, 154-156.

108. Ullah, S.; Ahmad, F.; Yusoff, P. S. M. M., Effect of Boric Acid and Melamine on the Intumescent Fire-Retardant Coating Composition for the Fire Protection of Structural Steel Substrates. *Journal of Applied Polymer Science* **2013,** *128*, 2983-2993.

109. Alongi, J.; Pošković, M.; Frache, A.; Trotta, F., Novel Flame Retardants Containing Cyclodextrin Nanosponges and Phosphorus Compounds to Enhance EVA Combustion Properties. *Polymer Degradation and Stability* **2010,** *95*, 2093-2100.

110. Dasari, A.; Yu, Z. Z.; Mai, Y. W.; Cai, G.; Song, H., Roles of Graphite Oxide, Clay and POSS durring the Combustion of Polyamide 6. *Polymer* **2009,** *50*, 1577-1587.

111. Kirschbaum, G. S., *Functional Mineral Fillers for Fire Performance and Smoke Suppression in Cable Formulations*. I O S Press: Amsterdam, 1997; pp 359-367.

112. Fischer, H., Polymer Nanocomposites: From Fundamental Research to Specific Applications. *Materials Science and Engineering: C* **2003,** *23*, 763-772.

113. Schmidt, D.; Shah, D.; Giannelis, E. P., New Advances in Polymer/Layered Silicate Nanocomposites. *Current Opinion in Solid State and Materials Science* **2002,** *6*, 205-212.

114. Usuki, A.; Kojima, Y.; Kawasumi, M.; Okada, A.; Fukushima, Y.; Kurauchi, T.; Kamigaito, O., Synthesis of Nylon 6-Clay Hybrid. *Journal of Materials Research* **1993,** *8*, 1179-1184.

115. Lan, T.; Pinnavaia, T., Clay-Reinforced Epoxy Nanocomposites. *Chem Mater* **1994,** *6*, 2216-2219.

116. Messersmith, P. B.; Giannelis, E. P., Synthesis and Characterization of Layered Silicate-Epoxy Nanocomposites. *Chem Mater* **1994,** *6*, 1719-1725.

117. Reichert, P.; Nitz, H.; Klinke, S.; Brandsch, R.; Thomann, R.; Mülhaupt, R., Poly(propylene)/Organoclay Nanocomposite Formation: Influence of Compatibilizer Functionality and Organoclay Modification. *Macromolecular Materials and Engineering* **2000,** *275*, 8-17.

118. Thostenson, E. T.; Ren, Z.; Chou, T. W., Advances in the Science and Technology of Carbon Nanotubes and their Composites: A Review. *Composites Science and Technology* **2001,** *61*, 1899-1912.

119. Gilman, J. W.; Kashiwagi, T.; Lichtenhan, J. D., Nanocomposites: A Revolutionary New Flame Retardant Approach. *SAMPE Journal* **1997,** *33*, 40-46.

120. Wang, Z.; Pinnavaia, T. J., Nanolayer Reinforcement of Elastomeric Polyurethane. *Chem Mater* **1998,** *10*, 3769-3771.

121. Dennis, H. R.; Hunter, D. L.; Chang, D.; Kim, S.; White, J. L.; Cho, J. W.; Paul, D. R., Effect of Melt Processing Conditions on the Extent of Exfoliation in Organoclay-based Nanocomposites. *Polymer* **2001,** *42*, 9513-9522.

122. Alexandre, M.; Dubois, P., Polymer-layered Silicate Nanocomposites: Preparation, Properties and Uses of a New Class of Materials. *Materials Science and Engineering: R: Reports* **2000,** *28*, 1-63.

123. Pavlidou, S.; Papaspyrides, C. D., A Review on Polymer–Layered Silicate Nanocomposites. *Progress in Polymer Science* **2008,** *33*, 1119-1198.

124. Paul, D. R.; Robeson, L. M., Polymer Nanotechnology: Nanocomposites. *Polymer* **2008,** *49*, 3187-3204.

125. Lebaron, P. C.; Wang, Z.; Pinnavaia, T. J., Polymer-layered Silicate Nanocomposites: An overview. *Applied Clay Science* **1999,** *15*, 11-29.

126. Yurekli, K.; Mitchell, C. A.; Krishnamoorti, R., Small-angle Neutron Scattering from Surfactant-assisted Aqueous Dispersions of Carbon Nanotubes. *Journal of the American Chemical Society* **2004,** *126*, 9902-9903.

127. Fornes, T. D.; Hunter, D. L.; Paul, D. R., Nylon-6 Nanocomposites from Alkylammonium-Modified Clay: The Role of Alkyl Tails on Exfoliation. *Macromolecules* **2004,** *37*, 1793-1798.

128. Yuan, Q.; Misra, R. D. K., Impact Fracture Behavior of Clay–reinforced Polypropylene Nanocomposites. *Polymer* **2006,** *47*, 4421-4433.

129. Devaprakasam, D.; Hatton, P. V.; Möbus, G.; Inkson, B. J., Nanoscale Tribology, Energy Dissipation and Failure Mechanisms of Nano- and Micro-silica Particle-filled Polymer Composites. *Tribol. Lett.* **2009,** *34*, 11-19.

130. Ajayan, P.; Tour, J., Materials Science: Nanotube Composites *Nature* **2007,** *447*, 1066.

131. Shen, J.; Han, X.; Lee, L. J., Nanoscaled Reinforcement of Polystyrene Foams using Carbon Nanofibers. *Journal of Cellular Plastics* **2006,** *42*, 105-126.

132. Goncalves, G.; Marques, P. A. A. P.; Barros-Timmons, A.; Bdkin, I.; Singh, M. K.; Emami, N.; Gracio, J., Graphene Oxide Modified with PMMA via ATRP as a Reinforcement Filler. *Journal of Materials Chemistry* **2010,** *20*, 9927-9934.

133. Beyer, G., Nanocomposites: A New Class of Flame Retardants for Polymers. *Plastics, Additives and Compounding* **2002,** *4*, 22-28.

134. Diez-Pascual, A. M.; Naffakh, M.; Marco, C.; Ellis, G.; Gomez-Fatou, M. A., High-performance Nanocomposites Based on Polyetherketones. *Prog. Mater. Sci.* **2012,** *57*, 1106-1190.

135. Gilman, J. W.; Jackson, C. L.; Morgan, A. B.; Harris, R.; Manias, E.; Giannelis, E. P.; Wuthenow, M.; Hilton, D.; Phillips, S. H., Flammability Properties of Polymer - Layered-silicate Nanocomposites. Polypropylene and Polystyrene Nanocomposites. *Chem Mater* **2000,** *12*, 1866-1873.

136. Cipiriano, B. H.; Kashiwagi, T.; Raghavan, S. R.; Yang, Y.; Grulke, E. A.; Yamamoto, K.; Shields, J. R.; Douglas, J. F., Effects of Aspect Ratio of MWNT on the Flammability Properties of Polymer Nanocomposites. *Polymer* **2007,** *48*, 6086-6096.

137. Kashiwagi, T.; Du, F.; Winey, K. I.; Groth, K. M.; Shields, J. R.; Bellayer, S. P.; Kim, H.; Douglas, J. F., Flammability Properties of Polymer Nanocomposites with Single-walled Carbon Nanotubes: Effects of Nanotube Dispersion and Concentration. *Polymer* **2005,** *46*, 471-481.

138. Iler, R. K., Multilayers of Colloidal Particles. *Journal of Colloid and Interface Science* **1966,** *21*, 569-594.

139. Decher, G.; Hong, J.-D., Buildup of Ultrathin Multilayer Films by a Self-assembly Process, 1 Consecutive Adsorption of Anionic and Ationic Bipolar Amphiphiles on Charged Surfaces. *Die Makromolekulare Chemie. Macromolecular Symposia* **1991,** *46*, 321-327.

140. Decher, G.; Hong, J. D., Buildup of Ultrathin Multilayer Films by a Self-assembly Process: II. Consecutive Adsorption of Anionic and Cationic Bipolar Amphiphiles and Polyelectrolytes on Charged Surfaces. *Berichte der Bunsengesellschaft für Physikalische Chemie* **1991,** *95*, 1430-1434.

141. Decher, G.; Schmitt, J.; Hong, J. D., Buildup of Ultrathin Multilayer Films by a Self-assembly Process: III. Consecutively Alternating Adsorption of Anionic and Cationic Polyelectrolytes on Charged Surfaces. *Thin Solid Films* **1992,** *210*, 831-835.

142. Mohwald, H.; Lvov, Y.; Decher, G.; Moehwald, H., Assembly, Structural Characterization, and Thermal Behavior of Layer-by-Layer Deposited Ultrathin Films of Poly(vinyl sulfate) and Poly(allylamine). *Langmuir* **1993,** *9*, 481-486.

143. Tao, A.; Kim, F.; Hess, C.; Goldberger, J.; He, R.; Sun, Y.; Xia, Y.; Yang, P., Langmuir−Blodgett Silver Nanowire Monolayers for Molecular Sensing Using Surface-Enhanced Raman Spectroscopy. *Nano Letters* **2003,** *3*, 1229-1233.

144. Cote, L. J.; Kim, F.; Huang, J. X., Langmuir-Blodgett Assembly of Graphite Oxide Single Layers. *Journal of the American Chemical Society* **2009,** *131*, 1043-1049.

145. Li, X. L.; Zhang, G. Y.; Bai, X. D.; Sun, X. M.; Wang, X. R.; Wang, E.; Dai, H. J., Highly Conducting Graphene Sheets and Langmuir-Blodgett Films. *Nature Nanotechnology* **2008,** *3*, 538-542.

146. Dierendonck, M.; De Koker, S.; De Rycke, R.; De Geest, B., Just Spray It - LbL Assembly Enters a New Age. *Soft Matter* **2014,** *10*, 804-807.

147. Krogman, K. C.; Lowery, J. L.; Zacharia, N. S.; Rutledge, G. C.; Hammond, P. T., Spraying Asymmetry into Functional Membranes Layer-by-Layer. *Nat Mater* **2009,** *8*, 512-518.

148. Krogman, K. C.; Zacharia, N. S.; Schroeder, S.; Hammond, P. T., Automated Process for Improved Uniformity and Versatility of Layer-by-Layer Deposition. *Langmuir* **2007,** *23*, 3137-3141.

149. Schaaf, P.; Voegel, J.-C.; Jierry, L.; Boulmedais, F., Spray-assisted Polyelectrolyte Multilayer Buildup: From Step-by-Step to Single-step Polyelectrolyte Film Constructions. *Advanced Materials* **2012,** *24*, 1001-1016.

150. An, M.; Hong, J.-D., Surface Modification of Hafnia with Polyelectrolytes Based on the Spin-coating Electrostatic Self-assembly Method. *Colloids and surfaces. A, Physicochemical and engineering aspects* **2009,** *348*, 301-304.

151. Lee, S.-S.; Hong, J.-D.; Kim, C.; Kim, K.; Koo, J.; Lee, K.-B., Layer-by-Layer Deposited Multilayer Assemblies of Ionene-type Polyelectrolytes Based on the Spin-coating Method. *Macromolecules* **2001,** *34*, 5358-5360.

152. Hagen, D. A.; Box, C.; Greenlee, S.; Xiang, F.; Regev, O.; Grunlan, J. C., High Gas Barrier Imparted by Similarly Charged Multilayers in Nanobrick Wall Thin Films. *RSC Advances* **2014,** *4*, 18354-18359.

153. Clark, S.; Montague, M.; Hammond, P., Ionic Effects of Sodium Chloride on the Templated Deposition of Polyelectrolytes Using Layer-by-Layer Ionic Assembly. *Macromolecules* **1997,** *30*, 7237-7244.

154. Dubas, S. T.; Schlenoff, J. B., Factors Controlling the Growth of Polyelectrolyte Multilayers. *Macromolecules* **1999,** *32*, 8153-8160.

155. Scholer, B.; Fery, A.; Schöler, B.; Cassagneau, T.; Caruso, F., Nanoporous Thin Films Formed by Salt-induced Structural Changes in Multilayers of Poly(acrylic acid) and Poly(allylamine). *Langmuir* **2001,** *17*, 3779-3783.

156. Shiratori, S. S.; Rubner, M. F., pH-dependent Thickness Behavior of Sequentially Adsorbed Layers of Weak Polyelectrolytes. *Macromolecules* **2000,** *33*, 4213-4219.

157. Dejugnat, C.; Mauser, T.; Djugnat, C.; Sukhorukov, G., Reversible pH-Dependent Properties of Multilayer Microcapsules Made of Weak Polyelectrolytes. *Macromolecular Rapid Communications* **2004,** *25*, 1781-1785.

158. Shutava, T.; Prouty, M.; Kommireddy, D.; Lvov, Y., pH Responsive Decomposable Layer-by-Layer Nanofilms and Capsules on the Basis of Tannic Acid. *Macromolecules* **2005,** *38*, 2850-2858.

159. Sukhishvili, S., Responsive Polymer Films and Capsules via Layer-by-Layer Assembly. *Current Opinion in Colloid & Interface Science* **2005,** *10*, 37-44.

160. Quinn, J.; Caruso, F., Thermoresponsive Nanoassemblies: Layer-by-Layer Assembly of Hydrophilic−Hydrophobic Alternating Copolymers. *Macromolecules* **2005,** *38*, 3414-3419.

161. Salomaki, M.; Vinokurov, I.; Kankare, J., Effect of Temperature on the Buildup of Polyelectrolyte Multilayers. *Langmuir* **2005,** *21*, 11232-11240.

162. Ye, S.; Wang, C.; Liu, X.; Tong, Z., Deposition Temperature Effect on Release Rate of Indomethacin Microcrystals from Microcapsules of Layer-by-Layer Assembled Chitosan and Alginate Multilayer Films. *Journal of Controlled Release* **2005,** *106*, 319-328.

163. Glinel, K.; Moussa, A.; Jonas, A. M.; Laschewsky, A., Influence of Polyelectrolyte Charge Density on the Formation of Multilayers of Strong Polyelectrolytes at Low Ionic Strength. *Langmuir* **2002,** *18*, 1408-1412.

164. Yang, J.; Zhang, Z.; Men, X.; Xu, X.; Zhu, X.; Zhou, X., Counterion Exchange to Achieve Reversibly Switchable Hydrophobicity and Oleophobicity on Fabrics. *Langmuir* **2011,** *27*, 7357-7360.

165. Xiang, F.; Tzeng, P.; Sawyer, J. S.; Regev, O.; Grunlan, J. C., Improving the Gas Barrier Property of Clay–Polymer Multilayer Thin Films Using Shorter Deposition Times. *Acs Appl Mater Inter* **2013,** *6*, 6040-6048.

166. Izquierdo, A.; Ono, S. S.; Voegel, J. C.; Schaaf, P.; Decher, G., Dipping versus Spraying: Exploring the Deposition Conditions for Speeding Up Layer-by-Layer Assembly. *Langmuir* **2005,** *21*, 7558-7567.

167. Carneiro-da-Cunha, M. G.; Cerqueira, M.; Cerqueira, M. A.; Carvalhoc, S.; Carvalho, S.; Quintas, M. A. C.; Teixeira, J. A.; Teixeira, J.; Vicente, A., Physical and Thermal Properties of a Chitosan/Alginate Nanolayered PET Film. *Carbohydr. Polym.* **2010,** *82*, 153-159.

168. Grunlan, J. C.; Choi, J. K.; Lin, A., Antimicrobial Behavior of Polyelectrolyte Multilayer Films Containing Cetrimide and Silver. *Biomacromolecules* **2005,** *6*, 1149-1153.

169. Huang, L.; Guo, G.; Liu, Y.; Chang, Q.; Xie, Y., Reduced Graphene Oxide-ZnO Nanocomposites for Flexible Supercapacitors. *Journal of Display Technology* **2012,** *8*, 373-376.

170. Li, Y.; Cui, P.; Wang, L.; Lee, K.; Lee, H., Highly Bendable, Conductive, and Transparent Film by an Enhanced Adhesion of Silver Nanowires. *Acs Appl Mater Inter* **2013,** *5*, 9155-9160.

171. Hirvikorpi, T.; Vaha Nissi, M.; Harlin, A.; Salomaki, M.; Areva, S.; Vähä Nissi, M.; Salomäki, M.; Korhonen, J.; Karppinen, M., Enhanced Water Vapor Barrier Properties for Biopolymer Films by Polyelectrolyte Multilayer and Atomic Layer Deposited Al2O3 Double-coating. *Applied Surface Science* **2011,** *257*, 9451-9454.

172. Svagan, A. J.; Åkesson, A.; Cárdenas, M.; Bulut, S.; Knudsen, J. C.; Risbo, J.; Plackett, D., Transparent Films Based on PLA and Montmorillonite with Tunable Oxygen Barrier Properties. *Biomacromolecules* **2012,** *13*, 397-405.

173. Hashide, R.; Yoshida, K.; Hasebe, Y.; Takahashi, S.; Sato, K.; Anzai, J.-i., Insulin-containing Layer-by-Layer Films Deposited on Poly(lactic acid) Microbeads for pH-controlled Release of Insulin. *Colloids and Surfaces B: Biointerfaces* **2012,** *89*, 242-247.

174. Hirsjarvi, S.; Peltonen, L.; Hirvonen, J., Layer-by-Layer Polyelectrolyte Coating of Low Molecular Weight Poly(lactic acid) Nanoparticles. *Colloids and Surfaces. B, Biointerfaces* **2006,** *49*, 93-99.

175. Dubas, S. T.; Kumlangdudsana, P.; Potiyaraj, P., Layer-by-Layer Deposition of Antimicrobial Silver Nanoparticles on Textile Fibers. *Colloids and Surfaces A: Physicochemical and Engineering Aspects* **2006,** *289*, 105-109.

176. Joshi, M.; Bhattacharyya, A.; Agarwal, N.; Parmar, S., Nanostructured Coatings for Super Hydrophobic Textiles. *Bulletin of Materials Science* **2012,** *35*, 933-938.

177. Robert, C.; Feller, J.; Castro, M., Sensing Skin for Strain Monitoring made of PC-CNT Conductive Polymer Nanocomposite Sprayed Layer-by-Layer. *Acs Appl Mater Inter* **2012,** *4*, 3508-3516.

178. Zhao, Y.; Tang, Y.; Wang, X.; Lin, T., Superhydrophobic Cotton Fabric Fabricated by Electrostatic Assembly of Silica Nanoparticles and its Remarkable Buoyancy. *Applied Surface Science* **2010,** *256*, 6736-6742.

179. Kim, Y. S.; Li, Y.-C.; Pitts, W. M.; Werrel, M.; Davis, R. D., Rapid Growing Clay Coatings to Reduce the Fire Threat of Furniture. *Acs Appl Mater Inter* **2014,** *6*, 2146-2152.

180. Liang, Z.; Susha, A.; Caruso, F., Gold Nanoparticle-based Core−Shell and Hollow Spheres and Ordered Assemblies Thereof. *Chem Mater* **2003,** *15*, 3176-3183.

181. Shenoy, D. B.; Antipov, A. A.; Sukhorukov, G. B.; Möhwald, H., Layer-by-Layer Engineering of Biocompatible, Decomposable Core−Shell Structures. *Biomacromolecules* **2003,** *4*, 265-272.

182. Peyratout, C. S.; Dähne, L., Tailor-made Polyelectrolyte Microcapsules: From Multilayers to Smart Containers. *Angewandte Chemie International Edition* **2004,** *43*, 3762-3783.

183. Wang, Y.; Caruso, F., Template Synthesis of Stimuli-Responsive Nanoporous Polymer-Based Spheres via Sequential Assembly. *Chem Mater* **2006,** *18*, 4089-4100.

184. Liang, Z.; Susha, A. S.; Yu, A.; Caruso, F., Nanotubes Prepared by Layer-by-Layer Coating of Porous Membrane Templates. *Advanced Materials* **2003,** *15*, 1849-1853.

185. Meng, X.; Yang, N.; Tan, X., Preparation of Polyelectrolyte Nanotubes by a Pressure-filter-template Technique Using Microporous Anodic Aluminum Oxide (AAO) as the Template. *Chin. J. Chem.* **2009,** *27*, 1925-1928.

186. Zhang, L.; Vidyasagar, A.; Lutkenhaus, J. L., Fabrication and Thermal Analysis of Layer-by-Layer Micro- and Nanotubes. *Current Opinion in Colloid & Interface Science* **2012,** *17*, 114-121.

187. Chaturbedy, P.; Jagadeesan, D.; Eswaramoorthy, M., pH-Sensitive Breathing of Clay within the Polyelectrolyte Matrix. *Acs Nano* **2010,** *4*, 5921-5929.

188. Choi, D.; Hong, J., Layer-by-Layer Assembly of Multilayer Films for Controlled Drug Release. *Arch. Pharm. Res.* **2014,** *37*, 79-87.

189. Chuang, H.; Hammond, P.; Smith, R., Polyelectrolyte Multilayers for Tunable Release of Antibiotics. *Biomacromolecules* **2008,** *9*, 1660-1668.

190. De Geest, B. G.; De Koker, S.; Immesoete, K.; Demeester, J.; De Smedt, S. C.; Hennink, W. E., Self-Exploding Beads Releasing Microcarriers. *Advanced Materials* **2008,** *20*, 3687-3691.

191. Granicka, L. H., Nanoencapsulation of Cells Within Multilayer Shells for Biomedical Applications. *J. Nanosci. Nanotechnol.* **2014,** *14*, 705-716.

192. Hammond, P. T., Building Biomedical Materials Layer-by-Layer. *Materials Today* **2012,** *15*, 196-206.

193. Macdonald, M. L.; Samuel, R. E.; Shah, N. J.; Padera, R. F.; Beben, Y. M.; Hammond, P. T., Tissue Integration of Growth Factor-eluting Layer-by-Layer Polyelectrolyte Multilayer Coated Implants. *Biomaterials* **2011,** *32*, 1446-1453.

194. Smith, R.; Riollano, M.; Leung, A.; Hammond, P., Layer-by-Layer Platform Technology for Small-molecule Delivery. *Angewandte Chemie (International ed.)* **2009,** *48*, 8974-8977.

195. Yoshida, K.; Hasebe, Y.; Takahashi, S.; Sato, K.; Anzai, J.-i., Layer-by-Layer Deposited Nano- and Micro-assemblies for Insulin Delivery: A Review. *Materials Science and Engineering: C* **2014,** *34*, 384-392.

196. Dam, H. H.; Caruso, F., Formation and Degradation of Layer-by-Layer Assembled Polyelectrolyte Polyrotaxane Capsules. *Langmuir* **2013,** *29*, 7203-7208.

197. Jing, J.; Szarpak Jankowska, A.; Guillot, R.; Pignot Paintrand, I.; Picart, C.; Auzély Velty, R., Cyclodextrin/Paclitaxel Complex in Biodegradable Capsules for Breast Cancer Treatment. *Chem Mater* **2013,** *25*, 3867-3873.

198. Sakr, O. S.; Borchard, G., Encapsulation of Enzymes in Layer-by-Layer (LbL) Structures: Latest Advances and Applications. *Biomacromolecules* **2013,** *14*, 2117-2135.

199. Wood, K. C.; Boedicker, J. Q.; Lynn, D. M.; Hammond, P. T., Tunable Drug Release from Hydrolytically Degradable Layer-by-Layer Thin Films. *Langmuir* **2005,** *21*, 1603-1609.

200. Wang, Y.; Angelatos, A. S.; Caruso, F., Template Synthesis of Nanostructured Materials via Layer-by-Layer Assembly. *Chem Mater* **2007,** *20*, 848-858.

201. Chen, B.; Liu, C.; Watanabe, M.; Hayashi, K., Layer-by-Layer Structured AuNP Sensors for Terpene Vapor Detection. *IEEE Sensors Journal* **2013,** *13*, 4212-4219.

202. Lutkenhaus, J. L.; Hammond, P. T., Electrochemically Enabled Polyelectrolyte Multilayer Devices: From Fuel Cells to Sensors. *Soft Matter* **2007,** *3*, 804-816.

203. Raoufi, N.; Surre, F.; Rajarajan, M.; Sun, T.; Grattan, K. T. V., Fiber Optic pH Sensor Using Optimized Layer-by-Layer Coating Approach. *IEEE Sensors Journal* **2014,** *14*, 47-54.

204. Skorb, E. V.; Andreeva, D. V., Layer-by-Layer Approaches for Formation of Smart Self-healing Materials. *Polymer Chemistry* **2013,** *4*, 4834-4845.

205. Lee, D.; Rubner, M. F.; Cohen, R. E., All-nanoparticle Thin-film Coatings. *Nano Letters* **2006,** *6*, 2305-2312.

206. Kwak, D.; Han, J. T.; Lee, J. H.; Lim, H. S.; Lee, D. H.; Cho, K., Facile Control of Thermo-responsive Wettability through an All-electrostatic Self-assembling Process. *Surface Science* **2008,** *602*, 3100-3105.

207. Liao, K.-S.; Fu, H.; Wan, A.; Batteas, J. D.; Bergbreiter, D. E., Designing Surfaces with Wettability that Varies in Response to Solute Identity and Concentration. *Langmuir* **2008,** *25*, 26-28.

208. Zhai, L., Stimuli-responsive Polymer Films. *Chemical Society Reviews* **2013,** *42*, 7148-7160.

209. Delcea, M.; Moehwald, H.; MÃ¶hwald, H.; Skirtach, A., Stimuli-responsive LbL Capsules and Nanoshells for Drug Delivery. *Advanced Drug Delivery Reviews* **2011,** *63*, 730-47.

210. Wang, A.; Tao, C.; Cui, Y.; Duan, L.; Yang, Y.; Li, J., Assembly of Environmental Sensitive Microcapsules of PNIPAAm and Alginate Acid and their Application in Drug Release. *Journal of Colloid and Interface Science* **2009,** *332*, 271-279.

211. Martins, G. V.; Mano, J. F.; Alves, N. M., Dual Responsive Nanostructured Surfaces for Biomedical Applications. *Langmuir* **2011,** *27*, 8415-8423.

212. Valmikinathan, C. M.; Chang, W.; Xu, J.; Yu, X., Self Assembled Temperature Responsive Surfaces for Generation of Cell Patches for Bone Tissue Engineering. *Biofabrication* **2012,** *4*, 1-9.

213. Pesirikan, N.; Chang, W.; Zhang, X.; Xu, J.; Yu, X., Characterization of Schwann Cells in Self-Assembled Sheets from Thermoresponsive Substrates. *Tissue Engineering Part A* **2013,** *19*, 1601-1609.

214. Podsiadlo, P.; Shim, B. S.; Kotov, N. A., Polymer/Clay and Polymer/Carbon Nanotube Hybrid Organic–Inorganic Multilayered Composites made by Sequential Layering of Nanometer Scale Films. *Coordination Chemistry Reviews* **2009,** *253*, 2835-2851.

215. Priolo, M. A.; Gamboa, D.; Grunlan, J. C., Transparent Clay-Polymer Nano Brick Wall Assemblies with Tailorable Oxygen Barrier. *Acs Appl Mater Inter* **2010,** *2*, 312-320.

216. Cussler, E. L.; Hughes, S. E.; Ward, W. J.; Arias, R., Barrier Membranes. *Journal of Membrane Science* **1988,** *38*, 161.

217. Tzeng, P.; Maupin, C. R.; Grunlan, J. C., Influence of Polymer Interdiffusion and Clay Concentration on Gas Barrier of Polyelectrolyte/Clay Nanobrick Wall Quadlayer Assemblies. *Journal of Membrane Science* **2014,** *452*, 46-53.

218. Choi, J. H.; Park, Y. W.; Park, T. H.; Song, E. H.; Lee, H. J.; Kim, H.; Shin, S. J.; Lau Chun Fai, V.; Ju, B.-K., Fuzzy Nanoassembly of Polyelectrolyte and Layered Clay Multicomposite toward a Reliable Gas Barrier. *Langmuir* **2012,** *28*, 6826-6831.

219. Ou, R.; Zhang, J.; Deng, Y.; Ragauskas, A., Polymer Clay Self-assembly Complexes on Paper. *Journal of Applied Polymer Science* **2007,** *105*, 1987-1992.

220. Bonderer, L. J.; Studart, A. R.; Woltersdorf, J.; Pippel, E.; Gauckler, L. J., Strong and Ductile Platelet-reinforced Polymer Films Inspired by Nature: Microstructure and Mechanical Properties. *Journal of Materials Research* **2009,** *24*, 2741-2754.

221. Podsiadlo, P.; Michel, M.; Lee, J.; Verploegen, E.; Wong Shi Kam, N.; Hammond, P. T.; Ball, V.; Qi, Y.; Hart, A. J.; Kotov, N., Exponential Growth of LbL Films with Incorporated Inorganic Sheets. *Nano Letters* **2008,** *8*, 1762-1770.

222. Peralta, S.; Habib-Jiwan, J.-L.; Jonas, A. M., Ordered Polyelectrolyte Multilayers: Unidirectional FRET Cascade in Nanocompartmentalized Polyelectrolyte Multilayers. *ChemPhysChem* **2009,** *10*, 137-143.

223. Ball, V.; Apaydin, K.; Laachachi, A.; Toniazzo, V.; Ruch, D., Changes in Permeability and in Mechanical Properties of Layer-by-Layer Films made from Poly(allylamine) and Montmorillonite Postmodified upon Reaction with Dopamine. *Biointerphases* **2012,** *7*, 59.

224. Lutkenhaus, J.; Olivetti, E.; Verploegen, E.; Cord, B.; Sadoway, D.; Hammond, P., Anisotropic Structure and Transport in Self-assembled Layered Polymer-Clay Nanocomposites. *Langmuir* **2007,** *23*, 8515-8521.

225. Hua, F.; Cui, T.; Lvov, Y. M., Ultrathin Cantilevers Based on Polymer−Ceramic Nanocomposite Assembled through Layer-by-Layer Adsorption. *Nano Letters* **2004,** *4*, 823-825.

226. de Villiers, M.; Otto, D.; Strydom, S.; Lvov, Y., Introduction to Nanocoatings Produced by Layer-by-Layer (LbL) Self-assembly. *Advanced Drug Delivery Reviews* **2011,** *63*, 701-715.

227. Min, J.; Braatz, R.; Hammond, P., Tunable Staged Release of Therapeutics from Layer-by-Layer Coatings with Clay Interlayer Barrier. *Biomaterials* **2014,** *35*, 2507-17.

228. Zhuk, A.; Mirza, R.; Sukhishvili, S., Multiresponsive Clay-containing Layer-by-Layer Films. *Acs Nano* **2011,** *5*, 8790-8799.

229. Laachachi, A.; Ball, V.; Apaydin, K.; Toniazzo, V.; Ruch, D., Diffusion of Polyphosphates into (Poly(allylamine)-Montmorillonite) Multilayer Films: Flame Retardant-intumescent Films with Improved Oxygen Barrier. *Langmuir* **2011,** *27*, 13879-13887.

230. Chang, S.; Slopek, R. P.; Condon, B.; Grunlan, J. C., Surface Coating for Flame-Retardant Behavior of Cotton Fabric Using a Continuous Layer-by-Layer Process. *Industrial & Engineering Chemistry Research* **2014,** *53*, 3805-3812.

231. Apaydin, K.; Laachachi, A.; Ball, V.; Jimenez, M.; Bourbigot, S.; Toniazzo, V.; Ruch, D., Polyallylamine–Montmorillonite as Super Flame Retardant Coating Assemblies by Layer-by-Layer Deposition on Polyamide. *Polymer Degradation and Stability* **2013,** *98*, 627-634.

232. Li, Y.-C.; Schulz, J.; Grunlan, J. C., Polyelectrolyte/Nanosilicate Thin-film Assemblies: Influence of pH on Growth, Mechanical Behavior, and Flammability. *Acs Appl Mater Inter* **2009,** *1*, 2338-2347.

233. Huang, G.; Liang, H.; Wang, X.; Gao, J., Poly(acrylic acid)/Clay Thin Films Assembled by Layer-by-Layer Deposition for Improving the Flame Retardancy Properties of Cotton. *Industrial & Engineering Chemistry Research* **2012,** *51*, 12299-12309.

234. Li, Y.-C.; Mannen, S.; Morgan, A. B.; Chang, S.; Yang, Y.-H.; Condon, B.; Grunlan, J. C., Intumescent All-Polymer Multilayer Nanocoating Capable of Extinguishing Flame on Fabric. *Advanced Materials* **2011,** *23*, 3926-3931.

235. Laufer, G.; Kirkland, C.; Morgan, A. B.; Grunlan, J. C., Intumescent Multilayer Nanocoating, Made with Renewable Polyelectrolytes, for Flame-retardant Cotton. *Biomacromolecules* **2012,** *13*, 2843-2848.

236. Carosio, F.; Laufer, G.; Alongi, J.; Camino, G.; Grunlan, J. C., Layer-by-Layer Assembly of Silica-based Flame Retardant Thin Film on PET Fabric. *Polymer Degradation and Stability* **2011,** *96*, 745-750.

237. Li, Y.-C.; Mannen, S.; Schulz, J.; Grunlan, J. C., Growth and Fire Protection Behavior of POSS-based Multilayer Thin Films. *Journal of Materials Chemistry* **2011,** *21*, 3060-3069.

238. Kim, Y. S.; Davis, R.; Cain, A. A.; Grunlan, J. C., Development of Layer-by-Layer Assembled Carbon Nanofiber-filled Coatings to Reduce Polyurethane Foam Flammability. *Polymer* **2011,** *52*, 2847-2855.

239. Alongi, J.; Carosio, F.; Malucelli, G., Influence of Ammonium Polyphosphate-/Poly(acrylic acid)-based Layer-by-Layer Architectures on the Char Formation in Cotton, Polyester and their Blends. *Polymer Degradation and Stability* **2012,** *97*, 1644-1653.

240. Carosio, F.; Alongi, J.; Malucelli, G., Layer-by-Layer Ammonium Polyphosphate-based Coatings for Flame Retardancy of Polyester–Cotton Blends. *Carbohydr. Polym.* **2012,** *88*, 1460-1469.

241. Laufer, G.; Kirkland, C.; Morgan, A. B.; Grunlan, J. C., Exceptionally Flame Retardant Sulfur-based Multilayer Nanocoating for Polyurethane Prepared from Aqueous Polyelectrolyte Solutions. *ACS Macro Letters* **2013,** *2*, 361-365.

242. Alongi, J.; Carosio, F.; Malucelli, G., Layer-by-Layer Complex Architectures Based on Ammonium Polyphosphate, Chitosan and Silica on Polyester-Cotton Blends: Flammability and Combustion Behaviour. *Cellulose* **2012,** *19*, 1041-1050.

243. Zhang, T.; Yan, H.; Wang, L.; Fang, Z., Controlled Formation of Self-extinguishing Intumescent Coating on Ramie Fabric via Layer-by-Layer Assembly. *Industrial & Engineering Chemistry Research* **2013,** *52*, 6138-6146.

244. Weil, E. D., Fire-protective and Flame-retardant Coatings - A State-of-the-art Review. *Journal of Fire Sciences* **2011,** *29*, 259-296.

245. Carosio, F.; Di Blasio, A.; Alongi, J.; Malucelli, G., Green DNA-based Flame Retardant Coatings Assembled through Layer-by-Layer. *Polymer* **2013,** *54*, 5148-5153.

246. Carosio, F.; Di Blasio, A.; Alongi, J.; Malucelli, G., Layer-by-Layer Nanoarchitectures for the Surface Protection of Polycarbonate. *European Polymer Journal* **2013,** *49*, 397-404.

247. Huang, G.; Wang, B.; Lu, H.; Mamedov, A.; Gupta, S., Material Characterization and Modeling of Single-Wall Carbon Nanotube/Polyelectrolyte Multilayer Nanocomposites. *Journal of Applied Mechanics* **2006,** *73*, 737-744.

248. Huang, G.; Yang, J.; Gao, J.; Wang, X., Thin Films of Intumescent Flame Retardant-Polyacrylamide and Exfoliated Graphene Oxide Fabricated via Layer-by-Layer Assembly for Improving Flame Retardant Properties of Cotton Fabric. *Industrial & Engineering Chemistry Research* **2012,** *51*, 12355-12366.

249. Zhang, T.; Yan, H.; Peng, M.; Wang, L.; Ding, H.; Fang, Z., Construction of Flame Retardant Nanocoating on Ramie Fabric via Layer-by-Layer Assembly of Carbon Nanotube and Ammonium Polyphosphate. *Nanoscale* **2013,** *5*, 3013-3021.

250. Bartholmai, M.; Schartel, B., Layered Silicate Polymer Nanocomposites: New Approach or Illusion for Fire Retardancy? Investigations of the Potentials and the Tasks using a Model System. *Polymers for Advanced Technologies* **2004,** *15*, 355-364.

251. Ploehn, H. J.; Liu, C. Y., Quantitative Analysis of Montmorillonite Platelet Size by Atomic Force Microscopy. *Industrial & Engineering Chemistry* **2006,** *45*, 7025.

252. Annabi-Bergaya, F., Layered Clay Minerals. Basic Research and Innovative Composite Applications. *Microporous and Mesoporous Materials* **2008,** *107*, 141-148.

253. Geddes, N. J.; Paschinger, E. M.; Furlong, D. N.; Caruso, F.; Hoffmann, C. L.; Rabolt, J. F., Surface Chemical Activation of Quartz Crystal Microbalance Gold Electrodes — Analysis by Frequency Changes, Contact Angle Measurements and Grazing Angle FTIR. *Thin Solid Films* **1995,** *260*, 192-199.

254. Nie, S.; Song, L.; Bao, C.; Qian, X.; Guo, Y.; Hong, N.; Hu, Y., Synergistic Effects of Ferric Pyrophosphate (FePP) in Intumescent Flame-retardant Polypropylene. *Polymers for Advanced Technologies* **2011,** *22*, 870-876.

255. Stone, D. H. Overview on the combustibility and testing of filing materials and fabrics for upholstered furniture. http://pfa.org/slideshows/facts/slide37.html.

256. Babrauskas, V.; Peacock, R. D., Heat Release Rate: The Single Most Important Variable in Fire Hazard. *Fire Safety Journal* **1992,** *18*, 255-272.

257. Krämer, R. H.; Zammarano, M.; Linteris, G. T.; Gedde, U. W.; Gilman, J. W., Heat Release and Structural Collapse of Flexible Polyurethane Foam. *Polymer Degradation and Stability* **2010,** *95*, 1115-1122.

258. Babrauskas, V., Related Quantities. Part A. In *Heat release in fires*, Babrauskas, V.; Grayson, S. J., Eds. 1992; pp 207-223.

259. Larsen, E. R., Fire Retardants (Halogenated). In *Kirk-Othmer Encyclopedia of Chemical Technology* 3rd ed.; 1980; Vol. 10, pp 373-395.

260. Lewin, M.; Weil, E. D., Physical Modes of Action of Halogenated Flame Retardants. In *Fire Retardant Materials*, Horrocks, A. R.; Price, D., Eds. Woodhead Publishing Ltd: Boca Raton, FL, 2001; pp 34-35.

261. Lefebvre, J.; Bastin, B.; Le Bras, M.; Duquesne, S.; Ritter, C.; Paleja, R.; Poutch, F., Flame Spread of Flexible Polyurethane Foam: Comprehensive Study. *Polymer Testing* **2004,** *23*, 281-290.

262. Wu, G. M.; Schartel, B.; Bahr, H.; Kleemeier, M.; Yu, D.; Hartwig, A., Experimental and Quantitative Assessment of Flame Retardancy by the Shielding Effect in Layered Silicate Epoxy Nanocomposites. *Combustion and Flame* **2012,** *159*, 3616-3623.

263. Zheng, X.; Wilkie, C. A., Flame Retardancy of Polystyrene Nanocomposites Based on an Oligomeric Organically-modified Clay Containing Phosphate. *Polymer Degradation and Stability* **2003,** *81*, 539-550.

264. Lindholm, J.; Brink, A.; Hupa, M. Cone Calorimeter - a Tool for Measuring Heat Release Rate 2009. http://www.ffrc.fi/FlameDays_2009/4B/LindholmPaper.pdf.

265. Wichman, I. S., Material Flammability, Combustion, Toxicity and Fire Hazard in Transportation. *Progress in Energy and Combustion Science* **2003,** *29*, 247-299.

266. Apaydin, K.; Laachachi, A.; Bour, J.; Toniazzo, V.; Ruch, D.; Ball, V., Polyelectrolyte Multilayer Films made from Polyallylamine and Short Polyphosphates: Influence of the Surface Treatment, Ionic Strength and Nature of the Electrolyte Solution. *Colloids and Surfaces A: Physicochemical and Engineering Aspects* **2012,** *415*, 274-280.

267. Isitman, N. A.; Gunduz, H. O.; Kaynak, C., Nanoclay Synergy in Flame Retarded/Glass Fibre Reinforced Polyamide 6. *Polymer Degradation and Stability* **2009,** *94*, 2241-2250.

268. Singh, H.; Jain, A. K., Ignition, Combustion, Toxicity, and Fire Retardancy of Polyurethane Foams: A Comprehensive Review. *Journal of Applied Polymer Science* **2009,** *111*, 1115-1143.

269. Aulin, C.; Salazar Alvarez, G.; Lindstrom, T., High strength, flexible and transparent nanofibrillated cellulose-nanoclay biohybrid films with tunable oxygen and water vapor permeability. *Nanoscale* **2012,** *4*, 6622-6628.

270. Mittal, V., Epoxy-Vermiculite Nanocomposites as Gas Permeation Barrier. *Journal of Composite Materials* **2008,** *42*, 2829-2839.

271. Takahashi, S.; Farrell, M.; Goldberg, H. A.; Feeney, C. A.; Karim, D. P.; O'Leary, K.; Paul, D. R., Gas Barrier Properties of Butyl Rubber/Vermiculite Nanocomposite Coatings. *Polymer* **2006,** *47*, 3083-3093.

272. Guin, T.; Guin, M.; Krecker, D.; Hagen, J.; Grunlan, Thick Growing Multilayer Nanobrick Wall Thin Films: Super Gas Barrier with Very Few Layers. *Langmuir* **2014,** *30*, 7057-7060.

273. Jang, W.-S.; Grunlan, J. C., Robotic Dipping System for Layer-by-Layer Assembly of Multifunctional Thin Films. *Review of Scientific Instruments* **2005,** *76*.

274. Priolo, M. A.; Holder, K. M.; Greenlee, S. M.; Grunlan, J. C., Transparency, Gas Barrier, and Moisture Resistance of Large-aspect-ratio Vermiculite Nanobrick Wall Thin Films. *Acs Appl Mater Inter* **2012,** *4*, 5529-5533.

275. Yang, Y. H.; Haile, M.; Park, Y. T.; Malek, F. A.; Grunlan, J. C., Super Gas Barrier of All-Polymer Multilayer Thin Films. *Macromolecules* **2011,** *44*, 1450-1459.

276. Stefanidou, M.; Athanaselis, S.; Spiliopoulou, C., Health Impacts of Fire Smoke Inhalation. *Inhalation Toxicology* **2008,** *20*, 761-766.

277. Priolo, M.; Holder, K.; Greenlee, S.; Grunlan, J., Transparency, gas barrier, and moisture resistance of large-aspect-ratio vermiculite nanobrick wall thin films. *Acs Appl Mater Inter* **2012,** *4*, 5529-33.

278. Abollino, O.; Giacomino, A.; Malandrino, M.; Mentasti, E., Interaction of Metal Ions with Montmorillonite and Vermiculite. *Applied Clay Science* **2008,** *38*, 227-236.

279. Ren, Q. A.; Zhang, Y.; Li, J. A.; Li, J. C., Synergistic Effect of Vermiculite on the Intumescent Flame Retardance of Polypropylene. *Journal of Applied Polymer Science* **2011,** *120*, 1225-1233.

280. Marcos, C.; Rodríguez, I., Some Effects of Trivalent Chromium Exchange of Thermo-exfoliated Commercial Vermiculite. *Applied Clay Science* **2014,** *90*, 96-100.

281. Chen, X. T.; Yin, Y. L.; Lu, J.; Chen, X. H., Preparation and Properties of Iron-based Flame-retardant Reinforcing Agent. *Journal of Fire Sciences* **2014,** *32*, 179-190.

282. Du, M.; Guo, B.; Jia, D., Thermal Stability and Flame Retardant Effects of Halloysite Nanotubes on Poly(propylene). *European Polymer Journal* **2006,** *42*, 1362-1369.

283. Kashiwagi, T.; Grulke, E.; Hilding, J.; Groth, K.; Harris, R.; Butler, K.; Shields, J.; Kharchenko, S.; Douglas, J., Thermal and Flammability Properties of Polypropylene/Carbon Nanotube Nanocomposites. *Polymer* **2004,** *45*, 4227-4239.

284. Zhu, J.; Uhl, F. M.; Morgan, A. B.; Wilkie, C. A., Studies on the Mechanism by which the Formation of Nanocomposites Enhances Thermal Stability. *Chem Mater* **2001,** *13*, 4649-4654.

285. Braun, U.; Schartel, B.; Fichera, M. A.; Jäger, C., Flame Retardancy Mechanisms of Aluminium Phosphinate in Combination with Melamine Polyphosphate and Zinc Borate in Glass-fibre Reinforced Polyamide 6,6. *Polymer Degradation and Stability* **2007,** *92*, 1528-1545.

286. Kandola, B. K., Flame Retardancy Design for Textile. In *Fire Retardancy of Polymeric Materials*, 2 ed.; Wilkie, C. A.; Morgan, A. B., Eds. CRS Press Taylor and Francis Group: Boca Raton, FL, 2010; pp 725-762.

287. Wyld, O. British Patent 551, 1735.

288. Lawson, J. R. *A History of Fire Testing*; National Institute of Standards and Technology: March 2009, 2009.

289. Horrocks, A. R.; Kandola, B. K.; Davies, P. J.; Zhang, S.; Padbury, S. A., Developments in Flame Retardant Textiles - A Review. *Polymer Degradation and Stability* **2005,** *88*, 3-12.

290. Bourbigot, S.; Le Bras, M.; Flambard, X.; Rochery, M.; Devaux, E.; Lichtenhan, J. D., *Polyhedral Oligomeric Silsesquioxanes: Application to Flame Retardant Textiles*. Royal Soc Chemistry: Cambridge, 2005; pp 189-201.

291. Lecoeur, E.; Vroman, I.; Bourbigot, S.; Lam, T. M.; Delobel, R., Flame Retardant Formulations for Cotton. *Polymer Degradation and Stability* **2001,** *74*, 487-492.

292. Horrocks, A. R., Developments in Flame Retardants for Heat and Fire Resistant Textiles— the Role of Char Formation and Intumescence. *Polymer Degradation and Stability* **1996,** *54*, 143-154.

293. Biesheuvel, P. M.; Cohen Stuart, M. A., Electrostatic Free Energy of Weakly Charged Macromolecules in Solution and Intermacromolecular Complexes Consisting of Oppositely Charged Polymers. *Langmuir* **2004,** *20*, 2785-2791.

294. Philipp, B.; Dautzenberg, H.; Linow, K.-J.; Kötz, J.; Dawydoff, W., Polyelectrolyte Complexes — Recent Developments and Open Problems. *Progress in Polymer Science* **1989,** *14*, 91-172.

295. Bertrand, P.; Jonas, A.; Laschewsky, A.; Legras, R., Ultrathin Polymer Coatings by Complexation of Polyelectrolytes at Interfaces: Suitable Materials, Structure and Properties. *Macromolecular Rapid Communications* **2000,** *21*, 319-348.

296. Wandrey, C.; Grigorescu, G.; Hunkeler, D., Study of Polyelectrolyte Complex Formation Applying the Synthetic Boundary Technique of Analytical Ultracentrifugation. *Progress in Colloid and Polymer Science* **2002,** *119*, 84-91.

297. Sukhishvili, S. A.; Kharlampieva, E.; Izumrudov, V., Where Polyelectrolyte Multilayers and Polyelectrolyte Complexes Meet. *Macromolecules* **2006,** *39*, 8873-8881.

298. Marsh, D. H.; Riley, D. J.; York, D.; Graydon, A., Sorption of Inorganic Nanoparticles in Woven Cellulose Fabrics. *Particuology* **2009,** *7*, 121-128.

299. Horrocks, A. R., Textiles. In *Fire Retardant Materials*, Horrocks, A. R.; Price, D., Eds. CRC Press LLC: Boca Raton, FL, 2001; pp 128-181.

300. Kandola, B. K.; Horrocks, A. R.; Price, D.; Coleman, G. V., Flame-retardant Treatments of Cellulose and their Influence on the Mechanism of Cellulose Pyrolysis. *Journal of Macromolecular Science, Part C: Polymer Reveiws* **1996,** *36*, 721-794.

301. Jimenez, M.; Duquesne, S.; Bourbigot, S., Intumescent Fire Protective Coating: Toward a Better Understanding of their Mechanism of Action. *Thermochimica Acta* **2006,** *449*, 16-26.

302. Moon, R. J.; Martini, A.; Nairn, J.; Simonsen, J.; Youngblood, J., Cellulose Nanomaterials Review: Structure, Properties and Nanocomposites. *Chemical Society Reviews* **2011,** *40*, 3941-3994.

303. Chinga-Carrasco, G., Cellulose Fibres, Nanofibrils and Microfibrils: The Morphological Sequence of MFC Components from a Plant Physiology and Fibre Technology Point of View. *Nanoscale Research Letters* **2011,** *6*, 417.

304. Larsson, E.; Sanchez, C. C.; Porsch, C.; Karabulut, E.; Wågberg, L.; Carlmark, A., Thermo-responsive Nanofibrillated Cellulose by Polyelectrolyte Adsorption. *European Polymer Journal* **2013,** *49*, 2689-2696.

305. Zammarano, M.; Krämer, R. H.; Harris, R.; Ohlemiller, T. J.; Shields, J. R.; Rahatekar, S. S.; Lacerda, S.; Gilman, J. W., Flammability Reduction of Flexible Polyurethane Foams via Carbon Nanofiber Network Formation. *Polymers for Advanced Technologies* **2008,** *19*, 588-595.

306. Chung, C.-L.; Gautier, C.; Campidelli, S.; Filoramo, A., Hierarchical Functionalisation of Single-Wall Carbon Nanotubes with DNA through Positively Charged Pyrene. *Chem Commun* **2010,** *46*, 6539-6541.

307. Backes, C.; Mundloch, U.; Ebel, A.; Hauke, F.; Hirsch, A., Dispersion of HiPco® and CoMoCAT® Single-Walled Nanotubes (SWNTs) by Water Soluble Pyrene Derivatives—Depletion of Small Diameter SWNTs. *Chemistry – A European Journal* **2010,** *16*, 3314-3317.

308. Dhawan, S. K.; Singh, N.; Venkatachalam, S., Shielding Behaviour of Conducting Polymer-Coated Fabrics in X-band, W-band and Radio Frequency Range. *Synthetic Metals* **2002,** *129*, 261-267.

309. Nuraje, N.; Asmatulu, R.; Cohen, R. E.; Rubner, M. F., Durable Antifog Films from Layer-by-Layer Molecularly Blended Hydrophilic Polysaccharides. *Langmuir* **2010,** *27*, 782-791.

310. Zhang, F.; Srinivasan, M. P., Cross-linked Polyimide–Polythiophene Composite Films with Reduced Surface Resistivities. *Thin Solid Films* **2005,** *479*, 95-102.

311. Yang, Y.-H.; Bolling, L.; Haile, M.; Grunlan, J. C., Improving Oxygen Barrier and Reducing Moisture Sensitivity of Weak Polyelectrolyte Multilayer Thin Films with Crosslinking. *RSC Advances* **2012,** *2*, 12355-12363.

312. Douglas Hayworth, P. D., Thermo Scientific Crosslinking Technical Handbook. Thermo Fisher Scientific Inc.: 2012.

313. Dai, J.; Jensen, A. W.; Mohanty, D. K.; Erndt, J.; Bruening, M. L., Controlling the Permeability of Multilayered Polyelectrolyte Films through Derivatization, Cross-Linking, and Hydrolysis. *Langmuir* **2001,** *17*, 931-937.

314. American Association of Textile Chemists and Colorists Test Method 124-2006.

APPENDIX A

LARGE-SCALE CONTINUOUS IMMERSION SYSTEM FOR LAYER-BY-LAYER DEPOSITION*

A.1 Introduction

Layer-by-layer (LbL) assembly is a powerful coating technology that suffers from a lack of industrial-scale processing tools. The LbL method is a simple, water-based technique that deposits various polymers, colloids, and/or molecules as thin films with tunable properties.[1-2] Nanocoatings created in this layered fashion have imparted numerous properties such as gas barrier,[3-5] electrical conductivity,[6-8] sensing,[9-11] anti-reflectivity,[12-15] antimicrobial,[16-17] drug delivery,[18-21] and flame-retardancy.[22-27] The deposition method involves the sequential exposure of a substrate to oppositely charged solutions, as illustrated in Figure A.1, and the cycle is repeated until the desired number of layers is reached. A single bilayer (BL) refers to a pair of positively and negatively-charged layers deposited using the LbL technique,[2] and film growth is typically driven by charge overcompensation on the surface of the last layer deposited.[1, 35-37]

*Parts of this chapter are reprinted with permission from Mateos, A. J.; Cain, A. A.; Grunlan, J. C., Large-Scale Continuous Immersion System for Layer-by-Layer Deposition of Flame Retardant and Conductive Nanocoatings on Fabric. *Industrial & Engineering Chemistry Research* **2014,** *53*, 6409-6416. © 2013 American Chemical Society,

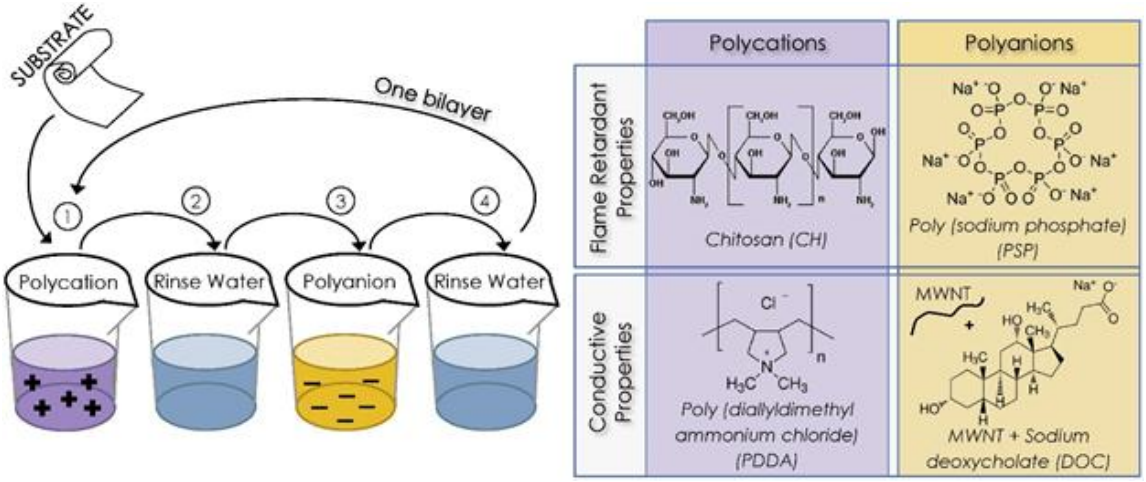

Figure A.1. Schematic of the layer-by-layer deposition process, where the substrate is immersed into polycation, polyanion, and deionized water rinse basins until the desired number of bilayers is achieved. The chemical structures shown above are used to produce the flame retardant and conductive behaviors imparted in this study.

The simplicity of this bottom-up processing technique and the tailorability of the thin film are spurring the development of new, and optimization of current, automated systems for larger-scale, faster production of reproducible multilayer assemblies. Several home-built robotic dipping systems have been designed to simulate the sequential adsorption process in an effort to probe fundamental interactions and structure-property relationships.[38-40] Other efforts to simplify and speed up the application of these nanocoatings involve the use of spraying as an alternative to dipping (or immersion).[41-44] As industrial interest in layer-by-layer assembly continues to increase, improvements to software/machine-design are being integrated into new automated systems (for both immersion and spray coating systems).[45-49]

The present study demonstrates a pilot-scale, automated, continuous system as a proof of concept for an industrial-scale immersion coating system capable of depositing layer-by-layer coatings onto large substrates. In an effort to highlight the versatility of this coating system, flame retardant and conductive multilayer recipes were deposited onto a model cotton fabric substrate. Fire behavior and antistatic properties were evaluated using two different nanocoating recipes. Continuously-coated samples were compared to hand-coated samples with regard to microstructure and behavior. These comparisons clearly demonstrate that the automated coating system is able to reproducibly fabricate thin films with consistent performance. This continuous immersion coater is a reliable technique that is expected to move LbL deposition towards more widespread commercial usage.

A.2 Experimental

A.2.1 Materials

Poly(sodium phosphate) (also known as sodium hexametaphosphate; crystalline, +200 mesh, 96%), chitosan (MW = 50-190 kDa, 75-85% deacetylated), poly(diallyldimethyl ammonium chloride) (MW = 100-200 kg/mol), branched polyethylenimine (MW = 25 kg/mol), sodium deoxycholate (≥ 97%), sodium hydroxide pellets (anhydrous) (reagent grade, ≥ 98%), and hydrochloric acid (ACS reagent, 37%) were purchased from Sigma-Aldrich (Milwaukee, WI). Multi-walled carbon nanotubes were obtained from Bayer MaterialScience (12-15 nm outer and 4 nm inner diameter and

1+ μm length, C ≥ 95 wt%, Leverkusen, Germany). Bleached, desized cotton print cloth (approximately of 3 oz/yd^2) was purchased from Testfabrics, Inc. (West Pittston, PA) and was soaked in pH 2 water immediately before use in an effort to induce a positive surface charge.[50] Large fabric swatches (10 x 180 in.) were coated with the continuous dipping system, and bench-scale fabric pieces (11 x 14 in.) were coated using the traditional hand dipping method. CH/PSP nanocoatings were deposited on P-doped, single-side-polished (100) silicon wafers (University Wafer, South Boston, MA) for ellipsometric thickness measurements.

A.2.2. Layer-by-layer (LbL) Deposition

All solutions were prepared with 18.2 MΩ deionized (DI) water. To improve adhesion to cotton, a 1.0 wt% of branched polyethylenimine (BPEI) was used as a primer layer for the flame retardant and conductive recipes. The conductive recipe consists of a positively-charged, aqueous solution of 0.25 wt% poly(diallyldimethyl ammonium chloride) (PDDA), and a negatively-charged dispersion of 0.05 wt% multi-walled carbon nanotubes (MWNT) stabilized with 1.0 wt% sodium deoxycholate (DOC). Prior to use, anionic solutions were sonicated at 20 W for 1 h, and slowly stirred for 0.5 h,[51] while cationic solutions were rolled for a minimum of 12 h to ensure full dissolution. The flame retardant recipe consists of 0.5 wt% positively-charged chitosan (CH) and 2.0 wt% negatively-charged poly(sodium phosphate) (PSP). After both polyion solutions had rolled for a minimum of 12 h, solution pH was adjusted to 4 prior

to deposition. Figure A.1 shows the chemical structures of deposition materials used in this study.

The automated system applies layer-by-layer nanocoatings by exposing sections of the fabric to deposition materials in a continuous, closed-loop fashion (Figure A.1). At each stage of the process, portions of the cotton fabric are submerged within the two polyelectrolyte solutions and two rinse stations. Each section of fabric is initially immersed in the cationic solution, and then passed from a water basin to an anionic solution, and finally to another water basin. A nip-roll technique was used to remove excess solution after each deposition. The coating machine continuously feeds the substrate through the looped system until the desired number of bilayers are applied. Deposition time is equal to the time in which each portion of the fabric is immersed. The stepper motor was used to set the immersion at 78 sec (0.093 in/sec). In order to directly compare microstructure and nanocoating properties, cotton fabric was also coated by hand with the same deposition time. All coated samples were dried in a 70 °C oven to remove moisture prior to evaluation and characterization.

A.2.3 Nanocoating Characterization

CH/PSP thickness was measured using an alpha-SE Ellipsometer (J. A. Woollam Co., Inc., Lincoln, NE). Surface images of uncoated and coated fabric were obtained using a JEOL JSM-6400 (JEOL Ltd., Tokyo, Japan). All samples were coated with 5 nm of platinum/palladium prior to imaging to reduce charging.

Thermal stability of uncoated fabric and CH/PSP-coated fabric was evaluated with vertical flame testing (VFT), according to ASTM D6413. Fabric samples were cut to size (3 x 12 in. strips), placed inside an automated vertical flammability cabinet (model VC-2; Govmark, Farmingdale, NY), and subjected to the direct flame of a Bunsen burner for 12 sec. The top of the main valve was situated 0.75 in. below each fabric sample. The term 'after flame' refers to the duration of time the flame persists on the cotton fabric after 12 sec. Hand-coated fabric samples were evaluated by vertical flame testing in triplicate. Two VFT samples were cut from four evenly spread sections along the length of the machine-coated fabric to assess the consistency of the nanocoating produced by the loop coater (i.e., fire behavior of eight 3 x 12 in. strips of continuously-coated fabric was evaluated using vertical flame testing).

A Signatone Pro4 four-point probe system (Gilroy, CA) with 0.4 mm probe tip diameter and 1.0 mm tip spacing was used to measure the sheet resistance of coated fabric. A LabVIEW program with SCB-68 shield I/O connector block (National Instruments Inc., Austin, TX) was connected to an Agilent E3644A DC power supply (Santa Clara, CA) and a Keithley digital multimeter (Cleveland, OH), which enabled the conductivity measurements. The selection process for machine coated sections to be analyzed was identical to that used for flammability analysis. The reported conductivity is an average of 10 sheet resistance measurements taken per sample, (five measurements per side). A SRM-110 surface resistivity meter (Pinion Products Corporation Inc., Los Fresnos, TX) was used for uncoated cotton due to its high resistivity (10^{11} Ω/□).

A.3. Results and Discussion

A.3.1 Continuous Layer-by-layer Coating System

Figure A.2a shows a schematic of the continuous immersion system developed to provide proof of concept for commercial-scale, continuous processing of nanocoatings deposited in a layer-by-layer fashion. The structural skeleton, constructed from t-slotted aluminum beams purchased from 80/20 Inc. (Columbia City, IN), provides the framework for a four-tiered system (e.g., 'electronics', 'excess removal', 'main', and 'ground'). The main houses 4 acrylic troughs (Figure A.2e), which were custom-made to minimize the amount of solution and water necessary for each experiment. The level above main (i.e., excess removal) supports the rollers (manufactured by Mid South Roller, Arlington, TX) that guide the substrate through the continuous coating system and remove excess material from the fabric after immersion in acrylic troughs. One

roller additionally functions as an adjustable tensioner for the closed loop system (Figure A.2c), while another is coupled with the NEMA 34 stepper motor, with a holding torque of 8.9 lb-ft and 1.8° resolution (purchased from National Instruments, Austin, TX). The stepper motor is located on the electronics level at the top of the coating system (Figure A.2d), which is controlled with a LabVIEW 2012 program to coordinate the substrate's position. In an effort to avoid polyelectrolyte contamination and reduce corrosion, hypalon and nylon parts were chosen for components immersed in water. Squeegee stations and water baths remove excess solution from the substrate after being dipped in either of the polyelectrolyte mixtures. A squeegee station consists of two spring-loaded rollers exerting pressure on the substrate, similar to a nip-roll, while the substrate passes between them. After being dipped into polyelectrolyte solutions, the fabric passes through a water bath and another squeegee station to remove excess material from the substrate.

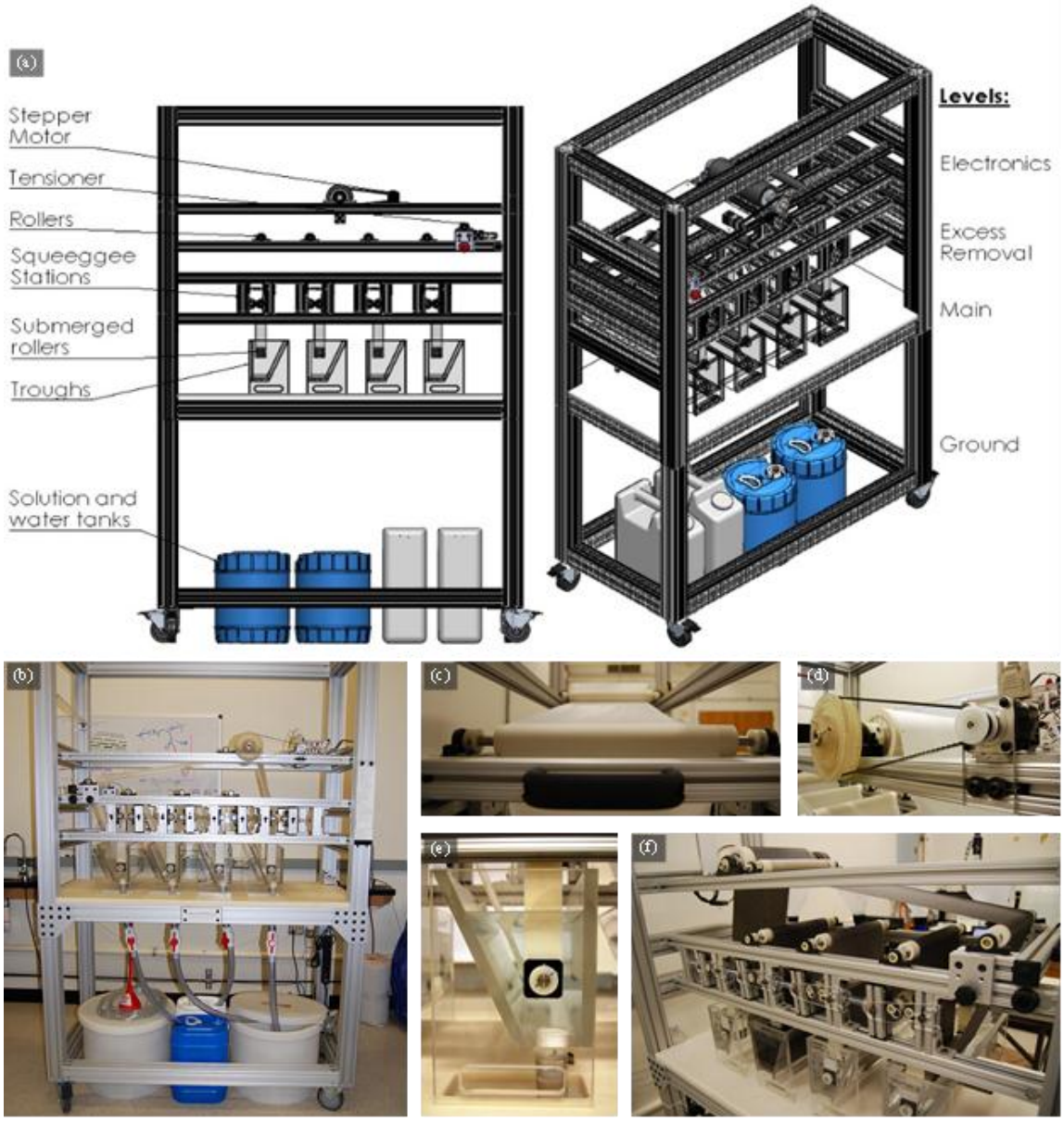

Figure A.2. Solidworks schematic and images of the continuous immersion system, with key components emphasized. (a) The four levels (electronics, excess removal, main, and ground) are noted in the isometric view (right). (b) Image of the actual pilot coater and pictures highlighting (c) the tensioner, (d) stepper motor and guide roller, and (e) solution trough. (f) Image of fabric being coated with the [PDDA/DOC-MWNT] antistatic recipe.

In an effort to maintain continuous motion and uniform deposition time over the length of the substrate, a section of the substrate is forfeited to allow for solution replenishing during the continuous process. PVC ball valves, and tubing purchased from U.S. Plastics Corp. (Lima, OH), connect the troughs to waste tanks resting at the ground level. One 17-gallon tank supplies water to the solution troughs and a similar tank is used to collect waste water. Two 5-gallon tanks are used to separately collect positively and negatively-charged solutions. A 13.8 VDC pump, purchased from McMaster-Carr (Chicago, IL), is used to transfer waste from these tanks.

A.3.2 Flame Retardant Fabric

Figure A.3a shows the growth of the CH/PSP multilayer thin film (measured with ellipsometry) as a function of the number of bilayers deposited. Alternate adsorption of chitosan and poly(sodium phosphate) solutions yields a flame resistant

nanocoating whose growth is characterized by both supralinear (1-16 BL) and linear (20-32 BL) regimes. Some researchers attribute the nonlinear portion, during initial layers, to island growth.[52] 20 and 30 BL of this multilayer system were applied to cotton fabric with the automated, continuous immersion system to evaluate the fire behavior of the nanocoating. These results were compared to nanocoatings created by traditional hand-coating methods to evaluate the efficacy of the pilot-scale coating system. Coating weight addition was determined by weighing the cotton before and after the thin film was applied. Residual weight after flame testing was similarly calculated. Weight measurements and flame test results are reported as a percentage of the original sample mass in Table A.1. Percentages for hand-coated fabric reflect the average flame test results for three vertical flame test pieces, while percentages for machine-coated fabric reflect the average flame test results for 8 vertical flame test pieces (2 VFT evaluations on 4 different sections of the 14 foot fabric).

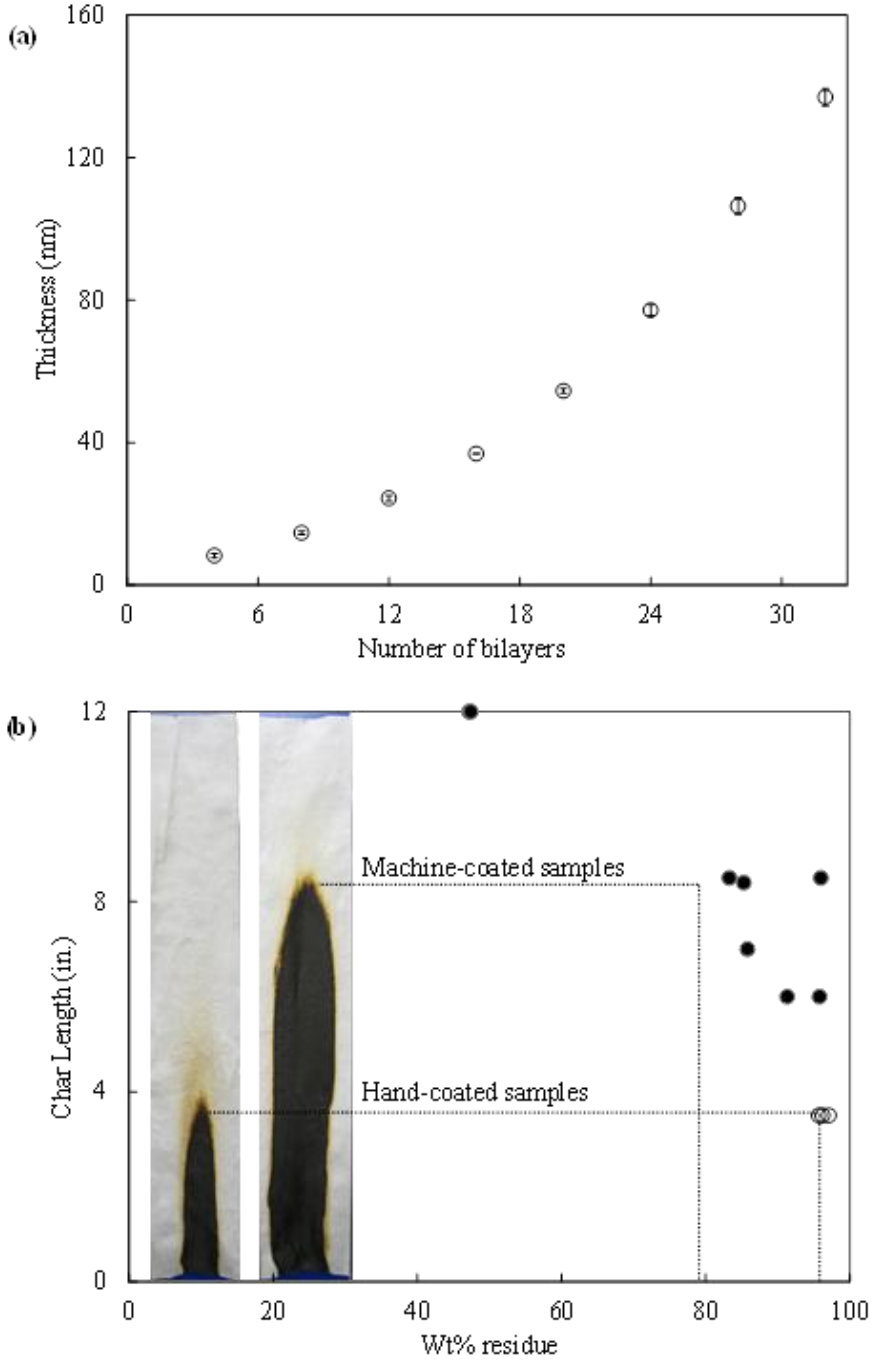

Figure A.3. (a) Ellipsometric thickness as a function of CH-PSP bilayers deposited on a silicon wafer. (b) Char length is plotted as a function of weight percent residue for 30 BL CH/PSP applied with the continuous coating system and by hand. The point where the dashed lines converge represents average values for both systems, and the inset images display the appearance of coated samples post flame testing.

Table A.1. Flame test results of CH/PSP coated fabric.

Sample	Wt Gain (%)	Wt Residue (%)	Time to Ignition (sec)	After Flame (sec)	After Glow (sec)
uncoated fabric	-	2.9 ± 0.5	0.8 ± 0.3	6.5 ± 1.7	25.9 ± 3.7
20 BL machine-coated	17.8	38.1 ± 7.2	0.9 ± 0.3	7.6 ± 3.4	0
20 BL hand-coated	15.8	60.4 ± 11.4	0.9 ± 0.2	3.5 ± 3.3	0
30 BL machine-coated	33.7	79.0 ± 20.1	1.5 ± 0.6	0*	0
30 BL hand-coated	35.9	96.3 ± 0.7	0.8 ± 0.1	0	0

*The value represents 5 VFT samples. The average 'After Flame' time for the other 3 samples is 16.6 ± 11.5 sec.

Both application methods result in similar weight addition for both 20 and 30 BL depositions (Table A.1). Control and coated fabric swatches are directly subjected to a Bunsen burner flame for 12 sec, as shown in Figure A.3b. Whereas cotton fabric is readily consumed by the flame, and remaining embers glow with heat for ~ 26 sec, LbL nanocoatings impart fire resistance to cotton fabric and eliminate after glow. The deposition materials used to create these multilayers are designed to reduce flammability of the substrates via a condensed phase mechanism called intumescence.[53-55] Heat activates the intumescent nature of the CH/PSP bilayers, transforming the film into a swollen, protective barrier that slows down mass transfer into the gas phase. It is believed that chitosan (and/or cotton fabric) acts as the carbon source and blowing agent, while poly(sodium phosphate) functions as the acid source, which dehydrates the carbon sources and creates the phosphorocarbonaceous heat shield that thermally insulates the underlying substrate.[53] The SEM micrographs in Figure A.4 show the transformation of the coating due to the application of heat (during vertical flame testing). The bubbling

observed on the postburn fabric is evidence of the intumescent flame retarding mechanism.

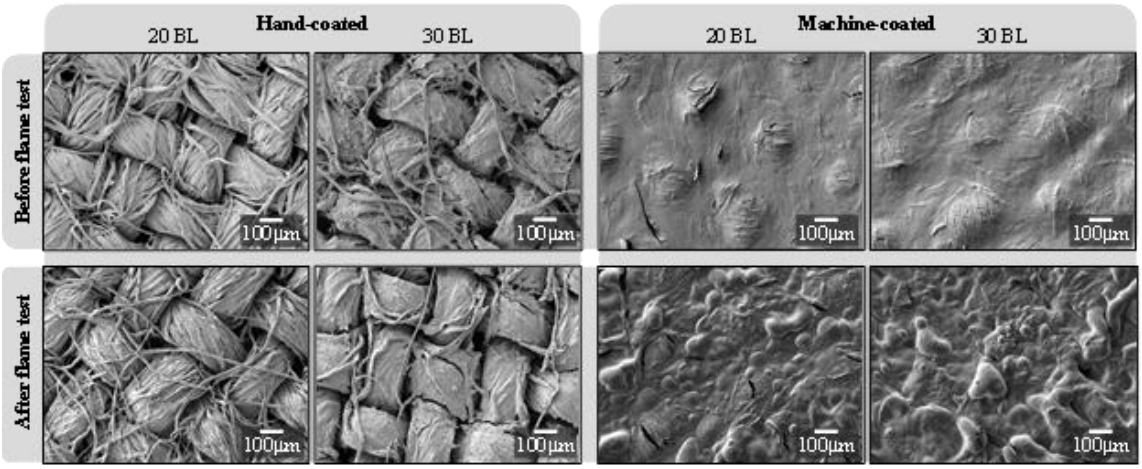

Figure A.4. SEM images of the coating morphology of CH/PSP coated fabric before (top row) and after (bottom row) flame testing.

Post vertical flame results of both application methods indicate 20 BL coatings do not provide enough of the deposited materials to effectively prevent flame spread (Table A.1). 30 BL nanocoatings applied with both application methods rendered fabric samples that self-extinguished during vertical flame testing. A coating weight addition of 35.9% was achieved with the hand-coating technique, and resulted in an average weight residue of 96.3% and an average char length of 3.5 inches after VFT. Flames self-extinguished on all 3 samples prior to the Bunsen burner flame being removed. Cotton fabric coated with the continuous immersion coating system gained 33.7 wt% coating addition. Flames on 5 out of the 8 VFT samples extinguished prior to the removal of the

Bunsen burner flame, yielding an average weight residue and char length of 90.8% and 7.2 inches, respectively. The other 3 VFT samples yielded an average residue and char length of 59.3% and 10.8 inches, respectively. Figure A.3b plots the residual weight left after each VFT as a function of char length for both machine and hand-coated fabric samples to better illustrate the performance of nanocoatings along the large substrate. The inset images display how samples look like after vertical flame testing, and the dashed lines represent the average value of each axis of the plot.

The slight variation in fire behavior is attributed to the difference in nanocoating morphologies created by each technique. The SEM micrographs of the coated fabric in Figure A.4 (before vertical flame testing) reveal that traditionally applied LbL coatings appear to deposit around cotton fibers while thin films applied by the continuous coating system appear to deposit the polyions on top of the fabric weave. If the majority of this applied nanocoating coalesced into a skin-like top coating, heat would more easily penetrate to the underlying cotton fabric through cracks in this thickly deposited thin film. In order to promote conformal coating of 'thickly growing systems', more aggressive rinsing stations should be incorporated into future designs and squeegee stations could be modified with texturized wringers. These adjustments may better imitate how excess material is removed from fabric when coated by hand (fabric coated by hand is wrung out prior to being submerged into the next solution). Although this comparison yields valuable information regarding this intumescent nanocoating, the focus of this study is to highlight the continuous coating system's ability to quickly produce multilayer nanocoatings that yield consistent results. All sections of the fabric

(10 x 180 in.) coated by the large-scale system exhibited very similar flammability characteristics for both 20 and 30 BL nanocoatings, which suggest that the automated system produces consistent coatings. Furthermore, this system outputs a 12-fold increase in quantity over the hand coating technique, produced by a single person.

A.3.3. Conductive Fabric

A second multilayer system, composed of poly(diallyldimethylammonium chloride) and multi-walled carbon nanotubes stabilized with sodium deoxycholate, was deposited to impart antistatic behavior to cotton fabric and to demonstrate the versatility of the continuous coating system. Similar systems, one containing single-walled carbon nanotubes with the same 1:20 (CNT:stabilizer) ratio,[56] and another with a 1:40 (CNT:stabilizer) ratio,[57] both grew linearly when deposited on silicon wafers. Five bilayers of [PDDA/DOC-MWNT] were deposited onto the fabric, which has an intrinsic sheet resistance of 10^{11} Ω/□. Machine-coated fabric and swatches coated by hand exhibit average sheet resistances of 1.4 x 10^{6} Ω/□ and 8.1 x 10^{4} Ω/□, respectively, as shown in Figure A.5a. The reported conductivity is an average of 10 sheet resistance measurements taken per sample (five measurements per side). This nanocoating improves the conductivity by 5 orders of magnitude, producing a surface resistivity adequate for antistatic applications.[58]

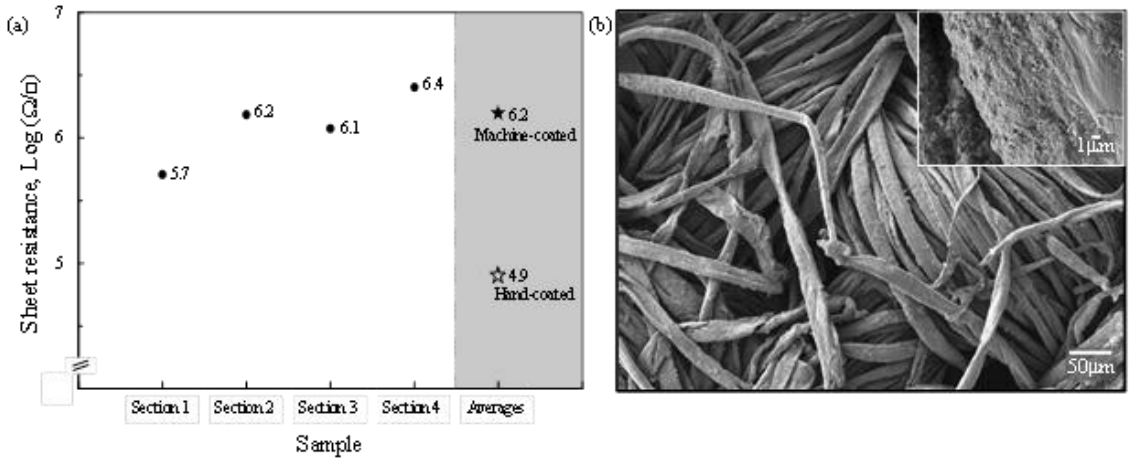

Figure A.5. (a) Sheet resistance of 5 [PDDA/DOC-MWNT] BL machine and hand-coated fabric. (b) SEM micrographs of continuously-coated fabric at low and high (inset) magnification.

The conductive fabric was imaged with SEM to better understand the morphology of the [PDDA/DOC-MWNT] layers (Figure A.5). The significant decrease in sheet resistance imparted by the 5 BL MWNT-based nanocoating, suggests that the loading of conductive material is at, or above, the percolation threshold.[59] These micrographs show that the conductive network forms around the weave structure. Inter-fiber linkages are present within this conformal nanocoating. Electrical conductivity of this thin film can easily be tuned by altering the number of bilayers deposited or varying the building blocks (e.g., the type of carbon nanotubes selected, sonication and exfoliation, surfactant type, etc.).[57] These thin films assembled with PDDA and DOC-stabilized MWNT further demonstrate the versatility of the continuous coating system.

A.4 Conclusions

A continuous immersion system, capable of efficiently depositing multilayer nanocoatings on a large scale was built and analyzed using various deposition recipes. The uniformity and physical properties of the coating system's fabric were directly compared to conventional bench-scale samples prepared by hand. CH/PSP multilayers were deposited on cotton fabric to impart flame retardant properties, while [PDDA/DOC-MWNT] bilayers were deposited on the same type of fabric to impart electrical conductivity (i.e., sheet resistance of 1.4×10^6 Ω/□). The coating system provides an acceleration of the LbL dipping process, while still imparting the desired properties of the applied nanocoatings. Further optimization of the continuous coating system could include a blade rinsing stage, after dip rinsing stations, and textured rollers in the squeegee stations to more effectively remove excess material from the substrate. This large-scale automated immersion device produces effective nanocoatings with consistent properties throughout the entire length of the coated fabric. Pairing these desired characteristics with the tailorability of the layer-by-layer assembly technique and the coater's potentially high rate of production, provides an excellent proof of concept for a commercially viable coating system.

REFERENCES

1. Ariga, K.; Hill, J. P.; Ji, Q., Layer-by-layer assembly as a versatile bottom-up nanofabrication technique for exploratory research and realistic application. *Phys. Chem. Chem. Phys.* **2007,** *9*, 2319-2340.

2. Decher, G., Schlenoff, J. B., *Multilayer Thin Films: Sequential Assembly of Nanocomposites Materials*. Wiley: New York, 2012.

3. Aulin, C.; Karabulut, E.; Tran, A.; Wagberg, L.; Lindstrom, T., Transparent Nanocellulosic Multilayer Thin Films on Polylactic Acid with Tunable Gas Barrier Properties. *Acs Appl Mater Inter* **2013,** *5*, 7352-7359.

4. Laufer, G.; Kirkland, C.; Cain, A. A.; Grunlan, J. C., Oxygen Barrier of Multilayer Thin Films Comprised of Polysaccharides and Clay. *Carbohydrate Polymers* **2013,** *95*, 299-302.

5. Priolo, M.; Holder, K.; Greenlee, S.; Stevens, B.; Grunlan, J., Precisely Tuning the Clay Spacing in Nanobrick Wall Gas Barrier Thin Films. *Chemistry of Materials* **2013,** *25*, 1649-1655.

6. Mihai, I.; Addiégo, F.; Del Frari, D.; Bour, J.; Ball, V., Associating oriented polyaniline and eumelanin in a reactive layer-by-layer manner: Composites with high electrical conductivity. *Colloids and Surfaces A: Physicochemical and Engineering Aspects* **2013,** *434*, 118-125.

7. Park, Y. T.; Ham, A. Y.; Yang, Y. H.; Grunlan, J. C., Fully Organic ITO Replacement through Acid Doping of Double-walled Carbon Nanotube Thin Film Assemblies. *RSC Advances* **2011,** *1*, 662-671.

8. Sarker, A.; Hong, J.-D., Layer-by-Layer Self-assembled Multilayer Films Composed of Graphene/Polyaniline Bilayers: High-energy Electrode Materials for Supercapacitors. *Langmuir* **2012,** *28*, 12637-12646.

9. Chen, B.; Liu, C.; Watanabe, M.; Hayashi, K., Layer-by-Layer Structured AuNP Sensors for Terpene Vapor Detection. *IEEE Sensors Journal* **2013,** *13*, 4212-4219.

10. Su, P.-G.; Shieh, H.-C., Flexible NO2 Sensors Fabricated by Layer-by-Layer Covalent Anchoring and In Situ Reduction of Graphene Oxide. *Sensors and Actuators B: Chemical* **2014,** *190*, 865-872.

11. Raoufi, N.; Surre, F.; Rajarajan, M.; Sun, T.; Grattan, K. T. V., Fiber Optic pH Sensor Using Optimized Layer-by-Layer Coating Approach. *IEEE Sensors Journal* **2014,** *14*, 47-54.

12. Eita, M.; Wagberg, L.; Muhammed, M.; Wågberg, L., Thin Films of Zinc Oxide Nanoparticles and Poly(acrylic acid) Fabricated by the Layer-by-Layer Technique: A Facile Platform for Outstanding Properties. *The Journal of Physical Chemistry C* **2012,** *116*, 4621-4627.

13. Li, X.; He, J.; Liu, W., Broadband Anti-reflective and Water-repellent Coatings on Glass Substrates for Self-cleaning Photovoltaic Cells. *Materials Research Bulletin* **2013,** *48*, 2522-2528.

14. Lee, H.; Alcaraz, M.; Rubner, M.; Cohen, R., Zwitter-wettability and Antifogging Coatings with Frost-resisting Capabilities. *ACS Nano* **2013,** *7*, 2172-2185.

15. Tan, W.; Du, Y.; Luna, L.; Khitass, Y.; Cohen, R.; Rubner, M., Templated Nanopores for Robust Functional Surface Porosity in Poly(methyl methacrylate). *Langmuir* **2012,** *28*, 13496-13502.

16. Gomes, A.; Gouveia, I.; Mano, J.; Queiroz, J., Layer-by-Layer Deposition of Antimicrobial Polymers on Cellulosic Fibers: A New Strategy to Develop Bioactive Textiles. *Polymers for Advanced Technologies* **2013,** *24*, 1005-1010.

17. Wang, B.-l.; Ren, K.-f.; Chang, H.; Wang, J.-l.; Ji, J., Construction of Degradable Multilayer Films for Enhanced Antibacterial Properties. *ACS Applied Materials & Interfaces* **2013,** *5*, 4136-4143.

18. Jing, J.; Szarpak Jankowska, A.; Guillot, R.; Pignot Paintrand, I.; Picart, C.; Auzély Velty, R., Cyclodextrin/Paclitaxel Complex in Biodegradable Capsules for Breast Cancer Treatment. *Chemistry of Materials* **2013,** *25*, 3867-3873.

19. Dam, H. H.; Caruso, F., Formation and Degradation of Layer-by-Layer Assembled Polyelectrolyte Polyrotaxane Capsules. *Langmuir* **2013,** *29*, 7203-7208.

20. Morton, S.; Poon, Z.; Hammond, P., The Architecture and Biological Performance of Drug-loaded LbL Nanoparticles. *Biomaterials* **2013,** *34*, 5328-5335.

21. Yi, Q.; Wen, D.; Sukhorukov, G., UV-cross-linkable Multilayer Microcapsules Made of Weak Polyelectrolytes. *Langmuir* **2012,** *28*, 10822-10829.

22. Li, Y.-C.; Mannen, S.; Morgan, A. B.; Chang, S.; Yang, Y.-H.; Condon, B.; Grunlan, J. C., Intumescent All-Polymer Multilayer Nanocoating Capable of Extinguishing Flame on Fabric. *Advanced Materials* **2011,** *23*, 3926-3931.

23. Cain, A. A.; Nolen, C. R.; Li, Y.-C.; Davis, R.; Grunlan, J. C., Phosphorous-filled Nanobrick Wall Multilayer Thin Film Eliminates Polyurethane Melt Dripping and Reduces Heat Release Associated with Fire. *Polymer Degradation and Stability* **2013,** *98*, 2645-2652.

24. Laufer, G.; Kirkland, C.; Morgan, A. B.; Grunlan, J. C., Exceptionally Flame Retardant Sulfur-based Multilayer Nanocoating for Polyurethane Prepared from Aqueous Polyelectrolyte Solutions. *ACS Macro Letters* **2013,** *2*, 361-365.

25. Carosio, F.; Di Blasio, A.; Alongi, J.; Malucelli, G., Green DNA-based Flame Retardant Coatings Assembled through Layer-by-Layer. *Polymer* **2013,** *54*, 5148-5153.

26. Apaydin, K.; Laachachi, A.; Ball, V.; Jimenez, M.; Bourbigot, S.; Toniazzo, V.; Ruch, D., Polyallylamine–Montmorillonite as Super Flame Retardant Coating Assemblies by Layer-by-Layer Deposition on Polyamide. *Polymer Degradation and Stability* **2013,** *98*, 627-634.

27. Zhang, T.; Yan, H.; Peng, M.; Wang, L.; Ding, H.; Fang, Z., Construction of Flame Retardant Nanocoating on Ramie Fabric via Layer-by-Layer Assembly of Carbon Nanotube and Ammonium Polyphosphate. *Nanoscale* **2013,** *5*, 3013-3021.

28. Li, Y.; Kim, J.; Shields, R.; Davis, Controlling Polyurethane Foam Flammability and Mechanical Behaviour by Tailoring the Composition of Clay-based Multilayer Nanocoatings. *Journal of Materials Chemistry A: Materials for Energy and Sustainability* **2013,** *1*, 12987.

29. Kim, Y. S.; Harris, R.; Davis, R., Innovative Approach to Rapid Growth of Highly Clay-filled Coatings on Porous Polyurethane Foam. *ACS Macro Letters* **2012,** *1*, 820-824.

30. Priolo, M. A.; Gamboa, D.; Holder, K. M.; Grunlan, J. C., Super Gas Barrier of Transparent Polymer−Clay Multilayer Ultrathin Films. *Nano Letters* **2010,** *10*, 4970-4974.

31. Erel, I.; Zhu, Z.; Zhuk, A.; Sukhishvili, S. A., Hydrogen-bonded Layer-by-Layer Films of Block Copolymer Micelles with pH-responsive Cores. *Journal of Colloid and Interface Science* **2011,** *355*, 61-69.

32. Zhuk, A.; Pavlukhina, S.; Sukhishvili, S., Hydrogen-bonded Layer-by-Layer Temperature-triggered Release Films. *Langmuir* **2009,** *25*, 14025-14029.

33. Sung, C.; Vidyasagar, A.; Hearn, K.; Lutkenhaus, J., Effect of Thickness on the Thermal Properties of Hydrogen-bonded LbL Assemblies. *Langmuir* **2012,** *28*, 8100-8109.
34. Kurapati, R.; Raichur, A., Composite Cyclodextrin–Calcium Carbonate Porous Microparticles and Modified Multilayer Capsules: Novel Carriers for Encapsulation of Hydrophobic Drugs. *Journal of Materials Chemistry B: Materials for Biology and Medicine* **2013,** *1*, 3175-3184.

35. Decher, G., Fuzzy Nanoassemblies: Toward Layered Polymeric Multicomposites. *Science* **1997,** *277*, 1232-1237.

36. Adamczyk, Z.; Zembala, M.; Kolasinska, M.; Warszynski, P., Characterization of polyelectrolyte multilayers on mica and oxidized titanium by streaming potential and wetting angle measurements. *Collods and Surfaces A* **2007,** *302*, 455-460.

37. Castelnovo, M.; Joanny, J.-F., Formation of Polyelectrolyte Multilayers. *Langmuir* **2000,** *16*, 7524-7532.

38. Dubas, S. T.; Schlenoff, J. B., Factors Controlling the Growth of Polyelectrolyte Multilayers. *Macromolecules* **1999,** *32*, 8153-8160.

39. Jin, W.; Toutianoush, A.; Tieke, B., Use of Polyelectrolyte Layer-by-Layer Assemblies as Nanofiltration and Reverse Osmosis Membranes. *Langmuir* **2003,** *19*, 2550-2553.

40. Okayama, Y.; Ito, T.; Shiratori, S., Optimization of the Feedback Constant Control for the Mass-controlled Layer-by-Layer Sequential Adsorption Technique for Polyelectrolyte Thin Films. *Thin Solid Films* **2001,** *393*, 132-137.

41. Krogman, K. C.; Zacharia, N. S.; Schroeder, S.; Hammond, P. T., Automated Process for Improved Uniformity and Versatility of Layer-by-Layer Deposition. *Langmuir* **2007,** *23*, 3137-3141.

42. Schlenoff, J. B.; Dubas, S. T.; Farhat, T., Sprayed Polyelectrolyte Multilayers. *Langmuir* **2000,** *16*, 9968-9969.

43. Izquierdo, A.; Ono, S. S.; Voegel, J. C.; Schaaf, P.; Decher, G., Dipping versus Spraying: Exploring the Deposition Conditions for Speeding Up Layer-by-Layer Assembly. *Langmuir* **2005,** *21*, 7558-7567.

44. Porcel, C. H.; Izquierdo, A.; Ball, V.; Decher, G.; Voegel, J. C.; Schaaf, P., Ultrathin Coatings and (Poly(glutamic acid)/Polyallylamine) Films Deposited by Continuous and Simultaneous Spraying. *Langmuir* **2004,** *21*, 800-802.

45. Jang, W.-S.; Grunlan, J. C., Robotic Dipping System for Layer-by-Layer Assembly of Multifunctional Thin Films. *Review of Scientific Instruments* **2005,** *76,103904*.

46. Gamboa, D.; Priolo, M. A.; Ham, A.; Grunlan, J. C., Note: Influence of Rinsing and Drying Routines on Growth of Multilayer Thin Films Using Automated Deposition System. *Review of Scientific Instruments* **2010,** *81*, 036103.

47. Mundra, P.; Otto, T.; Gaponik, N.; Eychmüller, A., Automated Setup for Spray Assisted Layer-by-Layer Deposition. *Review of Scientific Instruments* **2013,** *84*, 074101.

48. Fukao, N.; Kyung, K.-H.; Fujimoto, K.; Shiratori, S., Automatic Spray-LBL Machine Based on in-Situ QCM Monitoring. *Macromolecules* **2011,** *44*, 2964-2969.

49. Winterton, L.; Vogt, J.; Lally, J.; Stockinger, F. 1999.

50. Marsh, D. H.; Riley, D. J.; York, D.; Graydon, A., Sorption of Inorganic Nanoparticles in Woven Cellulose Fabrics. *Particuology* **2009,** *7*, 121-128.

51. Park, Y.-T.; Ham, A. Y.; Y.-H., Y.; C., G. J., Fully organic ITO replacement through acid doping of double-walled carbon nanotube thin film assemblies. *RSC Advances* **2011,** *1*, 662-671.

52. Schmitt, J.; Grunewald, T.; Decher, G.; Pershan, P. S.; Kjaer, K.; Losche, M., Internal Structure of Layer-by-Layer Adsorbed Polyelectrolyte Films: A Neutron and X-ray Reflectivity Study. *Macromolecules* **1993,** *26*, 7058-7063.

53. Weil, E. D., Fire-Protective and Flame-Retardant Coatings - A State-of-the-Art Review. *Journal of Fire Sciences* **2011,** *29*, 259-296.

54. Morgan, A. B.; Gilman, J., An overview of flame retardancy of polymeric materials: application, technology, and future directions. *Fire and Materials* **2013,** *37*, 259-279.

55. Jimenez, M.; Duquesne, S.; Bourbigot, S., Intumescent fire protective coating: Toward a better understanding of their mechanism of action. *Thermochimica Acta* **2006,** *449*, 16-26.

56. Park, Y. T.; Ham, A. Y.; Grunlan, J. C., Heating and Acid Doping Thin Film Carbon Nanotube Assemblies for High Transparency and Low Sheet Resistance. *Journal of Materials Chemistry* **2011,** *21*, 363-368.

57. Park, Y. T.; Ham, A. Y.; Grunlan, J. C., High Electrical Conductivity and Transparency in Deoxycholate-stabilized Carbon Nanotube Thin Films. *Journal of Physical Chemistry C* **2010,** *114*, 6325-6333.
58. Dhawan, S. K.; Singh, N.; Venkatachalam, S., Shielding Behaviour of Conducting Polymer-Coated Fabrics in X-band, W-band and Radio Frequency Range. *Synthetic Metals* **2002,** *129*, 261-267.

59. Grunlan, J. C.; Mehrabi, A. R.; Bannon, M. V.; Bahr, J. L., Water-based Single-walled-nanotube-fIlled Polymer Composite with an Exceptionally Low Percolation Threshold. *Advanced Materials* **2004,** *16*, 150-153.